https://ntrs.nasa.gov/search.jsp?R=19980228237 2020-06-15T23:26:07+00:00Z

N 62 70133

CASE FILE COPY

NASA MEMO 1-16-59A

NASA

MEMORANDUM

A NUMERICAL METHOD FOR CALCULATING THE WAVE DRAG OF A CONFIGURATION FROM THE SECOND DERIVATIVE OF THE AREA DISTRIBUTION OF A SERIES OF EQUIVALENT BODIES OF REVOLUTION

By Lionel L. Levy, Jr., and Kenneth K. Yoshikawa

Ames Research Center
Moffett Field, Calif.

NATIONAL AERONAUTICS AND SPACE ADMINISTRATION
WASHINGTON
April 1959

TABLE OF CONTENTS

NATIONAL AERONAUTICS AND SPACE ADMINISTRATION

MEMORANDUM 1-16-59A

A NUMERICAL METHOD FOR CALCULATING THE WAVE DRAG OF A CONFIGURATION FROM THE SECOND DERIVATIVE OF THE AREA DISTRIBUTION OF A SERIES OF EQUIVALENT BODIES OF REVOLUTION*

By Lionel L. Levy, Jr., and Kenneth K. Yoshikawa

SUMMARY

A method based on linearized and slender-body theories, which is easily adapted to electronic-machine computing equipment, is developed for calculating the zero-lift wave drag of single- and multiple-component configurations from a knowledge of the second derivative of the area distribution of a series of equivalent bodies of revolution. The accuracy and computational time required of the method to calculate zero-lift wave drag is evaluated relative to another numerical method which employs the Tchebichef form of harmonic analysis of the area distribution of a series of equivalent bodies of revolution.

The results of the evaluation indicate that the total zero-lift wave drag of a multiple-component configuration can generally be calculated most accurately as the sum of the zero-lift wave drag of each component alone plus the zero-lift interference wave drag between all pairs of components. The accuracy and computational time required of both methods to calculate total zero-lift wave drag at supersonic Mach numbers is comparable for airplane-type configurations. For systems of bodies of revolution both methods yield similar results with comparable accuracy; however, the present method only requires up to 60 percent of the computing time required of the harmonic-analysis method for two bodies of revolution and less time for a larger number of bodies.

INTRODUCTION

As shown in reference 1, the linearized theory value of the wave drag of any arbitrary configuration in a steady supersonic flow can be calculated from a knowledge of the second derivative of the area distribution of a series of equivalent bodies of revolution obtained from areas and

forces in oblique planes. For slender nonlifting configurations the wave-drag contribution of the force term is zero or is sufficiently small that it can be neglected. The zero-lift wave drag of such configurations is given to a good approximation by the supersonic area rule developed in reference 2. The infinite series form of the supersonic area rule in reference 2 utilizes a knowledge of the first derivative of the area distribution of the series of equivalent bodies of revolution obtained from only the areas in oblique planes. In reference 3 the supersonic area rule was expressed in a form which permits a numerical solution of the infinite series from a knowledge of the area distribution of the series of equivalent bodies of revolution.

In this report a method applicable to slender nonlifting configurations is developed which utilizes a knowledge of the second derivative of the area distribution of the equivalent bodies of revolution. The method is developed from the integral form of the wave-drag equation given in reference 1 for nonlifting configurations. By a simple approximation of the second derivative of the area distribution of the equivalent bodies of revolution, the zero-lift wave drag is expressed in a finite series which can be evaluated numerically. The finite series form of the present method is particularly attractive in its application to the calculation of zero-lift interference wave drag between any pair of components of a configuration.

The usefulness of the present method depends, of course, upon the availability of methods for finding the second derivative of the area distribution of equivalent bodies of revolution. Reference 4 contains information from which it is possible to calculate the second derivative of the area distribution of bodies of revolution. A method for finding the second derivative of the area distribution (as well as the first derivative and the area distribution) of wing and tail-surface components of the equivalent bodies of revolution is presented in an appendix.

The present method of zero-lift wave-drag calculation will be evaluated relative to the method of reference 3 with regard to accuracy and computational time required. Numerical values of zero-lift wave-drag solutions for several simple analytical shapes computed by the present method will be compared with numerical solutions obtained by the method of reference 3 and with analytical solutions. Equations of the area distribution, the first derivative of the area distribution, and the second derivative of the area distribution of two families of wings or tail surfaces will also be presented in an appendix.

SYMBOLS

a_{ij}	distance between the ith and jth values of coordinates in the free-stream direction (see eq. (41))
$A_n(\beta,\theta)$	coefficients of a Fourier sine series expansion of $S'(x,\beta,\theta)$
b	span of a wing or tail surface
b_o	span of an extended wing or tail surface (see sketch (c))
c_o	wing or tail-surface chord at the vertical plane of symmetry
$\tilde{c}(\eta)$	spanwise variation of the dimensionless half-chord of a wing or tail surface
d	lateral distance between the longitudinal axes of a pair of bodies of revolution
$D(\beta)$	wave drag or zero-lift wave drag of a configuration
$D(\beta,\theta)$	wave drag or zero-lift wave drag of an equivalent body of revolution of a configuration
I	total number of points specified on a given curve
$I(a_{ij},\beta d)$	integral function used to evaluate the zero-lift interference wave drag between a pair of bodies of revolution (see eqs. (40) and (43))
K	tangent of the sweep angle of the 50-percent chord line of any "sheared" panel of an extended wing or tail surface in dimensionless coordinates
$l(\beta,\theta)$	length of an equivalent body of revolution in the positive x direction, $l(\beta,\theta)+l_1(\beta,\theta)$ = total equivalent-body length
$l_1(\beta,\theta)$	length of an equivalent body of revolution in the negative x direction
$L(x,\beta,\theta)$	frontal projection of the lift distribution intercepted on a given configuration by a set of parallel oblique planes inclined to the [illegible]
M	free-stream Mach number
q	free-stream dynamic pressure

S	reference area upon which drag coefficient or dimensionless area is based
$S(x,\beta,\theta)$	frontal projection of the area distribution intercepted on a given configuration by a set of parallel oblique planes tangent to the Mach cones
$\Delta S''(x_i)$	increment between values of the second derivative of the area distribution of a configuration at points x_{i-1} and x_i
$S_m''(x)$	mean value of the second derivative of the area distribution of a configuration (see eq. (45))
t_o	maximum thickness of wing or tail surface at the vertical plane of symmetry
$t(x,y)$	thickness distribution of a wing or tail surface
x,y,z	Cartesian coordinates in the free-stream, spanwise, and thickness directions, respectively
$\alpha(\xi,\eta,K)$	transformation defined by equation (C17) which defines any point in the dimensionless extended plan form of a "sheared" wing or tail surface as the local dimensionless chord station measured from the 50-percent chord
β	$\sqrt{M^2-1}$
δ	longitudinal distance between the lateral axes of a pair of bodies of revolution
λ	taper ratio of a wing or tail surface; ratio of the tip chord to that at the vertical plane of symmetry
ξ,η,ζ	dimensionless Cartesian coordinates in the free-stream, spanwise, and thickness directions, respectively
$\tau(\alpha)$	dimensionless thickness distribution of the local airfoil section
$\tau(\xi,\eta,K)$	dimensionless thickness distribution of a "sheared" wing or tail surface
θ	angle defining the orientation of the parallel oblique planes tangent to the Mach cones (see sketch (a))
$\Phi(\eta)$	spanwise variation of the dimensionless thickness along lines of constant percent chord
ψ	$\tan^{-1}\beta \cos \theta$

Subscripts

B	body
E, H	body E or body H
H(E)	quantities measured in the coordinate system of body H but related by a transformation to the coordinate system of body E
i, j	ith and jth points, respectively, of the total number of points specified on a curve
l	lower limit of integration
n	nth term of a Fourier sine series expansion of $S'(x,\beta,\theta)$
R	reference
t	tip of a wing or tail surface
T	total
u	upper limit of integration
W	wing

Superscripts

'	differentiation with respect to a coordinate in the free-stream direction
~	dimensionless value of any symbol not specifically listed as such (also see appendix A)

METHOD

Review of Basic Theory

The linearized-theory value of the wave drag of any arbitrary configuration in a steady supersonic air flow is stated in reference 1 to be the average of the wave drag of a series of equivalent bodies of revolution and can be expressed analytically by

$$D(\beta) = \frac{1}{2\pi}\int_0^{2\pi} D(\beta,\theta)d\theta \tag{1}$$

where

$$D(\beta,\theta) = -\frac{q}{2\pi}\int_{-l_1(\beta,\theta)}^{l(\beta,\theta)}\int_{-l_1(\beta,\theta)}^{l(\beta,\theta)}\left[S''(x_1,\beta,\theta) - \frac{\beta}{2q}L'(x_1,\beta,\theta)\right]\left[S''(x_2,\beta,\theta) - \frac{\beta}{2q}L'(x_2,\beta,\theta)\right]\ln|x_1-x_2|\,dx_1dx_2 \tag{2}$$

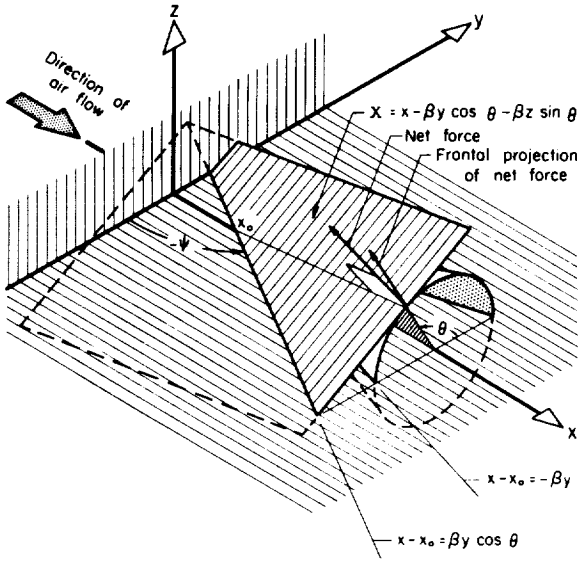

Sketch (a)

The quantity $S(x,\beta,\theta)$ is the frontal projection of the streamwise area distribution intercepted on the given configuration by parallel oblique planes tangent to the Mach cones. Similarly, $L(x,\beta,\theta)$ is the frontal projection of the lift distribution over the given configuration measured in the same oblique planes. The primes denote differentiation with respect to x. The coordinate system, angles, Mach planes, and the direction of the net force are defined in sketch (a).

In this report only slender nonlifting configurations will be considered. For these configurations $L(x,\beta,\theta)$ can be neglected and the zero-lift wave drag of the separate equivalent bodies of revolution for such configurations is given by

$$D(\beta,\theta) = -\frac{q}{2\pi}\int_{-l_1(\beta,\theta)}^{l(\beta,\theta)}\int_{-l_1(\beta,\theta)}^{l(\beta,\theta)} S''(x_1,\beta,\theta)S''(x_2,\beta,\theta)\ln|x_1-x_2|\,dx_1dx_2 \tag{3}$$

The analysis in reference 1 imposes no restriction on the slope of the area distribution at the ends of the equivalent bodies of revolution or of the given configuration. It should be noted that this freedom from end-condition restrictions requires rigorous adherence to the concept of the oblique planes when determining the area distribution of the equivalent bodies. However, for nonlifting slender pointed bodies of revolution, the normal cross-sectional area distribution can be used if the end conditions of the bodies are such that

$$S'(-l_1,\beta,\theta) = S'(l,\beta,\theta) = 0 \tag{4}$$

For isolated nonlifting slender pointed bodies of revolution for which the slope of the area distribution at the base is not zero, the normal cross-sectional area distribution can be used only if the zero-lift wave drag is calculated by slender-body theory. The zero-lift wave-drag equation given by slender-body theory for these isolated bodies of revolution is given in reference 5 and can be written

$$D = -\frac{q}{2\pi}\int_{-l_1}^{l}\int_{-l_1}^{l} S''(x_1)S''(x_2)\ln|x_1-x_2|\,dx_1dx_2 + q\left\{\frac{[S'(l)]^2}{2\pi}\ln\frac{2}{\beta R(l)} + \frac{S'(l)}{\pi}\int_{-l_1}^{l} S''(x_2)\ln|l-x_2|\,dx_2\right\} \tag{5}$$

where $R(l)$ is the radius at the base of the body. The lower limits of integration, $-l_1$, imply merely that the origin of the coordinate system need not be chosen at the half-body length. For bodies of revolution with zero slope of the area distribution at the base, $S'(l) = 0$, the second term of equation (5) vanishes and the resulting equation is identical to the equation (3) for equivalent bodies of revolution, once values of β and θ are specified.

The area distribution of a single body of revolution is independent of θ (but may change with β) and the linearized-theory value of the zero-lift wave drag is given by equation (3) without recourse to equation (1). Furthermore, if the body is sufficiently slender that neglecting the change in the area distribution with β produces only a negligible effect on the zero-lift wave drag, the linearized-theory value of the zero-lift wave drag of a slender body of revolution with $S'(l) = 0$ is identical to that given by slender-body theory. The body fineness ratio required in order to justify neglecting the effect of β on the body area distribution has been discussed in reference 4.

Approximations

Aside from the approximations basic to linearized and slender-body theories, only one approximation is necessary in order to express equations (3) and (5) in a finite series. This is an approximation of the second derivative of area distribution, $S''(x)$,[1] of the equivalent bodies of revolution.

[1]The variables β and θ have been intentionally omitted from the notation in the interest of simplicity and will be omitted throughout this report except in cases where these variables are necessary to the analysis. For bodies of revolution $S''(x) = S''(x,\beta)$. If the body is closed at the rear, l is constant, and if the body has a finite base, $l = l(\beta)$. For wings and tail surfaces $S''(x) = S''(x,\beta,\theta)$ and $l = l(\beta,\theta)$.

Let $S''(x)$ be approximated by constant values over small equal intervals; that is, a smooth curve is represented by a broken curve consisting of adjacent equal-length steps as shown in figure 1. The value of the second derivative of the area distribution at a given station, x, is considered to be approximately equal to the value at the beginning of the interval, station x_i, in which station x lies. This approximation can be expressed analytically as

$$S''(x) \approx S''(x_i) \quad \text{for} \quad x_i \leq x \leq x_{i+1}$$

If the difference between the values of the second derivative of the area distribution at two adjacent intervals is defined at the beginning of the right-hand interval as

$$\Delta S''(x_i) = S''(x_i) - S''(x_{i-1})$$

then $S''(x)$ can be approximated by

$$S''(x) \approx \sum_{i=1}^{i(x)} \Delta S''(x_i) \quad \text{for} \quad x_i \leq x \leq x_{i+1} \tag{6}$$

where the upper limit of summation defines the beginning of the interval in which station x lies. It should be noted that I points are employed to define $I-1$ intervals for the total length (see fig. 1).

Development of the Method

The present method for calculating zero-lift wave drag is developed from analyses which evaluate equations (3) and (5) in light of the approximation of $S''(x)$ described above.[2] All analyses in this section of the report will be made in physical or dimensional coordinates. Experience has shown, however, that in performing the actual drag calculations it is more convenient to use dimensionless coordinates. For this reason, procedures are given in appendix A for making various types of configurations dimensionless.

Single bodies of revolution, $S'(-l_1) = 0$, $S'(l) \neq 0$.- The general expression for the zero-lift wave drag of a slender pointed body of revolution is given by equation (5). It is convenient to write equation (5) as

[2]During the preparation of the present report a numerical method for calculating the zero-lift wave drag of bodies of revolution by electronic machines or desk calculators was published in reference 6. Application of the method of this reference also requires a knowledge of $S''(x)$ (exact or approximate) and may also be used to evaluate equations (3) and (5).

$$D = D_1 + D_2$$

where

$$D_1 = -\frac{q}{2\pi}\int_{-l_1}^{l}\int_{-l_1}^{l} S''(x_1)S''(x_2)\ln|x_1-x_2|\,dx_1dx_2 \tag{7}$$

and

$$D_2 = q\left\{\frac{[S'(l)]^2}{2\pi}\ln\frac{2}{\beta R(l)} + \frac{S'(l)}{\pi}\int_{-l_1}^{l} S''(x_2)\ln|l-x_2|\,dx_2\right\} \tag{8}$$

First consider the expression for D_1. Equation (7) can be written

$$D_1 = -\frac{q}{2\pi}\int_{-l_1}^{l} S''(x_2)F(x_2)\,dx_2 \tag{9}$$

where

$$F(x_2) = \int_{-l_1}^{l} S''(x_1)\ln|x_1-x_2|\,dx_1 \tag{10}$$

Using the form of equation (6) for the variable x_1 and using the fact that $S''(x)$ is approximated by a constant over each interval of the distribution (see fig. 1), one can write equation (10) as

$$F(x_2) \approx \sum_{i=1}^{I}\Delta S''(x_i)\int_{x_1=x_i}^{l}\ln|x_1-x_2|\,dx_1$$

and equation (9) becomes

$$D_1 \approx -\frac{q}{2\pi}\sum_{i=1}^{I}\Delta S''(x_i)\int_{-l_1}^{l} S''(x_2)\int_{x_1=x_i}^{l}\ln|x_1-x_2|\,dx_1dx_2 \tag{11}$$

Similarly, using the form of equation (6) for the variable x_2, one can write equation (11) as

$$D_1 \approx -\frac{q}{2\pi}\sum_{i=1}^{I}\sum_{j=1}^{I}\Delta S''(x_i)\Delta S''(x_j)\int_{x_2=x_j}^{l}\int_{x_1=x_i}^{l}\ln|x_1-x_2|\,dx_1dx_2 \tag{12}$$

After the double integration, equation (12) becomes

$$D_1 \approx -\frac{q}{4\pi}\sum_{i=1}^{I}\sum_{j=1}^{I}\Delta S''(x_i)\Delta S''(x_j)I_o(x_i,x_j) \tag{13}$$

where

$$I_o(x_i,x_j) = (l-x_i)^2\left(\ln|l-x_i| - \frac{3}{2}\right) + (l-x_j)^2\left(\ln|l-x_j| - \frac{3}{2}\right) - (x_i-x_j)^2\left(\ln|x_i-x_j| - \frac{3}{2}\right) \tag{14}$$

The order of the summation in equation (13) can be interchanged. This permits parts of equation (14) to be evaluated as constants. Hence, if the contribution to equation (13) of the first term in equation (14) is summed over i, the contribution of the second term of equation (14) is summed over j and the contribution of the second part of the third term of equation (14) is summed over both i and j, equation (13) can be written

$$D_1 \approx -\frac{q}{4\pi}\left\{K_1\sum_{j=1}^{I}\Delta S''(x_j)+K_2\sum_{i=1}^{I}\Delta S''(x_i)+K_3-\sum_{i=1}^{I}\sum_{j=1}^{I}\Delta S''(x_i)\Delta S''(x_j)I_1(x_i,x_j)\right\} \tag{15}$$

where

$$\left.\begin{aligned} K_1 &= \sum_{i=1}^{I}\Delta S''(x_i)(l-x_i)^2\left(\ln|l-x_i| - \frac{3}{2}\right) \\ K_2 &= \sum_{j=1}^{I}\Delta S''(x_j)(l-x_j)^2\left(\ln|l-x_j| - \frac{3}{2}\right) \\ K_3 &= \frac{3}{2}\sum_{i=1}^{I}\sum_{j=1}^{I}\Delta S''(x_i)\Delta S''(x_j)(x_i-x_j)^2 \end{aligned}\right\} \tag{16}$$

and

$$I_1(x_i,x_j) = (x_i-x_j)^2\ln|x_i-x_j| \tag{17}$$

Now consider the expression for D_2 given by equation (8). Using the form of equation (6) for the variable x_2 and the fact that $S''(x)$ is approximated by a constant over each interval of the distribution, one can write the second term of equation (8) as

$$G(x_2) = \frac{S'(l)}{\pi}\int_{-l_1}^{l} S''(x_2)\ln|l-x_2|dx_2 \approx \frac{S'(l)}{\pi}\sum_{j=1}^{I}\Delta S''(x_j)\int_{x_j}^{l}\ln|l-x_2|dx_2 \tag{18}$$

After the integration, equation (18) becomes

$$G(x_2) \approx \frac{S'(l)}{\pi}\sum_{j=1}^{I}\Delta S''(x_j)\left[(l-x_j)(\ln|l-x_j|-1)\right] \tag{19}$$

Again, since $S''(x)$ is approximated by a constant over each interval of the distribution, it can be shown that

$$\sum_{j=1}^{I}\Delta S''(x_j)(l-x_j) \approx S'(l) \tag{20}$$

and equation (19) becomes

$$G(x_2) \approx \frac{S'(l)}{\pi}\sum_{j=1}^{I}\Delta S''(x_j)J(x_j) - \frac{[S'(l)]^2}{\pi} \tag{21}$$

where

$$J(x_j) = (l-x_j)\ln|l-x_j| \tag{22}$$

Substituting equation (21) in equation (8)

$$D_2 \approx \frac{q}{\pi}\left\{\frac{1}{2}[S'(l)]^2\left[\ln\frac{2}{\beta R(l)} - 2\right] + S'(l)\sum_{j=1}^{I}\Delta S''(x_j)J(x_j)\right\} \tag{23}$$

Finally, the zero-lift wave drag of a slender pointed body of revolution with finite base area, such that $S'(l) \neq 0$, is given by the sum of equations (15) and (23) as

$$D \approx -\frac{q}{4\pi}\left[K_1\sum_{j=1}^{I}\Delta S''(x_j)+K_2\sum_{i=1}^{I}\Delta S''(x_i)+K_3-\sum_{i=1}^{I}\sum_{j=1}^{I}\Delta S''(x_i)\Delta S''(x_j)I_1(x_i,x_j)\right] +$$

$$\frac{q}{\pi}\left\{\frac{1}{2}[S'(l)]^2\left[\ln\frac{2}{\beta R(l)} - 2\right] + S'(l)\sum_{j=1}^{I}\Delta S''(x_j)J(x_j)\right\} \tag{24}$$

where K_1, K_2, K_3, and $I_1(x_i,x_j)$ are given by equations (16) and (17), respectively, and $J(x_j)$ is given by equation (22).

Single bodies of revolution, $S'(-l_1) = S'(l) = 0$.- For a slender body of revolution pointed at both ends or with finite base area such that $S'(l) = 0$ the last two terms of equation (24) become identically zero and the zero-lift wave drag of such bodies of revolution is given by equation (15). Equation (15) can be simplified for $S'(l) = 0$. For this condition, it can be seen from figure 1 (since $S''(x)$ is constant over each interval, $S'(x)$ is linear over each interval) that

$$\sum_{i=1}^{I} \Delta S''(x_i) = \sum_{j=1}^{I} \Delta S''(x_j) = 0 \quad \text{for} \quad S'(l) = 0 \tag{25}$$

Hence, the first two terms of equation (15) vanish. Further, upon substitution of equation (25) in equation (20) it is easily determined that

$$\sum_{i=1}^{I} \Delta S''(x_i)x_i = \sum_{j=1}^{I} \Delta S''(x_j)x_j = 0 \quad \text{for} \quad S'(l) = 0 \tag{26}$$

With equations (25) and (26) it can be further determined from equation (16) that K_3 is identically zero. Hence, for $S'(l) = 0$, equation (15) becomes

$$D_1 \approx \frac{q}{4\pi} \sum_{i=1}^{I} \sum_{j=1}^{I} \Delta S''(x_i)\Delta S''(x_j)I_1(x_i,x_j) \tag{27}$$

Finally it should be noted that $I_1(x_i,x_j) = 0$ for $i = j$ (see eq. (17)) and in view of symmetry of the matrix of the double summation with respect to i and j for a single body of revolution the zero-lift wave drag of equation (27) can be expressed as

$$D_1 \approx \frac{q}{2\pi} \sum_{i=2}^{I} \sum_{j=1}^{i-1} \Delta S''(x_i)\Delta S''(x_j)I_1(x_i,x_j) \tag{28}$$

Multiple-component configurations.- For configurations whose equivalent bodies of revolution satisfy the end conditions given by equation (4), the zero-lift wave drag of each equivalent body of revolution is given by equation (28). The zero-lift wave drag of the given configuration is determined by use of the results of equation (28) for each equivalent body of revolution in equation (1). If the end conditions of equation (4) are not satisfied, the results of equation (15) for each equivalent body of revolution (obtained from actual oblique areas) must be used in equation (1). It should be noted that equation (24) cannot be applied to calculate the total zero-lift wave drag of multiple-component configurations, since this equation is valid only for isolated bodies of revolution for which $S'(l) \neq 0$.

An analysis of the integral equation for a single equivalent body of revolution (eq. (3)) reveals that the total zero-lift wave drag of an equivalent body of revolution of a multiple-component configuration can be calculated as the sum of the zero-lift wave drag of each component alone plus the zero-lift interference wave drag between all possible pairs of components. For simplicity consider the complete wing shown by the solid lines in sketch (b). Each wing panel is considered to be one component of a multiple-component configuration. The dashed lines in sketch (b) represent the "sheared" configuration (described in ref. 7 for a given β and θ) whose normal area distribution is that of the equivalent body of revolution. From sketch (b) the total second derivative of the combined area distribution of the two wing panels (i.e., the equivalent body of revolution) is

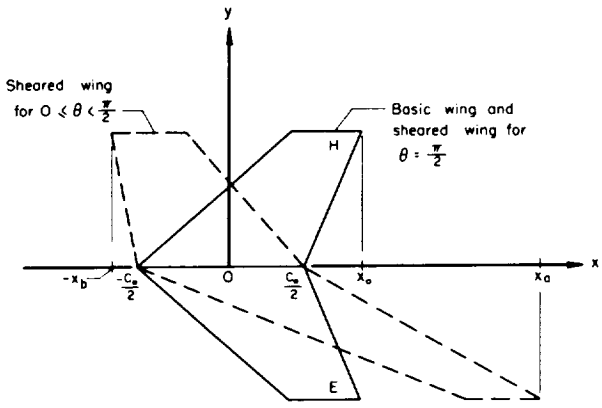

Sketch (b)

$$S_T''(x) = S_E''(x)+S_H''(x)$$

and the total zero-lift wave drag of the equivalent body of revolution is given by

$$D_T = -\frac{q}{2\pi}\int_{-x_b}^{x_a}\int_{-x_b}^{x_a}[S_E''(x_1)+S_H''(x_1)][S_E''(x_2)+S_H''(x_2)]\ln|x_1-x_2|dx_1dx_2 \tag{29}$$

Expanding the integrand of equation (29) yields

$$\begin{aligned} D_T = &-\frac{q}{2\pi}\int_{-x_b}^{x_a}\int_{-x_b}^{x_a}S_E''(x_1)S_E''(x_2)\ln|x_1-x_2|dx_1dx_2- \\ &\frac{q}{2\pi}\int_{-x_b}^{x_a}\int_{-x_b}^{x_a}S_H''(x_1)S_H''(x_2)\ln|x_1-x_2|dx_1dx_2- \\ &\frac{q}{\pi}\int_{-x_b}^{x_a}\int_{-x_b}^{x_a}S_E''(x_1)S_H''(x_2)\ln|x_1-x_2|dx_1dx_2 \end{aligned} \tag{30}$$

The first two terms of equation (30) represent the zero-lift wave drag alone of each component (wing panels E and H, respectively) of the equivalent body of revolution of the complete wing. The last term represents

the mutual zero-lift interference wave drag between the components of the equivalent body of revolution. Equations (29) and (30) indicate that the analysis is performed over the total length of the sheared configuration. Since the second derivative of the area distribution of each sheared wing panel (sketch (b)) is zero over some portion of the total length, equation (30) can obviously be written

$$D_T = -\frac{q}{2\pi}\int_{-\frac{c_o}{2}}^{x_a}\int_{-\frac{c_o}{2}}^{x_a} S_E''(x_1)S_E''(x_2)\ln|x_1-x_2|\,dx_1dx_2 -$$

$$\frac{q}{2\pi}\int_{-x_b}^{\frac{c_o}{2}}\int_{-x_b}^{\frac{c_o}{2}} S_H''(x_1)S_H''(x_2)\ln|x_1-x_2|\,dx_1dx_2 -$$

$$\frac{q}{\pi}\int_{-x_b}^{\frac{c_o}{2}}\int_{-\frac{c_o}{2}}^{x_a} S_E''(x_1)S_H''(x_2)\ln|x_1-x_2|\,dx_1dx_2 \qquad (31)$$

Equation (31) indicates that the analysis is performed over the individual lengths of each component of the sheared configuration. The analytical solutions of equations (30) and (31) yield identical results; however, as will be subsequently demonstrated, the approximate solutions of these two equations may differ.

For convenience, the first term of equations (30) and (31) will be designated as D_{EE}, the second term as D_{HH}, and the last term as D_{EH}. In the notation of the finite series form developed above, the approximate expressions for D_{EE}, D_{HH}, and D_{EH} are, for an analysis performed over the individual length of each equivalent-body component (eq. (31))

$$D_{EE} \approx \frac{q}{2\pi}\sum_{i=2}^{I_E}\sum_{j=1}^{i-1}\Delta S_E''(x_{E_i})\Delta S_E''(x_{E_j})I_1(x_{E_i},x_{E_j}) \qquad (32)$$

$$D_{HH} \approx \frac{q}{2\pi}\sum_{i=2}^{I_H}\sum_{j=1}^{i-1}\Delta S_H''(x_{H_i})\Delta S_H''(x_{H_j})I_1(x_{H_i},x_{H_j}) \qquad (33)$$

$$D_{EH} \approx \frac{q}{2\pi}\sum_{i=1}^{I_E}\sum_{j=1}^{I_H}\Delta S_E''(x_{E_i})\Delta S_H''(x_{H_j})I_1(x_{E_i},x_{H_j}) \qquad (34)$$

For an analysis performed over the total length of the equivalent body of revolution, equations (32) to (34) are applicable when the subscript

of the upper limit of summation is dropped and I represents the number of points used to divide the total length into equal intervals. Finally, the total zero-lift wave drag of the given configuration is, in accordance with equation (1),

$$D_T(\beta) = \frac{1}{2\pi}\int_0^{2\pi} D_{EE}(\beta,\theta)d\theta + \frac{1}{2\pi}\int_0^{2\pi} D_{HH}(\beta,\theta)d\theta + \frac{1}{2\pi}\int_0^{2\pi} D_{EH}(\beta,\theta)d\theta \tag{35}$$

Extending this procedure to configurations with more than two components the total zero-lift wave drag can obviously be calculated as the sum of the zero-lift wave drag of each component alone plus the mutual zero-lift interference wave drag between all possible pairs of components. On the other hand, if each equivalent body of revolution is treated as a single entity and its total zero-lift wave drag is calculated by equation (29), the total zero-lift wave drag of the given configuration is written in the form of equation (1) as

$$D_T(\beta) = \frac{1}{2\pi}\int_0^{2\pi} D_T(\beta,\theta)d\theta \tag{36}$$

Generally speaking, for a given β, the averaging process of equations (35) and (36) is performed graphically because the area distributions of the components of the equivalent bodies of revolution change with θ. The term "averaging process" implies integration with respect to θ and division of this result by 2π. In the special case of systems of slender bodies of revolution, whose individual-component area distributions do not change with θ, it is expedient to calculate the total zero-lift wave drag by equation (35) for an individual-length analysis. For this case the zero-lift wave drag of each component alone is calculated directly without recourse to averaging since the area distributions of all equivalent bodies of revolution for each component alone are identical. The interference wave drag between pairs of bodies, on the other hand, must be averaged, as the total area distributions of the equivalent bodies of revolution for pairs of components do change with θ. As a result of the present method for calculating zero-lift wave drag, it is possible, in this special case, to perform the averaging process analytically in closed form.

Interference between a pair of bodies of revolution, $S'(-l_1)=S'(l)=0$.- Consider the general arrangement of a pair of bodies of revolution, E and H, whose centers are longitudinally separated by a distance δ and whose axes are laterally separated by a distance d as shown in figure 2. Let each of the bodies satisfy the condition of equation (4), and let each body be sufficiently slender that the frontal projection of the area distribution formed from each body by the oblique planes can be considered to be the same as the normal cross-sectional area distribution of each

body (i.e., independent of β). The zero-lift interference wave drag between bodies E and H is given by the last term of equation (35). Preparatory to developing this term in finite series form, consider the area distribution of the equivalent bodies of revolution for the configuration of figure 2.

The area distribution (and all derivatives thereof) of each equivalent body of revolution of the configuration shown in figure 2 can be found in terms of sheared configurations in a manner similar to that employed in reference 7; that is, the area distribution of each equivalent body of revolution can be determined as the normal cross-sectional area distribution of a properly sheared configuration. For a specified β and θ, consider the trace in the xy plane of the oblique plane which passes through the center of body H (see fig. 2). Using the coordinate system of body E, the area distribution of the equivalent body of revolution at x_{E_1} would consist of the frontal projection of the area of body E at x_{E_1} plus the frontal projection of the area of body H at $x_H = 0$. Within the slenderness requirements of the theory, this projected area is the same as the normal cross-sectional area of a configuration consisting of body E and of body H shown by the dashed lines in figure 2. In other words, body H is sheared a distance $|\beta d \cos \theta|$ rearward for $0 \leq \theta < \pi/2$ and forward for $\pi/2 < \theta \leq \pi$. The total area distribution of the equivalent body of revolution consists of the sum of the normal cross-sectional area distribution of body E plus that of body H properly translated. Since the effect of θ on the area distribution of the equivalent bodies of revolution is merely the translation or shearing of one of the original bodies, the second derivative of the area distribution of body H can be determined relative to the coordinate system of body H and related to the coordinate system of body E by the transformation (see fig. 2)

$$x_{H(E)} = x_H + \delta + \beta d \cos \theta \tag{37}$$

When equations (34) and (37) are combined, the last term of equation (35) becomes

$$D_{EH}(\beta d) \approx \frac{q}{2\pi} \left\{ \frac{1}{2\pi} \int_0^{2\pi} \sum_{i=1}^{I_E} \sum_{j=1}^{I_H} \Delta S_E''(x_{E_i}) \Delta S_H''(x_{H_j}) I_1[x_{E_i}, x_{H(E)_j}] d\theta \right\} \tag{38}$$

where from equations (17) and (37)

$$\begin{aligned} I_1(x_{E_j}, x_{H(E)_j}) &= I_1[x_{E_i}, x_{H(E)_j}, \beta d, \theta] \\ &= (x_{E_i} - x_{H_j} - \delta - \beta d \cos \theta)^2 \ln \left| x_{E_i} - x_{H_j} - \delta - \beta d \cos \theta \right| \end{aligned} \tag{39}$$

To simplify the notation, equation (39) is written

$$I_2(a_{ij},\beta d,\theta) = (a_{ij}-\beta d \cos\theta)^2 \ln|a_{ij}-\beta d \cos\theta| \tag{40}$$

where

$$a_{ij} = |x_{E_i}-(x_{H_j}+\delta)| \tag{41}$$

For both bodies $\Delta S''(x)$ is independent of θ and it can be determined with the aid of figure 2 that the sheared configurations are symmetrical for $0 \leq \theta \leq \pi$ and $\pi \leq \theta \leq 2\pi$; therefore equation (38) can be written

$$D_{EH}(\beta d) \approx \frac{q}{2\pi} \sum_{i=1}^{I_E} \sum_{j=1}^{I_H} \Delta S_E''(x_{E_i}) \Delta S_H''(x_{H_j}) I(a_{ij},\beta d) \tag{42}$$

where

$$I(a_{ij},\beta d) = \frac{1}{\pi} \int_0^{\pi} I_2(a_{ij},\beta d,\theta) d\theta \tag{43}$$

A detailed evaluation of equation (43) is given in closed form in appendix B in terms of the dimensionless coordinates described in appendix A.

Equation (42) is also applicable to nonlifting slender bodies of revolution whose equivalent-body area distributions are not considered identical to the normal cross-sectional area distribution of the body, but are dependent upon β. For these cases $I(a_{ij},\beta d)$ of equation (42) is unchanged but $\Delta S''(x)$ must be replaced by $\Delta S''(x,\beta)$ where $\Delta S''(x,\beta)$ is obtained for each body from the second derivative of the frontal projection of the area distribution formed from each body by the oblique planes.

The importance of equation (42) is that for each βd it yields the zero-lift interference wave drag between a pair of bodies of revolution from a single set of calculations by an electronic computing machine (punch cards). Thus, with tabulated values of equation (43), a single set of calculations evaluates each term of equation (35). On the other hand, to evaluate equation (36) a separate set of calculations for each value of θ and an integration are required. Consequently, it is immediately apparent that the total zero-lift wave drag of a system of slender bodies of revolutions can he calculated more rapidly and more accurately if the system is subdivided into components and an individual-length analysis is used.

Equation (42) is valid for all β, d, and δ greater than or equal to zero. Several interesting results are indicated by equation (42) when combinations of these variables are zero. If β and/or d equals zero the averaging process is automatically eliminated (see eqs. (40) and (43)). In this case equation (42) yields the same result as equation (34). In

particular, if $\beta d = 0$ by virtue of the fact that $d = 0$ the body axes are coincident and for this condition equation (42) is applicable to each pair of components of the equivalent bodies of revolution of airplane-type configurations. For the very special case of two identical bodies of revolution arranged so that $d = \delta = 0$, the result of equation (42), for any $\beta \geq 0$, is exactly twice that of equation (27); that is, the zero-lift interference wave drag, at any supersonic Mach number, between a pair of identical bodies of revolution whose axes are superimposed is twice the zero-lift wave drag of either body alone. A bar over the subscripts denote pairs of bodies of revolution which satisfy these conditions; thus

$$D_{\overline{EH}}(\beta) = 2D_{\overline{EE}}(\beta) = 2D_{\overline{HH}}(\beta) \tag{44}$$

Equation (44) is also valid for a pair of identical bodies of revolution which satisfy the conditions $\beta = \delta = 0$ and $d \neq 0$, and for the equivalent bodies of revolution of a complete wing for $\beta \geq 0$ and $\theta = \pi/2$ (see sketch (b)). The latter result is immediately obvious from equation (31), since, for $\theta = \pi/2$, $S_E''(x) = S_H''(x)$, $-x_b = -c_o/2$, and $x_a = x_o$.

Interference between a pair of bodies of revolution, $S'(-l_1) = 0$, $S'(l) \neq 0$.- It may seem logical that the same procedure employed above for a pair of bodies of revolution with $S'(-l_1)=S'(l)=0$ can be used to develop a zero-lift interference wave-drag equation for a pair of bodies of revolution with $S'(-l_1) = 0$ and $S'(l) \neq 0$ merely by using equation (37) to evaluate $J(x_j)$ of equation (24) in analytical form for all $0 \leq \theta \leq \pi$. Unfortunately, this is not the case. It will be recalled that equation (24) was developed from slender-body theory for an isolated body of revolution. However, a zero-lift interference wave-drag equation for bodies of revolution with these end conditions can be developed by using equation (37) and the proper limits of integration for each body in equation (7). Following the same analysis as that used for equation (7), an equation similar to equation (15) will evolve. The new expressions for K_1, K_2, and K_3 will be a function of l_E, l_H, x_i, x_j, βd, δ, and $\cos\theta$. The last term will be identical to the unaveraged expression of equation (38). Each term of the new equation can be averaged analytically in closed form. The averaged expression for the last term of the new equation will, of course, be given by equation (42). It is to be emphasized that for bodies of revolution with $S'(-l_1) = 0$ and $S'(l) \neq 0$ it is mandatory to use the second derivative of the frontal projection of the area distribution formed from each body by the oblique planes.

Procedure for Applying the Method

Zero-lift wave drag.- Application of the equations developed above depends upon the geometry of the configuration being considered. The equations of this report to be used to calculate the zero-lift wave drag

of each component of an equivalent body of revolution and the zero-lift interference wave drag between pairs of components of an equivalent body are summarized in table I for several configurations together with the averaging process generally required to obtain the zero-lift wave drag of the given configuration.

As a result of the basic approximation of $S''(x)$ each of the equations listed in table I is easily adapted to electronic-machine computing techniques, in particular, to punch-card computing machines. Values of $I_1(x_i,x_j)$ of equation (28) and of $I_2(x_{E_i},x_{H_j})$ of equation (34) can be obtained from values of $I(a_{ij},\beta d)$ of equation (42) for $\beta d = 0$. Hence, if the present method is to be adopted, cards for the values of $I(a_{ij},\beta d)$ can be punched for many values of the arguments and permanently stored for reuse with values of $\Delta S''(x)$ of a particular configuration to be analyzed. This accomplished, the problem of the application of the present method resolves itself into the question of how the values of $\Delta S''(x)$ at the points which divide $S''(x)$ into equal intervals are to be recorded on punch cards. Generally it will not be possible, or even feasible, to calculate $\Delta S''(x)$ at each of these points. Therefore, the procedure employed is to record the values of $S''(x)$ on a set of punch cards with the aid of an electronic machine called a telereader; that is, one can determine $S''(x)$ at the desired points from a plot of $S''(x)$ vs. x. Then, as noted earlier,

$$\Delta S''(x_i) = S''(x_i)-S''(x_{i-1})$$

This procedure has been found to yield numerical solutions of the zero-lift wave-drag equations in very good agreement with analytical solutions of equation (3) for configurations with no singular points in $S''(x)$. When singularities occur in $S''(x)$, the telereader yields values of $S''(x)$ in the region of the singular points which are subject to errors. These errors have been found to have a predominant influence on the calculated wave-drag results when singularities occur at the ends of the distribution. When singular points in $S''(x)$ occur in the inboard region of the distribution these errors have been found to have only a small effect on the accuracy of the calculations. In order to circumvent the detrimental effect of singularities at the ends of $S''(x)$, it was reasoned that, since $S''(x)$ was approximated by constant values over equal intervals, $S'(x)$ is linearly approximated over these intervals and could be determined by the telereader from plots of a continuous variation of $S'(x)$ vs. x. Then it becomes a simple matter to define a mean value of the second derivative of the area distribution as

$$S_m''(x) = \frac{S'(x_{i+1})-S'(x_i)}{x_{i+1}-x_i} \quad \text{for} \quad x_i \leq x \leq x_{i+1} \tag{45}$$

from which $\Delta S_m''(x)$ is easily obtained. The results of many calculations, not presented here in the interest of brevity, demonstrate that the use

of $S_m''(x)$ rather than $S''(x)$ yields zero-lift wave-drag results which are invariably more accurate for distributions with singularities. The use of $S_m''(x)$ rather than $S''(x)$ for distributions with no singularities reduces the accuracy of the calculations by less than one tenth of a percent. Consequently, it is recommended that $S_m''(x)$ always be used in the present method. All calculations of this report made by the present method have employed $S_m''(x)$.

A final point of procedure in applying the present method concerns the arbitrary choice of the number of points selected to divide the second derivative of the area distribution into equal intervals. Obviously, the number of points selected will affect the accuracy of the zero-lift wave-drag calculations in a manner similar to that which the choice of the number of terms of the infinite series affects the accuracy of the results obtained by the method of references 2 or 3. It has been found in the present analysis and in reference 3 that 201 points (200 equal intervals) is a practical limit for which punch-card computing machines should be programed. The results of many calculations indicate that in some special cases as few as 101 points, or even less, yield zero-lift wave-drag results with acceptable accuracy. However, the most accurate results have been found to be consistently obtained with 201 points. Consequently, all calculations used to evaluate the present method have employed 201 points. The results of a special detailed analysis of the effect of the choice of the number and the location of equally spaced points on the zero-lift wave drag of one configuration are presented in the next section of this report.

The development of the present method for calculating zero-lift wave drag and the outline of the procedure for applying the method have merely presumed that the second derivative of the area distribution ($S''(x)$ or $S_m''(x)$) is available for all components of all equivalent bodies of revolution of a configuration. The actual determination of these distributions is probably the greatest task required in order to perform zero-lift wave-drag calculations by the present method. An analytical procedure for computing $S(x)$ for wings and tail surfaces is available in reference 7 and has been expanded in reference 8 for wings (with arbitrary thickness distributions) in the presence of bodies. A method for finding $S(x)$ and $S'(x)$ (from which $S_m''(x)$ is obtained) is given in reference 4 for bodies of revolution and wing and tail-surface components of equivalent bodies. Because the area distribution of wing and tail-surface components of equivalent bodies of revolution changes with β and θ, and because the airfoil-section thickness distribution is not generally available in analytical form, the graphical method of reference 4 can become tedious. The need for a more simplified method for finding $S(x)$, $S'(x)$, and even $S''(x)$ for wings and tail surfaces, obviously, exists. To satisfy this need a simplified method has been developed for the analytical calculation of $S(x)$, $S'(x)$, and $S''(x)$. The formulation of analytical expressions for these distributions obviously depends upon an analytical expression for the plan-form thickness distribution. Analytical approximations of the airfoil-section thickness distribution as well as the complete

plan-form thickness distribution are given in appendix C. The analytical expressions are given in terms of a single parameter which identifies each of the sheared configuration plan forms described in references 7 and 8. This single parameter combines the dependence of the sheared plan forms upon both β and θ. The analytical method for calculating $S(x)$, $S'(x)$, and $S''(x)$ is presented in appendix D.

Wave drag.- The general form of equation (15) can be employed to calculate the linear-theory wave drag for planar and nonplanar lifting configurations when, in addition to the second derivative of the area distribution, the force term of equation (2) is known. When the force term is also known the second derivative of the area distribution of each equivalent body of revolution is represented by the combined term

$$S''(x,\beta,\theta) - \frac{\beta}{2q} L'(x,\beta,\theta)$$

and for a specified β and θ equation (2) has the same form as equation (3). Hence in equation (15) one merely replaces $\Delta S''(x)$ by

$$\Delta\left[S''(x) - \frac{\beta}{2q} L'(x)\right]$$

If it is desirable to separate the effects of thickness and lift on the wave drag, equation (2) can be expanded by multiplying out the integrand. This manipulation yields three terms for the wave drag of each equivalent body. Two of the terms, identical or similar in form to equation (3), represent the separate contributions to the wave drag of thickness and lift and can be evaluated using the form of equation (15). The third term, similar in form to the last term of equations (30) and (31), represents the interference wave drag between thickness and lift and can be evaluated using the form of equation (42) with values of $I(a_{ij},\beta d)$ for $\beta d = 0$. In general, $L'(x,\beta,\theta)$ is difficult to obtain; however, a review of the literature revealed that reference 9 provides a systematic method for computing wing pressure distributions for wings with subsonic leading edges and supersonic trailing edges. From this information it is possible to obtain $L(x,\beta,\theta)$ and $L'(x,\beta,\theta)$. A procedure for finding these quantities in terms of the lift distribution of sheared wings is briefly outlined in appendix E for wings with zero taper ratio.

Vortex drag.- The general form of equation (15) can also be used to calculate the vortex drag of a finite-span wing. The familiar form of the equation for the vortex drag is

$$D_V = -\frac{\rho}{4\pi}\int_{-\frac{b}{2}}^{\frac{b}{2}}\int_{-\frac{b}{2}}^{\frac{b}{2}} \Gamma'(y_1)\Gamma'(y_2)\ln|y_1-y_2|\,dy_1 dy_2 \qquad (46)$$

where ρ is the free-stream density and $\Gamma'(y)$ is the slope of the spanwise circulation distribution. Equation (46) is identical in form to equation (7). By means of the same approximation of $\Gamma'(y)$ as was used for $S''(x)$, the vortex drag can be calculated by equation (15) with q, $\Delta S''(x)$, x, and l replaced by $\rho/2$, $\Delta\Gamma'(y)$, y, and $b/2$, respectively.

EVALUATION OF THE METHOD

The method will be evaluated by calculating the zero-lift wave drag of several bodies of revolution and comparing the results with those obtained by analytical solutions (when available) and by the method of reference 3. The calculations are restricted to Mach number 1 in order to avoid the integration required of the method of reference 3 at Mach numbers greater than 1. Subsequently, the merits of the present method for Mach numbers greater than 1 will be briefly examined. The two basic arrangements of the bodies considered in the evaluation are presented in figure 3. As shown in figures 3(a) and 3(b) the body centers are separated longitudinally a distance $\delta = 0$ ($\tilde{\delta} = 0$) and $\delta = 2l$ ($\tilde{\delta} = 2$), respectively. For these arrangements the wave-drag analysis is performed over the total lengths $2l$ and $4l$, respectively. For the arrangement of bodies with $\delta = 0$ the wave-drag analysis is also performed over the alternate length $4l$ as indicated in figure 3(c). Equations defining the dimensionless area distribution of the bodies used in these arrangements are given below:

Body	Equation of area distribution	
1	$\tilde{S}_1(\xi) = \frac{4}{3}(1-\xi^2)^{3/2}$	(47)
2	$\tilde{S}_2(\xi) = \frac{8}{5}(1-\xi^2)^{5/2}$	(48)
3	$\tilde{S}_3(\xi) = \frac{64}{35}(1-\xi^2)^{7/2}$	(49)
4	$\tilde{S}_4(\xi) = \frac{128}{63}(1-\xi^2)^{9/2}$	(50)
5	$\tilde{S}_5(\xi) = \frac{4}{3}\xi(1-\xi^2)^{3/2}$	(51)
6	$\tilde{S}_6(\xi) = \frac{8}{5}\xi(1-\xi^2)^{5/2}$	(52)
7	$\tilde{S}_7(\xi) = \frac{64}{35}\xi(1-\xi^2)^{7/2}$	(53)
8	$\tilde{S}_8(\xi) = \frac{128}{63}\xi(1-\xi^2)^{9/2}$	(54)

For each body $-1 \leq \xi \leq 1$. Equations (47) to (50) are even functions with the coefficients so chosen that the dimensionless value of the volume of each body is $\pi/2$. Equations (51) to (54) are odd functions corresponding

to bodies 1 to 4, respectively, and the volume of each of the bodies 5 to 8 is obviously zero. It should be noted that bodies 1 and 5 have singularities in $\tilde{S}''(\xi)$ at both ends (i.e., at $\xi = -1$ and $\xi = 1$).

Comparisons will be made of the total zero-lift wave drag for several pairs of bodies, the separate contribution of each body alone to the total, and the separate contribution of the interference between bodies. The interference drag results will be considered first, since, as discussed in the METHOD section and amplified in the following paragraphs, these results provide information from which calculations can be made of both the total wave drag of a pair of bodies and the contribution of each body to the total. Before presenting the results of the calculations it is desirable to mention the specific computing procedures employed for the bodies considered herein. These specific computing procedures were employed in order to obtain consistently the most accurate results by each method.

Only the zero-lift interference wave drag was calculated by an electronic computing machine for both the present method and the method of reference 3. Values of $\tilde{S}(\xi)$ and $\tilde{S}_m''(\xi)$ were calculated at each of the 201 points from equations (47) to (54). The existing machine-computing program at Ames Research Center for the method of reference 3 yields directly, for a given value of $\beta \cos \theta$ and up to 49 terms, only the total zero-lift wave-drag results based on an analysis performed over the total length of a configuration. However, interference drag results were obtained by a special manipulation of the data obtained from the existing program. This manipulation is described in appendix F which presents the computing procedure used in this report for the method of reference 3.

Four significant figures were retained for all machine-computed calculations of the interference drag results for both methods. For the configurations of figure 3(b) with singularities in $\tilde{S}''(\xi)$ at the ends of at least one body, only two significant figures were possible in the case of the present method. This loss of significant figures is a direct result of the large values of $\tilde{S}_m''(\xi)$ at and near the ends of the body.

The total zero-lift wave drag of a pair of bodies of revolution is given by the sum of the contribution to the total of each body alone and the interference between bodies (see eq. (35)). The body-alone contribution can be determined from the interference results in accordance with equation (44). Hence, by combining equations (35) and (44) the following equations can be written for the dimensionless total zero-lift wave drag:

$$\tilde{D}_T = \frac{1}{2} \tilde{D}_{\overline{EE}}(a) + \frac{1}{2} \tilde{D}_{\overline{HH}}(a) + \tilde{D}_{EH}(a) \tag{55}$$

for the configurations of figure 3(a),

$$\tilde{D}_T = \frac{1}{2}\tilde{D}_{\overline{EE}}(c) + \frac{1}{2}\tilde{D}_{\overline{HH}}(c) + \tilde{D}_{EH}(b) \tag{56}$$

for a total-length analysis of the bodies in figure 3(b), and

$$\tilde{D}_T = \frac{1}{2}\tilde{D}_{\overline{EE}}(a) + \frac{1}{2}\tilde{D}_{\overline{HH}}(a) + \tilde{D}_{EH}(b) \tag{57}$$

for an individual-length analysis of the bodies in figure 3(b). In equations (55) to (57) the terms in parentheses designate that part of figure 3 which indicates the configuration length over which the wave-drag analysis is performed.

Accuracy of Calculations for Interference

The dimensionless zero-lift interference wave drag for the bodies in the arrangements of figure 3 is presented in table II. Rough sketches of figures 3(a), 3(b), and 3(c) are duplicated in the column headings to indicate the arrangement of the bodies and the length over which the wave-drag analysis is performed. In column 1 of table II are tabulated all possible combinations of pairs of bodies whose area distributions are defined by equations (47) to (54). Note that the bodies with singularities in $S''(\xi)$ at the ends are marked with an asterisk. Columns 2 and 3 of table II list the analytical values of the wave drag. For $\tilde{\delta} = 2$ the analytical solution of the last term of equation (31) for nonidentical bodies has not, as yet, been obtained; therefore, analytical solutions for only identical pairs of bodies are presented in column 3. However, it is felt that the pairs of identical bodies with $\tilde{\delta} = 2$ are sufficient to evaluate the accuracy of the present method for calculating zero-lift wave drag.

Bodies with $\tilde{\delta} = 0$.- For all pairs of bodies in the arrangement of figure 3(a) for which data are available both methods yield zero-lift interference wave-drag solutions which are accurate to within a fraction of 1 percent of the analytical solutions (compare columns 2, 4, and 7 of table II). For configurations with no singularities or discontinuities in $\tilde{S}''(\xi)$ the method of reference 3 yields exactly the analytical solutions. The data of columns 5 and 8 of table II are included merely as data from which the body-alone contribution to the total zero-lift wave drag can be obtained for configurations of figure 3(b) which are analyzed over the total length of the configurations. It will be noted that analytical solutions for configurations of figures 3(a) and 3(c) are identical (see column 2 of table II); whereas, the numerical solutions by both methods are less accurate for the configurations of figure 3(c).

Bodies with $\tilde{\delta} = 2$.- For all pairs of bodies in the arrangement of figure 3(b) for which data are available both methods yield zero-lift

interference wave-drag solutions which are accurate to within a fraction of 1 percent of the analytical solutions for pairs of bodies with no singularities or discontinuities in $\tilde{S}''(\xi)$ (compare columns 3, 6, and 9 of table II). For pairs of bodies, at least one of which has singularities in $\tilde{S}''(\xi)$ at the ends, the method of reference 3 and the present method yield zero-lift interference wave-drag solutions which are accurate to within -8 and +14 percent of the analytical solutions, respectively. However, these figures are percentages of small values of the interference. Furthermore, it should be recalled that with the use of the existing machine-computing program the results for these bodies by the present method are based on only two significant figures. Bodies 1 and 5, for which calculations by the present method are in greatest error, are bodies with singularities at the ends which have minimum zero-lift wave drag at transonic speeds for a given volume and length and a given first moment of area, respectively. For these reasons an evaluation of the accuracy of the zero-lift wave-drag results computed by the present method for these bodies should constitute the most severe test of the method.

Accuracy of Calculations for Body Alone

In view of the simple relationship given by equation (44) between the zero-lift wave drag for a body alone and the interference between a pair of identical bodies with $\delta = 0$, body-alone results have not been tabulated. It is obvious, however, that both methods yield numerical solutions for the body-alone zero-lift wave drag which are accurate to within a fraction of 1 percent of the analytical solutions.

Accuracy of Calculations for Total Configurations

The dimensionless total zero-lift wave-drag results for only pairs of identical bodies in both basic arrangements of figure 3 have been calculated using the data of table II in equations (55) to (57) and are presented in table III. These pairs of bodies are considered sufficient to evaluate the accuracy of total zero-lift wave-drag calculations by the present method in that these bodies represent the extreme deviations from the analytical solutions and are generally typical of all the pairs of bodies in their demonstration of the effect of the different lengths used in the analysis. The data in parentheses in table III indicate the percent deviation from the analytical solutions.

Bodies with $\tilde{\delta} = 0$.- Since the total zero-lift wave drag for these bodies was obtained from the zero-lift interference wave drag of these bodies, it is clear that the accuracy of the total wave-drag results for these bodies is consistent with that of the interference wave-drag results; that is, for all pairs of bodies in table III both methods yield total

zero-lift wave-drag solutions which are accurate to within a fraction of 1 percent of the analytical solutions (compare columns 2, 4, and 5 of table III). For configurations with no singularities or discontinuities in $\tilde{S}''(\xi)$ at the ends, the method of reference 3 yields exactly the analytical solutions.

Bodies with $\tilde{\delta} = 2$.- Total zero-lift wave drag for these bodies can be calculated from an individual- or a total-length analysis. As noted in the METHOD section and demonstrated in column 3 of table III, the configuration length used in the analysis does not influence the analytical solutions. The length does, however, affect the numerical solutions. The effect is small for the simple bodies of revolution of this report, even for bodies with singularities at the ends of $S''(\xi)$ (see table III). Preliminary calculations for a more general airplane-type configuration indicate, however, that the influence of the length may not be small for such configurations in that $S''(\xi)$ of the sheared wings of many equivalent bodies is discontinuous. Therefore, the authors feel that some discussion of the length is warranted for the present configurations even though, in this case, the effect is small.

For pairs of bodies with no singularities or discontinuities in $\tilde{S}''(\xi)$ both methods yield results which are accurate to within one third of 1 percent of the analytical solutions regardless of the length of analysis (compare columns 3, 7, and 9 for the present method and columns 3, 6, and 8 for the method of ref. 3). Even though the deviations from the analytical solutions are very small for each length of analysis, a definite trend toward more accurate solutions for the individual-length analysis is evidenced by the results for these bodies. For pairs of bodies with singularities in $\tilde{S}''(\xi)$ at the ends (bodies 1x1 and 5x5) both methods yield results which are accurate to within ±3 percent of the analytical solutions. The same trend toward more accurate solutions for the individual-length analysis is evidenced by the results for these latter bodies for the method of reference 3 but not, however, for the present method. In spite of these seemingly anomalous results for the present method, and even though the effect of length of analysis is small, the data of table III indicate that both methods yield comparable total zero-lift wave-drag solutions which are in closer agreement with analytical solutions when the wave-drag analysis is performed over the individual lengths of the bodies.

Bodies with $0 < \tilde{\delta} < 2$ and $\tilde{\delta} > 2$.- The total zero-lift wave-drag calculations at Mach number 1 (or at any supersonic Mach number) for pairs of bodies arranged with these values of $\tilde{\delta}$ will be more accurate than those discussed above for $\tilde{\delta} = 2$ if the wave-drag analysis is always based on an individual-length analysis. The body-alone contribution to the total zero-lift wave drag is, of course, independent of $\tilde{\delta}$; but both the accuracy and magnitude of the interference contribution are affected by $\tilde{\delta}$. As $\tilde{\delta}$ becomes less than 2, the interference calculations become more accurate as a result of a larger number of points of the 201-point

analysis lying on each body. As the value of $\tilde{\delta}$ increases beyond 2, the interference calculations are subject to greater inaccuracies, yet the magnitude of this portion of the wave drag diminishes to an almost negligibly small percentage of the total zero-lift wave drag.

Accuracy of Calculations at Mach Numbers Greater Than 1 for Total Configurations

A complete evaluation of the present method as a tool for calculating total zero-lift wave drag (eq. (35)) should include an evaluation of the accuracy of the method at Mach numbers greater than 1 for the configurations of this report as well as the more general airplane-type configurations. No quantitative evaluation of this aspect of the accuracy will be made; however, from the information available in this and the previous section of this report it is possible to make a qualitative evaluation.

Pairs of bodies of revolution.- The area distribution of each body does not change with θ; therefore, the zero-lift wave drag of each body alone is obtained, with comparable accuracy, from a single set of calculations by each method. The area distribution of the combined bodies of each equivalent body of revolution does change with θ. For the method of reference 3 the zero-lift interference wave drag between bodies must be computed for several values of θ and the results averaged as discussed relative to equations (35) and (36); whereas, for the present method the zero-lift interference wave drag is obtained from a single set of calculations, analytically averaged for all θ. As a result of the averaging process required of the method of reference 3, it can be stated that the present method yields the more direct and probably the more accurate total zero-lift wave-drag results for systems of bodies of revolution.

Airplane-type configurations.- The area distribution of the various components of airplane-type configurations changes with θ. Hence, for these configurations both methods, in general, yield total zero-lift wave-drag results with a comparable accuracy. If a particular configuration contains several body-of-revolution components such as the airplane-type configuration shown in table I, the present method will probably yield more accurate results for the reasons mentioned above concerning the zero-lift interference wave drag between bodies of revolution.

Computational Time Required

An evaluation of the computational time required by the present method is equally as important to the complete evaluation of the method as is an evaluation of the accuracy of the method. Just as the most

accurate zero-lift wave-drag values obtainable by the present method and the method of reference 3 were used to effect an equitable evaluation of the relative accuracy of the methods, so it is desired to evaluate the relative computational time for both methods on the basis of equitable electronic-computing machine techniques. Accordingly, this evaluation will be based upon the following assumptions:

i. The zero-lift wave-drag equations for an equivalent body of revolution for both methods are programed in such a manner to permit calculations of the total zero-lift wave drag of multiple-component configurations from separate calculations of the zero-lift wave drag of each component alone plus the zero-lift interference wave drag between components.

ii. The initial data for each method are obtained by a telereader from a plot of $\tilde{S}(\xi)$ or $\tilde{S}'(\xi)$ vs. ξ, as the case may be. It should be recalled that values of $\tilde{S}_m''(\xi)$ are calculated from values of $\tilde{S}'(\xi)$ according to equation (53), and this operation is assumed to be included in the program.

iii. $\tilde{S}(\xi)$ and $\tilde{S}'(\xi)$ are obtained for wings and tail surfaces by an analytical method similar to that presented in appendix D.

The present method and the method of reference 3 require the same computing time to calculate the total zero-lift wave drag of any configuration at Mach number 1. If plots of the distributions are available, calculations for one equivalent body of revolution require up to 1-1/2 hours from the beginning of the telereader operation to the final answer. For configurations with components whose equivalent body area distributions change with θ, both methods require the same computational time because the time required to calculate the total zero-lift wave drag of each equivalent body is identical and the averaging process can be performed similarly for both methods. For configurations consisting entirely of body-of-revolution components, both methods require the same time to calculate the zero-lift wave drag of each body alone. The present method, however, affords a saving in time required to calculate the zero-lift interference wave drag between pairs of bodies because the averaging process cannot be performed similarly for both methods. The present method inherently averages the interference contribution of all pairs of equivalent bodies with a single set of calculations; whereas, by the method of reference 3, the averaging process must be performed for the results of a finite number of pairs of equivalent bodies of revolution. Consequently, the saving in time is directly proportional to the number of pairs of equivalent bodies (or values of θ) necessary to define the integrand of the last term of equation (35). For example, for two bodies of revolution (the minimum required for interference) a minimum of five equivalent bodies is required. Hence, zero-lift interference wave-drag calculations by the present method would only require 20 percent of the computing time required of the method of reference 3, and the total

zero-lift wave-drag calculations would require 60 percent of the computing time required of the method of reference 3. If more than five equivalent bodies were required, the saving in computing time would be even greater, as would be the case for a system of more than two bodies of revolution.

Ultimate Capabilities of the Present Method

The analyses presented in this report have developed a numerical method for calculating zero-lift wave drag which employs a knowledge of the second derivative of the area distribution of a configuration and which is easily adaptable to electronic-machine computing equipment. The ultimate desire, however, is the development of a method for computing zero-lift wave drag by ordinary desk computing techniques. As a result of a detailed analysis of the effect of the choice of the number and the location of the points used to divide $\tilde{S}_m''(\xi)$ into equal intervals, such a method appears possible for components of a configuration. Presented in figure 4 are the results of this detailed analysis for a single body of revolution whose area distribution is composed of three parabolic arcs. The dimensionless zero-lift wave drag tabulated in figure 4 demonstrates that as few as 25 points yield a solution accurate to within 1.75 percent of the analytical solution. This suggests that by a judicious choice of intervals (not necessarily equal) a fewer number of points may be considered which will yield numerical solutions in almost exact agreement with analytical solutions and thereby make desk calculations feasible. Preliminary calculations indicate that zero-lift wave-drag values of any one component of a configuration which are essentially identical to the analytical values can be obtained with as few as 10 unequal intervals if the intervals are systematically determined from information concerning the source strengths which define the geometry of the component.

CONCLUDING REMARKS

A numerical method based on linearized and slender-body theories, which is easily adapted to electronic-machine computing equipment, has been developed for calculating the wave drag of single- and multiple-component configurations from a knowledge of the second derivative of the area distribution of a series of equivalent bodies of revolution. Zero-lift wave-drag results have been calculated at a Mach number of 1 for several simple analytical shapes (bodies of revolution) by the present method and by a method which employs the Tchebichef form of harmonic analysis of the configuration area distribution. The relative accuracy and computational time required of both methods to calculate zero-lift wave drag at a Mach number of 1 have been evaluated by comparing the zero-lift wave-drag solutions for these simple shapes computed by both methods with those obtained from analytical solutions of the wave-drag

equations. From these results it was possible to evaluate also the relative accuracy and computational time required of both methods to calculate the zero-lift wave drag at supersonic speeds. The following remarks are warranted as a result of these evaluations.

For the pairs of bodies considered in this report at a Mach number of 1, both methods yield numerical solutions for the zero-lift wave drag of each body alone to an accuracy of a fraction of 1 percent of the analytical solutions. Calculations by both numerical methods of the zero-lift interference wave drag between bodies were generally accurate to within a fraction of 1 percent; however, in some special cases for which the interference was small, these results were accurate to within only -8 and +14 percent of the analytical values for the harmonic analysis and the present method, respectively. Total zero-lift wave-drag solutions generally were calculated more accurately as the sum of the zero-lift wave drag of each body alone plus the interference between bodies. All total drag results for bodies with no singularities or discontinuities in the second derivative of their area distributions were accurate to within a fraction of 1 percent of the analytical solutions, and for bodies with singularities the results were accurate to within 3 percent of the analytical solutions. Both methods required the same computing time.

For total zero-lift wave-drag calculations at supersonic Mach numbers, the relative accuracy and computing time required by both methods is comparable for airplane-type configurations. For systems of bodies of revolution both methods yield similar results with comparable accuracy; however, the present method only requires up to 60 percent of the computing time required of the harmonic-analysis method for two bodies of revolution and less time for a larger number of bodies.

Ames Research Center
National Aeronautics and Space Administration
Moffett Field, Calif., Oct. 17, 1958

APPENDIX A

DIMENSIONLESS ZERO-LIFT WAVE-DRAG EQUATIONS

In order to take advantage of the decrease in the number of parameters resulting from similarity considerations and to facilitate the calculations, the quantities defined in the METHOD section will be made dimensionless. The procedures presented apply to all of the sheared or equivalent configurations previously discussed. However, in the interest of simplicity, the dependence of the quantities upon β and θ will be omitted from the notation.

To establish a general dimensionless coordinate system each coordinate is divided by a characteristic length, areas are divided by some reference area, volumes are divided by some reference volume, and so on. In this manner the relationship between dimensional and dimensionless lengths and longitudinal area distributions can be written

$$\xi = \frac{x}{k_x} \tag{A1}$$

$$\eta = \frac{y}{k_y} \tag{A2}$$

$$\zeta = \frac{z}{k_z} \tag{A3}$$

$$\tilde{S}(\xi) = \frac{l}{S_R} S(x) \qquad \text{for} \begin{Bmatrix} -l_1 \le x \le l \\ -\frac{l_1}{k_x} \le \xi \le \frac{l}{k_x} \end{Bmatrix} \tag{A4}$$

where k_x, k_y, and k_z are characteristic lengths in the x, y, and z directions, respectively, and S_R is the reference area. From a differentiation of equations (A1) and (A4) the relationship between the derivatives of the dimensional and dimensionless area distributions are found to be

$$\tilde{S}'(\xi) = \frac{k_x}{S_R} S'(x) \tag{A5}$$

$$\tilde{S}''(\xi) = \frac{k_x^2}{S_R} S''(x) \tag{A6}$$

With the aid of equations (A1) to (A6), the general relationship between the dimensional and dimensionless zero-lift wave drag can be shown to be

$$D = \left(\frac{S_R}{k_x}\right)^2 q\tilde{D} \tag{A7}$$

Values of the characteristic lengths and reference areas are tabulated below for bodies of revolution and wings or tail surfaces.

Configuration	k_x	k_y	k_z	S_R
Body of revolution	$l_1=l$	---	---	S_o
Wing or tail surface	$c_o/2$	$b_o/2$	t_o	$t_o(b_o/2)$

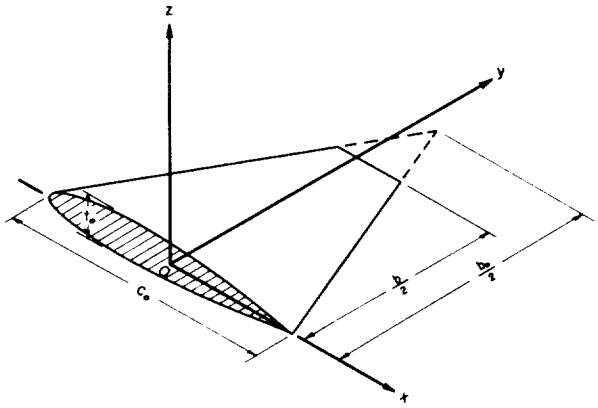

Sketch (c)

The characteristic length l or l_1 is the half-body length and S_o is the maximum frontal area of the body. The characteristic lengths for wings or tail surfaces are shown in sketch (c). By means of equations (A1) to (A6) and the above table, the dimensionless zero-lift wave-drag equations for both the present method and the method of reference 3 can be determined as discussed in the following paragraphs.

PRESENT METHOD

Single Body of Revolution, $S'(-l_1) = 0$, $S'(l) \neq 0$

The zero-lift wave drag for this kind of body is given by equation (5), from which the dimensionless form is determined to be

$$\tilde{D} = -\frac{1}{2\pi}\int_{-1}^{1}\int_{-1}^{1}\tilde{S}''(\xi_1)\tilde{S}''(\xi_2)(\ln|\xi_1-\xi_2|+\ln l)d\xi_1 d\xi_2 +$$

$$\frac{1}{\pi}\left\{\frac{[\tilde{S}'(1)]^2}{2}\left[\ln\frac{2}{\beta\tilde{R}(1)} - \ln\sqrt{S_o}\right] + \tilde{S}'(1)\int_{-1}^{1}\tilde{S}''(\xi_2)(\ln|1-\xi_2|+\ln l)d\xi_2\right\} \tag{A8}$$

In accordance with equations (7) and (8), the dimensionless expressions $\tilde{D}_1$ and $\tilde{D}_2$ are given by the first and second terms of equation (A8), respectively.

Single Body of Revolution, $S'(-l_1) = S'(l) = 0$

For this kind of body the second term of equation (A8) is identically zero and the dimensionless zero-lift wave drag is given by only the first term. This first term can be simplified, however, for bodies of revolution with $\tilde{S}'(-1) = \tilde{S}'(1) = 0$. After an integration by parts, it is a simple matter to show that the $ln\ l$ term vanishes. Hence,

$$\tilde{D}_1 = -\frac{1}{2\pi}\int_{-1}^{1}\int_{-1}^{1}\tilde{S}''(\xi_1)\tilde{S}''(\xi_2)ln|\xi_1-\xi_2|d\xi_1 d\xi_2 \qquad (A9)$$

Multiple-Component Configurations

The general relationship between the dimensional and dimensionless equations for an equivalent body of revolution of a multiple-component configuration is given by equation (A7). The total zero-lift wave drag of an equivalent body of revolution of a two-component configuration can be expressed by the unaveraged expression for equation (35). Hence, if each component is made dimensionless with respect to its own characteristic length and reference area, the relationship between the dimensional and dimensionless total zero-lift wave-drag equations is

$$D_T = \left(\frac{S_R}{k_x}\right)_E^2 q\tilde{D}_{EE} + \left(\frac{S_R}{k_x}\right)_H^2 q\tilde{D}_{HH} + \left(\frac{S_R}{k_x}\right)_E\left(\frac{S_R}{k_x}\right)_H q\tilde{D}_{EH} \qquad (A10)$$

Experience has demonstrated that in the majority of cases it is more convenient to make the complete configuration dimensionless with respect to only one of the components. In this case equation (A7) is applicable to the total configuration and values of S_R and k_x are used for only one (either) component.

In view of the foregoing, the dimensionless finite-series form of the zero-lift wave-drag equations developed in the METHOD section of this report can be obtained if $\Delta S''(x)$, x, and l are replaced by $\Delta\tilde{S}''(\xi)$, ξ, and l/k_x, respectively, and if the logarithm terms of the equations for $\tilde{D}_2$ and/or $\tilde{D}_1$ are properly evaluated. As a typical example, the dimensionless zero-lift wave-drag equation for a single body of revolution with $S'(-l_1) = S'(l) = 0$ can be written (see eq. (28))

$$\tilde{D}_1 \approx \frac{1}{2\pi} \sum_{i=2}^{I} \sum_{j=1}^{i-1} \Delta\tilde{S}''(\xi_i)\Delta\tilde{S}''(\xi_j)\tilde{I}_1(\xi_i,\xi_j) \tag{A11}$$

where, from equation (17),

$$\tilde{I}_1(\xi_i,\xi_j) = (\xi_i-\xi_j)^2 \ln|\xi_1-\xi_2| \tag{A12}$$

METHOD OF REFERENCE 3

Use of equations (A1) and (A5) in equations (F4), (F2), and (F3) yields the dimensionless zero-lift wave-drag equation for an equivalent body of revolution for the method of reference 3

$$\tilde{D} = \frac{\pi}{4} \sum_{n=1}^{\infty} n\tilde{A}_n^2 \tag{A13}$$

where

$$\tilde{A}_n = \frac{2}{\pi} \int_{-\pi}^{0} \frac{\partial\tilde{S}(\xi)}{\partial\xi} \sin(n\varphi)d\varphi \tag{A14}$$

and

$$\xi = \left(\frac{l_1+l}{2k_x}\right) \cos\varphi \tag{A15}$$

SIMILARITY CONSIDERATIONS

With the definitions of k_x, k_y, k_z, and S_R tabulated above, a general expression for the wave drag, at any supersonic Mach number, for a system of bodies of revolution is

$$D_B = \left(\frac{S_o}{l}\right)^2 q\tilde{D}_B\left(\beta\,\frac{d}{l}\right) \tag{A16}$$

where

$$\tilde{D}_B\left(\beta\,\frac{d}{l}\right) = \frac{1}{2\pi}\int_{0}^{2\pi} \tilde{D}_B\left(\beta\,\frac{d}{l},\,\theta\right) d\theta$$

and for an airplane-type configuration is

$$D_W = \left(t_o \frac{b_o}{c_o}\right)^2 q\tilde{D}_W\left(\beta \frac{b_o}{c_o}\right) \tag{A17}$$

where

$$\tilde{D}_W\left(\beta \frac{b_o}{c_o}\right) = \frac{1}{2\pi}\int_o^{2\pi} \tilde{D}_W\left(\beta \frac{b_o}{c_o}, \theta\right) d\theta$$

Dividing both sides of equations (A16) and (A17) by q and a proper reference area, one obtains the wave-drag coefficient

$$C_{D_B} = \frac{1}{S_B}\left(\frac{S_o}{l}\right)^2 \tilde{D}_B\left(\beta \frac{d}{l}\right) \tag{A18}$$

$$C_{D_W} = \frac{1}{S_W}\left(t_o \frac{b_o}{c_o}\right)^2 \tilde{D}_W\left(\beta \frac{b_o}{c_o}\right) \tag{A19}$$

For bodies of revolution $S_B = S_o = \pi/4{d_o}^2$, where d_o is the maximum diameter of the body. For airplane-type configurations $b^2/S_W = A$, the aspect ratio of the wing and $t_o/c_o = \tau_o$, the maximum thickness ratio of the airfoil section. Therefore equations (A18) and (A19) can be written

$$C_{D_B} = \pi\left(\frac{d_o}{2l}\right)^2 \tilde{D}_B\left(\beta \frac{d}{l}\right) \tag{A20}$$

$$C_{D_W} = A{\tau_o}^2\left(\frac{b_o}{b}\right)^2 \tilde{D}_W\left(\beta \frac{b_o}{c_o}\right) \tag{A21}$$

Equations (A20) and (A21) demonstrate the advantage to be gained from similarity considerations which are afforded as a result of wave-drag calculations made in a dimensionless coordinate system. From equations (A20) and (A21), it is clear that dimensionless wave-drag calculations of a single configuration, in effect, yield the wave-drag coefficients for an entire family of related configurations. The wave-drag coefficients of geometrically similar families of bodies of revolution are related by the fineness ratio of the bodies, and those for geometrically similar airplane-type configurations are related by the aspect ratio and maximum thickness ratio of the wings.

APPENDIX B

EVALUATION OF THE INTERFERENCE INTEGRAL FOR PAIRS OF BODIES OF REVOLUTION

In the METHOD section of this report the zero-lift interference wave drag between a pair of bodies with $S(-l_1) = S(l) = 0$, in the arrangement shown in figure 2, is given by equation (42). If the complete configuration is made dimensionless with respect to body E, that is, both x coordinates are divided by l_E and both area distributions are divided by S_{E_o}, equation (42) can be written (see appendix A)

$$D_{EH}(\tilde{B}) = \frac{q}{2\pi}\left(\frac{S_o}{l}\right)^2 \sum_{i=1}^{I_E} \sum_{j=1}^{I_H} \Delta\tilde{S}_E''(\xi_{E_i})\Delta\tilde{S}_H''(\xi_{H_j})\tilde{I}(\tilde{a}_{ij},\tilde{B}) \tag{B1}$$

where

$$\tilde{I}(\tilde{a}_{ij},\tilde{B}) = \frac{1}{\pi}\int_o^\pi (\tilde{a}_{ij}-\tilde{B}\cos\theta)^2 l_n|\tilde{a}_{ij}-\tilde{B}\cos\theta|d\theta \tag{B2}$$

$$\tilde{a}_{ij} = \xi_{E_i}-(\xi_{H_j}+\tilde{\delta}) \tag{B3}$$

$$\tilde{B} = \frac{\beta d}{l_E} \tag{B4}$$

This appendix will evaluate the integral function defined by equations (B2) to (B4). Using the substitution

$$\gamma = \frac{\tilde{a}_{ij}}{\tilde{B}} \tag{B5}$$

one can write equation (B2) as

$$\tilde{I}(\tilde{a}_{ij},\tilde{B}) = \tilde{B}^2\left[\frac{1}{\pi}\int_o^\pi \frac{1}{2}(\gamma-\cos\theta)^2 l_n(\gamma-\cos\theta)^2 d\theta + l_n\tilde{B}\,\frac{1}{\pi}\int_o^\pi (\gamma-\cos\theta)^2 d\theta\right] \tag{B6}$$

Let

$$K(\gamma) = \frac{1}{\pi}\int_o^\pi \frac{1}{2}(\gamma-\cos\theta)^2 l_n(\gamma-\cos\theta)^2 d\theta \tag{B7}$$

If the integrand of equation (B7) is grouped as $\ln(\gamma-\cos\theta)^2$ and $1/2(\gamma-\cos\theta)^2 d\theta$, integration by parts yields

$$K(\gamma) = \left(\gamma^2 + \frac{1}{2}\right) \ln|\gamma+1| - \left(\gamma^2 + \frac{1}{2}\right) \frac{1}{\pi}\int_0^\pi \frac{\theta \sin\theta}{\gamma-\cos\theta}\, d\theta +$$

$$2\gamma \frac{1}{\pi}\int_0^\pi \frac{\sin^2\theta}{\gamma-\cos\theta}\, d\theta - \frac{1}{2}\frac{1}{\pi}\int_0^\pi \frac{\sin^2\theta \cos\theta}{\gamma-\cos\theta}\, d\theta \qquad \text{(B8)}$$

Since

$$\frac{\sin^2\theta}{\gamma-\cos\theta} = \frac{1-\cos^2\theta}{\gamma-\cos\theta} = \gamma+\cos\theta - \frac{\gamma^2-1}{\gamma-\cos\theta}$$

and

$$\frac{\sin^2\theta \cos\theta}{\gamma-\cos\theta} = \frac{\cos\theta-\cos^3\theta}{\gamma-\cos\theta} = \cos^2\theta+\gamma\cos\theta+(\gamma^2-1) - \frac{\gamma(\gamma^2-1)}{\gamma-\cos\theta}$$

equation (B8), after the indicated integration of the simple terms is performed, can be written

$$K(\gamma) = \left(\gamma^2 + \frac{1}{2}\right) \ln|\gamma+1| + \frac{1}{2}\left(3\gamma^2 + \frac{1}{2}\right) - \left(\gamma^2 + \frac{1}{2}\right) \frac{1}{\pi}\int_0^\pi \frac{\theta \sin\theta}{\gamma-\cos\theta}\, d\theta -$$

$$\frac{3}{2}\gamma\left(\gamma^2-1\right) \frac{1}{\pi}\int_0^\pi \frac{d\theta}{\gamma-\cos\theta} \qquad \text{(B9)}$$

If the integrand of the first integral expression in equation (B9) is grouped as θ and $(\sin\theta/\gamma-\cos\theta)d\theta$, integration by parts yields

$$\frac{1}{\pi}\int_0^\pi \frac{\theta \sin\theta}{\gamma-\cos\theta}\, d\theta = \ln|\gamma+1| - \frac{1}{\pi}\int_0^\pi \ln(\gamma-\cos\theta)d\theta \qquad \text{(B10)}$$

Now

$$\frac{1}{\pi}\int_0^\pi \ln(\gamma-\cos\theta)d\theta = \ln\frac{1}{2}\left(|\gamma|+\sqrt{\gamma^2-1}\right) \quad \text{for} \quad |\gamma| \geq 1 \qquad \text{(B11)}$$

The partial derivative with respect to γ of the left-hand side of equation (B11) is zero for $|\gamma| < 1$. This demonstrates that the integral expression is independent of γ and hence has a constant value for $|\gamma| < 1$. The constant is evaluated as $\ln 2$. Therefore

$$\frac{1}{\pi}\int_0^{\pi} \frac{\theta \sin\theta}{\gamma-\cos\theta}\,d\theta = \begin{cases} \ln|\gamma+1| + \ln 2 - \ln(|\gamma|+\sqrt{\gamma^2-1}) & \text{for } |\gamma| \geq 1 \\ \ln|\gamma+1| + \ln 2 & \text{for } |\gamma| < 1 \end{cases} \tag{B12}$$

The last integral expression in equation (B9) is evaluated as follows:

$$\frac{1}{\pi}\int_0^{\pi} \frac{d\theta}{\gamma-\cos\theta} = \begin{cases} \frac{1}{\pi}\left[\frac{2}{\sqrt{\gamma^2-1}} \tan^{-1}\left(\frac{\sqrt{\gamma^2-1}\tan\frac{1}{2}\theta}{\gamma-1}\right)\right]_0^{\pi} & \text{for } |\gamma| > 1 \\ \frac{1}{\pi}\left[\frac{1}{\sqrt{1-\gamma^2}} \ln\frac{\sqrt{1-\gamma^2}\tan\frac{1}{2}\theta+(1+\gamma)}{\sqrt{1-\gamma^2}\tan\frac{1}{2}\theta-(1+\gamma)}\right]_0^{\pi} & \text{for } |\gamma| \leq 1 \end{cases}$$

Therefore

$$\frac{1}{\pi}\int_0^{\pi} \frac{d\theta}{\gamma-\cos\theta} = \begin{cases} \frac{1}{\sqrt{\gamma^2-1}} & \text{for } \gamma > 1 \\ \frac{-1}{\sqrt{\gamma^2-1}} & \text{for } \gamma < -1 \\ 0 & \text{for } |\gamma| \leq 1 \end{cases} \tag{B13}$$

From equations (B12) and (B13) equation (B9) reduces to

$$K(\gamma) = \begin{cases} \frac{1}{2}\left(3\gamma^2+\frac{1}{2}\right) - \left(\gamma^2+\frac{1}{2}\right)\ln 2 + \left(\gamma^2+\frac{1}{2}\right)\ln(|\gamma|+\sqrt{\gamma^2-1}) - \frac{3}{2}|\gamma|\sqrt{\gamma^2-1} & \text{for } |\gamma| > 1 \\ \frac{1}{2}\left(3\gamma^2+\frac{1}{2}\right) - \left(\gamma^2+\frac{1}{2}\right)\ln 2 & \text{for } |\gamma| \leq 1 \end{cases} \tag{B14}$$

The second integral of equation (B6) evaluates simply as

$$\frac{1}{\pi}\int_0^{\pi} (\gamma-\cos\theta)^2 d\theta = \gamma^2 + \frac{1}{2} \tag{B15}$$

By means of equations (B5), (B7), (B14), and (B15), equation (B6) is written

$$\tilde{I}(\tilde{a}_{ij},\tilde{B}) = \tilde{B}^2 \left\{ K\left(\frac{\tilde{a}_{ij}}{\tilde{B}}\right) + \left[\left(\frac{\tilde{a}_{ij}}{\tilde{B}}\right)^2 + \frac{1}{2}\right] \ln \tilde{B} \right\} \tag{B16}$$

where $K(\tilde{a}_{ij}/\tilde{B})$ is given by equations (B5) and (B14). Equation (B16) can be further simplified by applying the conditions for bodies of revolution with $\tilde{S}'(1) = 0$. The terms of the equation resulting from substitution of equation (B16) in equation (B1) which are constant or are proportional to $\tilde{a}_{ij}$ and $\tilde{a}_{ij}^2$ will vanish as a result of the conditions imposed for all values of $\tilde{a}_{ij}$ by equations (25) and (26) for zero area gradient at the ends of a body of revolution. Therefore, equation (B16) can be written

$$I(\tilde{a}_{ij},\tilde{B}) = \begin{cases} \left(\tilde{a}_{ij}^2 + \frac{1}{2}\tilde{B}^2\right)\left[\ln\left(|\tilde{a}_{ij}| + \sqrt{\tilde{a}_{ij}^2 - \tilde{B}^2}\right) - \ln \tilde{B}\right] - \frac{3}{2}|\tilde{a}_{ij}|\sqrt{\tilde{a}_{ij}^2 - \tilde{B}^2} & \text{for } |\tilde{a}_{ij}| > \tilde{B} \\ 0 & \text{for } |\tilde{a}_{ij}| \leq \tilde{B} \end{cases} \tag{B17}$$

From figure 2 it can be seen that $\tilde{B}$ is the dimensionless longitudinal distance defined by the intersection of the Mach wave ($\beta d \cos\theta = \beta d$ for $\theta = 0^\circ$) with the axes of both bodies. Also, $\tilde{a}_{ij}$ is the dimensionless longitudinal distance between pairs of points, one on each body, used in the double summation of equation (B1). Consequently, $\tilde{I}(\tilde{a}_{ij},\tilde{B}) = 0$ for $|\tilde{a}_{ij}| \leq \tilde{B}$ has the important physical interpretation that any parts of a configuration which lie on or outside the Mach cones from the nose and tail of the configuration do not contribute to the interference wave drag.

Wing and tail-surface components of equivalent bodies of revolution have coincident axes ($d = 0$); therefore, the dimensionless zero-lift interference wave drag between such equivalent-body components can be calculated by the present method with values of $\tilde{I}(\tilde{a}_{ij},0)$. The zero-lift interference wave drag between the actual components must, however, be obtained from a graphical averaging process. Values of $\tilde{I}(\tilde{a}_{ij},0)$ are calculated directly from equation (B2) with $\tilde{B} = 0$. Values of $\tilde{I}(\tilde{a}_{ij},\tilde{B})$ have been calculated for $0 \leq \tilde{a}_{ij} \leq 3.10$ in increments of 0.01 and $0 \leq \tilde{B} \leq 3.0$ in intervals of 0.2 and are presented in table IV. A value of $\tilde{a}_{ij} = 3.1$ corresponds to a longitudinal separation of component centers of 1.1 half-component lengths of the largest component and should be adequate for most practical configurations.

APPENDIX C

AN ANALYTICAL APPROXIMATION OF AIRFOIL-SECTION AND PLAN-FORM THICKNESS DISTRIBUTIONS

The area distribution of a wing or tail surface depends upon the thickness distribution of the plan form which, in turn, depends upon the thickness distribution of the airfoil section. The plan-form area and thickness distributions can not be expressed in analytical form unless such an expression is available for the airfoil-section thickness distribution. In some cases the airfoil-section thickness distribution is available in analytical form; for example, that for the NACA four-digit-series airfoil sections is given by a power series. In many other cases, such as the NACA 6-series airfoil sections, the thickness distribution is not available in analytical form; however, the thickness distribution is, in general, accurately specified at many airfoil-section chord stations. The slope of the airfoil-section thickness distribution is always known for at least one chord station, usually at the chord station for maximum thickness, where the slope of the thickness distribution is zero. In this appendix a simple approximation of the airfoil-section thickness distribution will be made which affords an analytical expression for the thickness distribution from a knowledge of the thickness at specified chord stations and the slope of the thickness distribution for at least one chord station. With this information, an analytical expression for the plan-form thickness distribution of wings and tail surfaces will also be determined. The distributions will be determined in the dimensionless coordinate system described in appendix A.

Airfoil-Section Thickness Distribution

The thickness distribution of an airfoil section is generally specified at a sufficient number of chord stations that it can be approximated quite accurately by a series of adjacent parabolic-arc segments of continuous slope. Concerning zero-lift wave-drag calculations, errors introduced into the calculation of $\tilde{S}(\xi)$, $\tilde{S}'(\xi)$, or $\tilde{S}''(\xi)$ by this approximation are far less significant than those inherent in the various numerical calculation methods for the wave drag.

Consider the dimensionless airfoil-section thickness distribution and its derivatives shown in sketch (d). The thickness distribution is

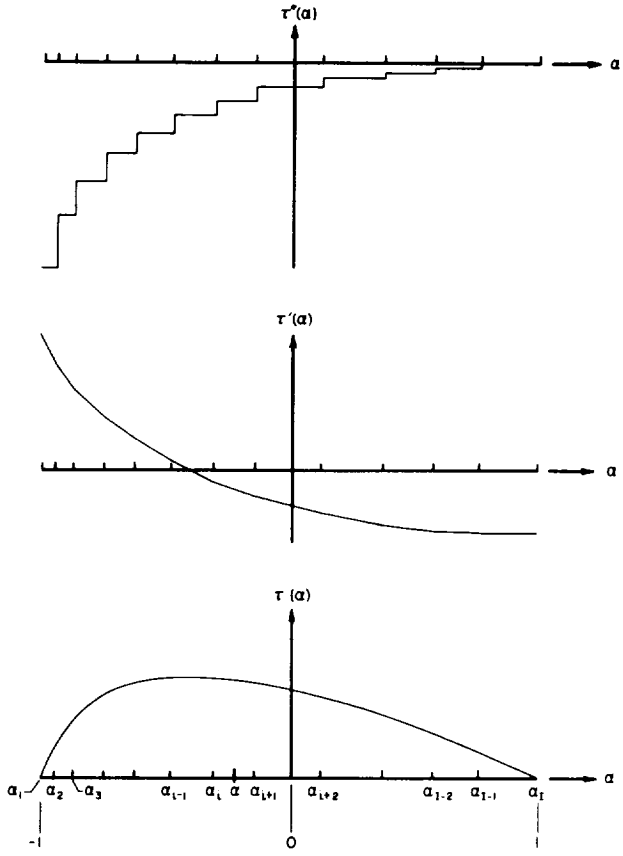

Sketch (d)

expressed analytically as

$$\tau(\alpha) = f(\alpha) \qquad \text{for} \quad -1 \leq \alpha \leq 1 \tag{C1}$$

where $f(\alpha)$ is a function of α which defines the shape of the thickness distribution and α is the dimensionless chord station measured positive and negative in the free-stream direction from the 50-percent chord as the origin. It should be recalled that the chord station defined in this manner is made dimensionless with respect to the half chord of the airfoil section. The function $f(\alpha)$ can be determined analytically as a series of adjacent parabolic-arc segments of continuous slope when the following conditions are satisfied:

i. Each parabolic segment satisfies the given thickness at two consecutive chord stations, α_i and α_{i+1}.

ii. The slope of the thickness distribution is continuous and is known for at least one chord station.

The function $f(\alpha)$ can be written for a parabolic arc through two consecutive points, α_i and α_{i+1}, such that

$$\tau(\alpha) = a(\alpha-\alpha_i)^2+b(\alpha-\alpha_{i+1})^2+c(\alpha-\alpha_i)(\alpha-\alpha_{i+1}) \quad \text{for} \quad \alpha_i \leq \alpha \leq \alpha_{i+1} \tag{C2}$$

also

$$\tau'(\alpha) = 2a(\alpha-\alpha_i)+2b(\alpha-\alpha_{i+1})+c[2\alpha-(\alpha_i+\alpha_{i+1})] \quad \text{for} \quad \alpha_i \leq \alpha \leq \alpha_{i+1} \tag{C3}$$

and

$$\tau''(\alpha) = 2(a+b+c) \quad \text{for} \quad \alpha_i \leq \alpha \leq \alpha_{i+1} \tag{C4}$$

With $\tau(\alpha_i)$, $\tau(\alpha_{i+1})$, and $\tau'(\alpha_{i+1})$ known, the constants in equations (C2) to (C4) can be determined as

$$a = \frac{\tau(\alpha_{i+1})}{(\alpha_{i+1}-\alpha_i)^2} \tag{C5}$$

$$b = \frac{\tau(\alpha_i)}{(\alpha_{i+1}-\alpha_i)^2} \tag{C6}$$

$$c = -2a + \frac{\tau'(\alpha_{i+1})}{\alpha_{i+1}-\alpha_i} \tag{C7}$$

Since $\tau'(\alpha)$ is linear and $\tau''(\alpha)$ is constant over each segment of parabolic arc, it is more convenient to express $\tau'(\alpha)$ at each α_i as

$$\tau'(\alpha_i) = \tau'(\alpha_{i+1})-(\alpha_{i+1}-\alpha_i)\tau''(\alpha) \tag{C8}$$

At each predetermined chord station, α_i, of the actual airfoil section $\tau(\alpha) = \tau(\alpha_i)$ where $\tau(\alpha_i)$ is known, $\tau'(\alpha) \approx \tau'(\alpha_i)$ where $\tau'(\alpha_i)$ is given by equation (C8), but is known for at least one value of α_i, and $\tau''(\alpha) \approx \tau''(\alpha_i)$ where $\tau''(\alpha_i)$ is given by equation (C4).

To illustrate the procedure for finding $\tau(\alpha)$, $\tau'(\alpha)$, and $\tau''(\alpha)$ consider a simple parabolic-arc airfoil section and an NACA 6XA00Y airfoil section. For the parabolic-arc airfoil section the known conditions are

i. $\tau(\alpha_i) = \tau(-1) = 0$

ii. $\tau(\alpha_{i+1}) = \tau(0) = 1$

iii. $\tau'(\alpha_{i+1}) = \tau'(0) = 0$

iv. $\alpha_{i+1}-\alpha_i = 1$

From conditions i and iv in equation (C6) b = 0; from conditions ii and iv in equation (C5) a = 1; and from conditions iii and iv and the fact that a = 1 in equation (C7) c = -2; hence, from equations (C2) to (C4)

$$\tau(\alpha) = 1-\alpha^2$$

$$\tau'(\alpha) = -2\alpha$$

$$\tau''(\alpha) = -2$$

For the NACA 6XA00Y airfoil section the known conditions are

i. $0.6 \leq \alpha \leq 1$ $\tau(\alpha)$ is given for $\alpha_{i+1}-\alpha_i = 0.1$

$\tau(\alpha)$ is linear, hence $\tau'(0.6)$ can be found

ii. $-0.8 \leq \alpha \leq 0.6$ $\tau(\alpha)$ given for $\alpha_{i+1}-\alpha_i = 0.1$

iii. $-0.95 \leq \alpha \leq -0.8$ $\tau(\alpha)$ given for $\alpha_{i+1}-\alpha_i = 0.05$

iv. $-1 \leq \alpha \leq -0.95$ $\tau(\alpha)$ given for $\alpha_{i+1}-\alpha_i = 0.025$

From condition i, $\tau(\alpha_i)$ is given and

$$\tau'(\alpha_i) = \frac{\tau(\alpha_{i+1})-\tau(\alpha_i)}{\alpha_{i+1}-\alpha_i} \qquad (C9)$$

$$\tau''(\alpha_i) = 0$$

To continue from condition i, $\tau'(0.6)$ must be found and used with condition ii. From equation (C9)

$$\tau'(0.6) = \frac{\tau(1)-\tau(0.6)}{1-0.6} = 2.5[\tau(1)-\tau(0.6)] \qquad (C10)$$

At $\alpha = 0.5$, from condition ii and the result of equation (C10), a, b, and c are found from equations (C5) to (C7). In equation (C7) $\tau'(\alpha_{i+1}) = \tau'(0.6)$. Next $\tau''(0.5)$ is found from equation (C4). Then sufficient information is available to calculate $\tau'(0.5)$ from equation (C8). With $\tau'(0.5)$ the above steps are repeated and conditions ii to iv are used until $\tau(-1)$, $\tau'(-1)$, and $\tau''(-1)$ are determined.

Wing Plan-Form Thickness Distribution

Consider those wings which satisfy the following conditions.

i. The boundaries of the wing are such that the plan form and the spanwise variation of the local chord can be expressed analytically.

ii. The wing has the same basic airfoil section at all spanwise stations; that is, only spanwise variations in thickness and/or thickness ratio are allowed.

iii. The thickness distribution of the basic airfoil section can be expressed analytically as described in the preceding part of this appendix.

iv. The spanwise variation of the thickness along lines of constant percent chord can be expressed analytically.

Actually, condition ii can be relaxed to include wings with one basic airfoil section out to a discontinuity in plan form, for example, a fence or extended leading edge, and a different basic airfoil section from the discontinuity out to the wing tip. In such cases each portion of the plan form is treated as a separate entity.

Consider the one wing panel of a typical plan form shown by the solid lines in sketch (e) in dimensionless coordinates. If the abcissa of any

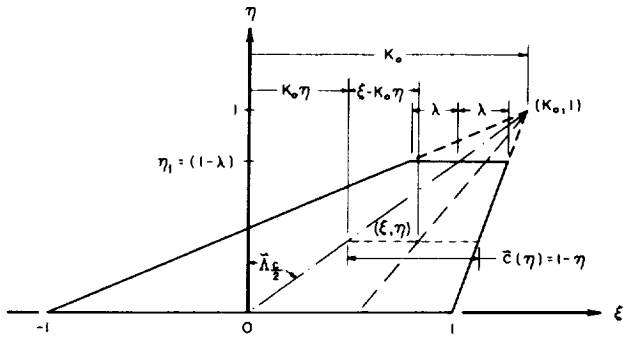

Sketch (e)

point in the plan form is measured from the local 50-percent chord station and this distance is divided by the half chord of the local airfoil section, any point in the plan form, (ξ,η), can be expressed as a chord station of the local dimensionless airfoil section. With the aid of sketch (e) this is accomplished by the transformation

$$\alpha(\xi,\eta) = \frac{\xi - K_o\eta}{\bar{c}(\eta)} \qquad \text{(C11)}$$

where K_o is the tangent of the sweep angle of the 50-percent chord line of the extended wing panel and $\tilde{c}(\eta)$ is the local half chord. All points in the plan form which yield the same value of $\alpha(\xi,\eta)$ define lines of constant percent chord (see long dashed line in sketch (e)), and since the basic airfoil section is the same at all spanwise stations, the dimensionless thickness of the local dimensionless airfoil section is constant along these lines. Therefore, the thickness at any point in the plan form can be found as the product of the thickness at the proper chord station of the basic airfoil section and a term which allows for the spanwise variation of the thickness along lines of constant percent chord. If $\Phi(\eta)$ represents the known analytical spanwise variation of the thickness along lines of constant percent chord, an analytical expression for the wing plan-form thickness distribution is

$$\tau(\xi,\eta) = \Phi(\eta)\tau[\alpha(\xi,\eta)] \tag{C12}$$

where $\tau[\alpha(\xi,\eta)]$ is a known analytical expression for the basic airfoil section and $\alpha(\xi,\eta)$ is given by equation (C11).

Equation (C12) is applicable to all generalized wings which satisfy conditions i to iv above. For instance, if the plan form is such that the 50-percent chord line is nonlinear, equation (C12) is applicable when equation (C11) takes the more general form

$$\alpha(\xi,\eta) = \frac{\xi - K_o\eta + f(\eta)}{\tilde{c}(\eta)}$$

In this case $f(\eta)$ describes the nonlinearity of the 50-percent chord line.

Equations (C11) and (C12) can be modified in a very simple manner to yield the plan-form thickness distribution, and hence

$$\tilde{S}\left(\xi,\ \beta\frac{b_o}{c_o},\ \theta\right)$$

$$\tilde{S}'\left(\xi,\ \beta\frac{b_o}{c_o},\ \theta\right)$$

and

$$\tilde{S}''\left(\xi,\ \beta\frac{b_o}{c_o},\ \theta\right)$$

for sheared wing components of the equivalent bodies of revolution required when calculating the zero-lift wave drag of an airplane-type configuration. Consider the complete wing shown in figure 5. The traces in the ξ,η plane of the intersection of the oblique planes and the ξ,η plane define an angle $\tilde{\psi}$ with the η axis such that

$$\tilde{\psi} = \tan^{-1}\beta \frac{b_o}{c_o} \cos \theta$$

Hence, the traces through the extended wing tips and the ξ axis (see lines XX and YY in fig. 5) define a longitudinal distance $|\beta(b_o/c_o)\cos \theta|$. In accordance with reference 5 each element of the upper (positive η direction) wing panel is sheared a distance $|\beta(b_o/c_o)\cos \theta|\eta$ forward and each element of the lower (negative η direction) wing panel is sheared a distance $|\beta(b_o/c_o)\cos \theta|\eta$ rearward for $0 \leq \theta < \pi/2$ (see the dashed lines in fig. 5). From figure 5 it can be seen that the tangent of the sweep angle of the sheared 50-percent chord line of the upper and lower extended wing panels can be defined, respectively, as

$$K_U = K_o - \beta \frac{b_o}{c_o} \cos \theta \tag{C13}$$

$$K_L = K_o + \beta \frac{b_o}{c_o} \cos \theta \tag{C14}$$

The quantity K, rather than β and θ, can be used to define the shearing of the wing panels. The upper and lower wing panels are related in a simple manner by

$$K_U + K_L = 2K_o \tag{C15}$$

It will be recalled that the tangent of the sweep angle of the 50-percent chord of the extended wing panel is used in equation (C11) to define the parameter α. Hence, if K_o in equation (C11) is replaced by K, the plan-form thickness distribution of the wing panels of the various sheared configurations can be written

$$\tau(\xi,\eta,K) = \Phi(\eta)\tau[\alpha(\xi,\eta,K)] \tag{C16}$$

where

$$\alpha(\xi,\eta,K) = \frac{\xi - K\eta}{\tilde{c}(\eta)} \tag{C17}$$

and K is defined by equations (C13) and (C14).

In calculating the area distribution and derivatives of the area distribution for the various sheared configurations, the above means of identifying the sheared configurations permits the use of only one variable, K, to define these distributions. This will be demonstrated by the sample calculations of appendix D.

The equations derived above for the dimensionless wing plan-form thickness distributions are also applicable to tail surfaces when the characteristic lengths $c_o/2$, $b_o/2$, and $t_o/2$ for the tail surfaces are used to obtain dimensionless coordinates in the x, y, and z directions, respectively. For horizontal tail surfaces, equations (C13) and (C14) are used with $\theta_{HT} = \theta_W$. For vertical tail surfaces, equation (C14) is used with $\theta_{VT} = \theta_W+\pi/2$. The sheared configurations for vertical tail surfaces are symmetrical in π rather than $\pi/2$.

APPENDIX D

AN APPROXIMATE ANALYTICAL METHOD FOR CALCULATING AREA DISTRIBUTIONS AND THEIR DERIVATIVES FOR SHEARED WINGS OR TAIL SURFACES

The analytical expressions which will be developed in this appendix for calculating the area distribution, the first derivative of the area distribution, and the second derivative of the area distribution are applicable to wings or tail surfaces which satisfy the following conditions:

i. The spanwise variation of the 50-percent chord line is known analytically.

ii. The boundaries of the plan form, the spanwise variation of the local chord, and that of the thickness along lines of constant percent chord can be expressed analytically.

iii. The same airfoil section is employed at all spanwise stations.

iv. The thickness of the airfoil section is known at a sufficient number of chord stations to permit an analytical approximation of the airfoil-section thickness distribution in the manner described in appendix C.

Consider the typical half plan form for wings and tail surfaces shown in dimensionless coordinates in figure 6. The figure represents all trapezoidal-type half plan forms with taper ratio, $0 \leq \lambda < 1$. The general form of the equations which will be developed for the various distributions is also applicable to the case for $\lambda = 1$. The details of the solutions for this case, however, are simpler than those for $0 \leq \lambda < 1$. The differences will be pointed out later when some sample calculations are presented. The solid lines in figure 6 represent any half plan form with $0 < \lambda < 1$, and the short dashed lines represent the extended half plan form. It should be noted the actual half plan form and the extended half plan form are identical for $\lambda = 0$. It should also be noted that all equations are based upon extended half plan form.

EXACT EQUATIONS FOR THE DISTRIBUTIONS

The dimensionless area distribution of any half plan form and its sheared configurations is given by

$$\tilde{S}(\xi,K) = \int_{\eta_l(\xi,K)}^{\eta_u(\xi,K)} \tau(\xi,\eta,K)d\eta \tag{D1}$$

Differentiation of equation (D1) with respect to ξ yields the first derivative of the area distribution of the half plan form

$$\tilde{S}'(\xi,K) = \int_{\eta_l(\xi,K)}^{\eta_u(\xi,K)} \frac{\partial\tau(\xi,\eta,K)}{\partial\xi}\, d\eta + \tau(\xi,\eta_u,K)\frac{d\eta_u}{d\xi} - \tau(\xi,\eta_l,K)\frac{d\eta_l}{d\xi} \tag{D2}$$

Differentiation of equation (D2) with respect to ξ yields the second derivative of area distribution of the half plan form

$$\tilde{S}''(\xi,K) = \int_{\eta_l(\xi,K)}^{\eta_u(\xi,K)} \frac{\partial^2\tau(\xi,\eta,K)}{\partial\xi^2}\, d\eta + \frac{\partial\tau(\xi,\eta_u,K)}{\partial\xi}\frac{d\eta_u}{d\xi} + \frac{d\tau(\xi,\eta_u,K)}{d\xi}\frac{d\eta_u}{d\xi} +$$

$$\tau(\xi,\eta_u,K)\frac{d^2\eta_u}{d\xi^2} - \frac{\partial\tau(\xi,\eta_l,K)}{\partial\xi}\frac{d\eta_l}{d\xi} - \frac{d\tau(\xi,\eta_l,K)}{d\xi}\frac{d\eta_l}{d\xi} -$$

$$\tau(\xi,\eta_l,K)\frac{d^2\eta_l}{d\xi^2} \tag{D3}$$

In equations (D1) to (D3) $\tau(\xi,\eta,K)$ is the plan-form thickness distribution of any of the sheared configurations and is given by

$$\tau(\xi,\eta,K) = \Phi(\eta)\tau[\alpha(\xi,\eta,K)] \tag{C16}$$

where $\Phi(\eta)$ is the known analytical spanwise variation of the thickness along lines of constant-percent chord, $\tau[\alpha(\xi,\eta,K)]$ is the local airfoil-section dimensionless thickness at a given percent chord, $\alpha(\xi,\eta,K)$ defines lines of constant-percent chord for any point (ξ,η) in the plan form and is given by

$$\alpha(\xi,\eta,K) = \frac{\xi - K\eta}{\tilde{c}(\eta)} \tag{C17}$$

and K is given by equation (C13) or (C14). The upper and lower limits of integration, $\eta_u(\xi,K)$ and $\eta_l(\xi,K)$, respectively, are the boundaries of the half plan form. Also $\partial\tau(\xi,\eta,K)/\partial\xi$ is continuous between limits of integration.

To evaluate equations (D1) to (D3) it is convenient to make a change of variable from η to α in accordance with equation (C17). In this

manner one can subsequently make use of the fact that $\tau''(\alpha)$ is constant over each interval of parabolic arc which approximates the airfoil-section thickness distribution (see appendix C). With this change of variable let

$$\alpha = \alpha(\xi,\eta,K) \tag{D4}$$

$$\left.\begin{aligned} \eta_u &= \eta_u(\xi,K) \\ \eta_l &= \eta_l(\xi,K) \end{aligned}\right\} \tag{D5}$$

and from equation (C17) the new lower and upper limits of integration become, respectively,

$$\left.\begin{aligned} \alpha_l &= \alpha(\xi,\eta_l,K) \\ \alpha_u &= \alpha(\xi,\eta_u,K) \end{aligned}\right\} \tag{D6}$$

The change of variable for each term of equations (D1) to (D3) which contains a function of $\tau(\xi,\eta,K)$ can be made by means of equations (C16), (C17), and (D4) and various combinations of their partial and total derivatives. Thus,

$$\tau(\xi,\eta,K) = \Phi(\eta)\tau(\alpha) \tag{D7}$$

$$\frac{\partial\tau(\xi,\eta,K)}{\partial\xi} = \Phi(\eta)\tau'(\alpha)\frac{\partial\alpha}{\partial\xi} \tag{D8}$$

$$\frac{\partial^2\tau(\xi,\eta,K)}{\partial\xi^2} = \Phi(\eta)\tau''(\alpha)\left(\frac{\partial\alpha}{\partial\xi}\right)^2 \tag{D9}$$

$$\frac{d\tau(\xi,\eta,K)}{d\xi} = \Phi(\eta)\tau'(\alpha)\frac{\partial\alpha}{\partial\xi} + \left[\frac{d\Phi(\eta)}{d\eta}\tau(\alpha)+\Phi(\eta)\tau'(\alpha)\frac{\partial\alpha}{\partial\eta}\right]\frac{d\eta}{d\xi} \tag{D10}$$

Exact Equation for $\tilde{S}(\xi,K)$

Substituting equations (D7) in equation (D1) and making the change of variable from η to α

$$\tilde{S}(\xi,K) = \int_{\alpha_l}^{\alpha_u} \Phi(\alpha,\xi,K)\tau(\alpha)\frac{d\eta}{d\alpha}\,d\alpha \tag{D11}$$

Grouping the integrand of equation (D11) as $\tau(\alpha)$ and

$$\Phi(\alpha,\xi,K)\ \frac{d\eta}{d\alpha}\ d\alpha$$

integration by parts yields

$$\tilde{S}(\xi,K) = [\tau(\alpha)\psi(\alpha,\xi,K)]_{\alpha_l}^{\alpha_u} - \int_{\alpha_l}^{\alpha_u} \tau'(\alpha)\psi(\alpha,\xi,K)d\alpha \qquad (D12)$$

where

$$\psi(\alpha,\xi,K) = \int \Phi(\alpha,\xi,K)\ \frac{d\eta}{d\alpha}\ d\alpha \qquad (D13)$$

After integration by parts of the second term in equation (D12)

$$\tilde{S}(\xi,K) = [\tau(\alpha)\psi(\alpha,\xi,K)-\tau'(\alpha)\Gamma(\alpha,\xi,K)]_{\alpha_l}^{\alpha_u} + \int_{\alpha_l}^{\alpha_u} \tau''(\alpha)\Gamma(\alpha,\xi,K)d\alpha \qquad (D14)$$

where

$$\Gamma(\alpha,\xi,K) = \int \psi(\alpha,\xi,K)d\alpha \qquad (D15)$$

Exact Equation for $\tilde{S}'(\xi,K)$

Substituting equation (D8) and equation (D7), evaluated at η_u and η_l, in equation (D2) and making the change of variable from η to α yields

$$\tilde{S}'(\xi,K) = \int_{\alpha_l}^{\alpha_u} \Phi(\alpha,\xi,K)\tau'(\alpha)\ \frac{\partial\alpha}{\partial\xi}\ \frac{d\eta}{d\alpha}\ d\alpha + \Phi(\eta_u)\tau(\alpha_u)\ \frac{d\eta_u}{d\xi} - \Phi(\eta_l)\tau(\alpha_l)\ \frac{d\eta_l}{d\xi} \qquad (D16)$$

Grouping the integrand of equation (D16) as $\tau'(\alpha)$ and

$$\Phi(\alpha,\xi,K)\ \frac{\partial\alpha}{\partial\xi}\ \frac{d\eta}{d\alpha}\ d\alpha$$

integration by parts yields

$$\tilde{S}'(\xi,K) = [\tau'(\alpha)\Omega(\alpha,\xi,K)]_{\alpha_l}^{\alpha_u} - \int_{\alpha_l}^{\alpha_u} \tau''(\alpha)\Omega(\alpha,\xi,K)d\alpha + \Phi(\eta_u)\tau(\alpha_u)\ \frac{d\eta_u}{d\xi} - \Phi(\eta_l)\tau(\alpha_l)\ \frac{d\eta_l}{d\xi} \qquad (D17)$$

where

$$\Omega(\alpha,\xi,K) = \int \Phi(\alpha,\xi,K)\ \frac{\partial\alpha}{\partial\xi}\ \frac{d\eta}{d\alpha}\ d\alpha \qquad (D18)$$

Exact Equation for $\tilde{S}''(\xi,K)$

Substituting equations (D9), and equations (D7), (D8), and (D10), evaluated at η_u and η_l, in equation (D3), making the change of variable from η to α and collecting the terms

$$\tilde{S}''(\xi,K) = \int_{\alpha_l}^{\alpha_u} \tau''(\alpha)\Lambda(\alpha,\xi,K)d\alpha + \left(2\frac{\partial\alpha_u}{\partial\xi} + \frac{\partial\alpha_u}{\partial\eta_u}\frac{d\eta_u}{d\xi}\right)\Phi(\eta_u)\tau'(\alpha_u)\frac{d\eta_u}{d\xi} +$$

$$\left[\frac{d\Phi(\eta_u)}{d\eta_u}\left(\frac{d\eta_u}{d\xi}\right)^2 + \Phi(\eta_u)\frac{d^2\eta_u}{d\xi^2}\right]\tau(\alpha_u) - \left(2\frac{\partial\alpha_l}{\partial\xi} + \frac{\partial\alpha_l}{\partial\eta_l}\frac{d\eta_l}{d\xi}\right)$$

$$\Phi(\eta_l)\tau'(\alpha_l)\frac{d\eta_l}{d\xi} - \left[\frac{d\Phi(\eta_l)}{d\eta_l}\left(\frac{d\eta_l}{d\xi}\right)^2 + \Phi(\eta_l)\frac{d^2\eta_l}{d\xi^2}\right]\tau(\alpha_l) \qquad (D19)$$

where

$$\Lambda(\alpha,\xi,K) = \Phi(\alpha,\xi,K)\left(\frac{\partial\alpha}{\partial\xi}\right)^2\frac{d\eta}{d\alpha} \qquad (D20)$$

Limits of Integration

The limits of integration in the equations for the various distributions depend upon the plan form being considered. For practical half plan forms only four limits of integration need be considered - the chord on the ξ axis, the leading edge, the trailing edge, and the finite tip for half plan forms with $0 < \lambda \leq 1$. It should be noted that integration over the half plan form in the η direction is transformed, by equation (C17), to an integration over the basic airfoil section in the α (or ξ) direction. Furthermore, the limits of α integration never exceed ± 1 regardless of the value of ξ. The limits of α integration as determined from figure 6 and equation (C17) for the actual and extended half plan forms are tabulated below:

Limits of α integration				
Limit, location	Value	Type of limit	Where applicable	
ξ axis	ξ	Lower	$-1 \le \xi \le 1$	All K
Leading edge	-1	Upper	$-1 < \xi \le K$	$K > -1$
		Lower	$K \le \xi < -1$	$K \le -1$
Finite tip $(0 < \lambda < 1)$	$\frac{\xi - K\eta_t}{\tilde{c}(\eta)}$	Upper (actual half plan form)	$(K\eta_t - \lambda) \le \xi \le (K\eta_t + \lambda)$	All K
		Lower (extended tip)		
Trailing edge	1	Upper	$K \le \xi < 1$	$K < 1$
		Lower	$1 < \xi \le K$	$K \ge 1$

Presented in figures 7(a) and 7(b) for half plan forms with $0 < \lambda < 1$ and $\lambda = 0$, respectively, are the regions and limits of α integration for all possible values of K. It should be noted that the distributions of the actual half plan forms with $0 < \lambda < 1$ (fig. 7(a)) are found by subtracting from the distributions of the extended half plan forms, for values of $(K\eta_t - \lambda) \le \xi \le (K\eta_t + \lambda)$, the distributions for the extended tip defined by $\eta_t \le \eta \le 1$. It is for this reason that the half plan forms are made dimensionless with respect to the extended half plan form. Note also that the upper limit of integration is always constant (either -1 or 1) and the equations for the distributions can be expressed as a function of the lower limit. More important, however, this treatment of the limits of integration permits the calculation of the distributions for the half plan forms with $0 < \lambda < 1$ from a very simple manipulation of the basic data for the extended half plan forms. This procedure will be explained in detail in the sample calculations. Similarly, in the case of an airplane-type configuration, the distributions of the exposed half plan forms can be conveniently found from the basic data of the extended half plan forms.

It now remains to investigate the effect of the limits of integration on the terms in equations for the distributions (eqs. (D14), (D17), and (D19)) which are evaluated at the limits. Only the terms in these equations which contain $\tau(\alpha)$ and/or $d\eta/d\xi$, evaluated at the limits, will vanish when the values of ξ are such that the limits of integration of the half plan form are

i. Along the ξ axis, in which case $d\eta_l/d\xi = 0$.

ii. Along the leading edge, in which case $\tau(\alpha_u) = \tau(-1) = 0$ or $\tau(\alpha_l) = \tau(-1) = 0$.

iii. Along the finite tip, in which case $d\eta_u/d\xi = 0$ or $d\eta_l/d\xi = 0$ when η_t is the lower limit of the extended half plan form.

iv. Along the trailing edge if the basic airfoil section has or is assumed to have zero thickness at the trailing edge, in which case $\tau(\alpha_u) = \tau(1) = 0$ or $\tau(\alpha_l) = \tau(1) = 0$.

APPROXIMATE EQUATIONS FOR THE DISTRIBUTIONS

The approximate equations for $\tilde{S}(\xi,K)$, $\tilde{S}'(\xi,K)$, and $\tilde{S}''(\xi,K)$ will be determined by examining equations (D14), (D17), and (D19), respectively, in the light of the approximation of the airfoil-section thickness distribution made in appendix C. It will be noted that each of equations (D14), (D17), and (D19) contains a term of the form

$$\int_{\alpha_l}^{\alpha_u} \tau''(\alpha) f(\alpha,\xi,K)\,d\alpha \tag{D21}$$

For the approximation made in appendix C, $\tau''(\alpha) \approx \tau''(\alpha_i)$ = a constant for $\alpha_i \le \alpha \le \alpha_{i+1}$ (see sketch (d)). Therefore, if the integration in expression (D21) is performed as the sum of integrations over the intervals $\alpha_{i+1}-\alpha_i$, $\tau''(\alpha_i)$ can be taken outside the integral sign for each interval. The sum of the individual integrations which make up the integration of the expression (D21) can have two forms, depending on whether α_u is less than or greater than α_l. The form of the integration for these two cases can be determined with the aid of figure 8 which defines the stepwise limits and direction of α integration. Case I, for which $\alpha_u < \alpha_l$ applies, regardless of plan form, when $\xi \le K$; and Case II, for which $\alpha_u > \alpha_l$ applies, regardless of plan form, when $\xi > K$.

With the aid of figure 8 and the approximation in appendix C, the expression (D21) can be written

$$\begin{aligned}\int_{\alpha_l}^{\alpha_u} \tau''(\alpha) f(\alpha,\xi,K)\,d\alpha \approx\ & \tau''(\alpha_l) \int_{\alpha_l}^{\alpha_{i(\alpha_l)}} f(\alpha,\xi,K)\,d\alpha + \\ & \sum_{i=i(\alpha_l)}^{U+1} \tau''(\alpha_{i-1}) \int_{\alpha_i}^{\alpha_{i-1}} f(\alpha,\xi,K)\,d\alpha + \\ & \tau''(\alpha_{U-1}) \int_{\alpha_U}^{\alpha_u} f(\alpha,\xi,K)\,d\alpha \qquad \text{for Case I}\end{aligned} \tag{D22}$$

and

$$\int_{\alpha_l}^{\alpha_u} \tau''(\alpha) f(\alpha,\xi,K)d\alpha \approx \tau''(\alpha_l) \int_{\alpha_l}^{\alpha_{i(\alpha_l)+1}} f(\alpha,\xi,K)d\alpha + \sum_{i=i(\alpha_l)+1}^{U-1} \tau''(\alpha_i) \int_{\alpha_i}^{\alpha_{i+1}} f(\alpha,\xi,K)d\alpha + \tau''(\alpha_U) \int_{\alpha_U}^{\alpha_u} f(\alpha,\xi,K)d\alpha \quad \text{for Case II} \tag{D23}$$

If α_l and α_u can be made to coincide with α_{i-1} and α_U for Case I and with α_{i+1} and α_U for Case II, the first and last terms of equations (D22) and (D23) will vanish. This can be accomplished for the first terms by choosing ξ such that α_l always corresponds to a value of α_i for which the airfoil-section thickness is specified, and for the last terms by always integrating to the leading or trailing of the extended half plan form (i.e., $\alpha_u = \alpha_U = \mp 1$). As mentioned earlier, this is accomplished for half plan forms with $0 < \lambda < 1$ by subtracting the distributions of the extended tip from those for the extended half plan forms.

The approximate equations for $\tilde{S}(\xi,K)$, $\tilde{S}'(\xi,K)$, and $\tilde{S}''(\xi,K)$ are found by substituting the form of equations (D22) and (D23), with the proper integrand, in the integral term of the exact equation for each distribution. For $\tilde{S}(\xi,K)$, equation (D14), $f(\alpha,\xi,K) = \Gamma(\alpha,\xi,K)$. For $\tilde{S}'(\xi,K)$, equation (D17), $f(\alpha,\xi,K) = \Omega(\alpha,\xi,K)$. For $\tilde{S}''(\xi,K)$, equation (D19), $f(\alpha,\xi,K) = \Lambda(\alpha,\xi,K)$. The terms of equations (D14), (D17), and (D19) which are evaluated at the limits of integration are treated in the same manner as discussed in connection with the exact equations for the distributions.

SAMPLE CALCULATIONS

Complete Half Plan Forms, $0 \leq \lambda < 1$

The area distribution, the first derivative of the area distribution, and the second derivative of the area distribution will be calculated for the families of half plan forms shown in figure 7. The airfoil sections will be considered to have a linear spanwise variation in thickness along lines of constant percent chord, and, for simplicity, will be considered to have zero thickness at the trailing edge.[3] The spanwise variation of the half chord is given by

[3]Generally, the thickness at the trailing edge of the airfoil section is sufficiently small that it can be considered to be zero without introducing any appreciable error in the distributions. Any small error which might be introduced, however, has a negligible effect upon the zero-lift wave-drag calculations.

$$\tilde{c}(\eta) = 1-\eta \tag{D24}$$

From equations (C17) and (D24)

$$\alpha = \frac{\xi - K\eta}{1-\eta} \tag{D25}$$

and

$$\eta = 1 - \frac{\xi - K}{\alpha - K} \tag{D26}$$

The linear spanwise variation of the thickness along lines of constant percent chord is

$$\Phi(\eta) = 1-C\eta \quad \text{for} \quad 0 \leq \eta \leq 1 \tag{D27}$$

where

$$C = \frac{1-\sigma}{1-\lambda} \quad \text{for} \quad 0 \leq \lambda < 1 \tag{D28}$$

In equation (D28) σ is the ratio of the airfoil-section thickness at the finite tip to that at the vertical plane of symmetry, and λ is the taper ratio of the actual half plan form being considered. For the spanwise thickness variation, C is normally defined by only the numerator of equation (D28). In the present case, however, the factor $1/1-\lambda$ is required in order that equation (D27) be valid for $0 \leq \eta \leq 1$. This factor is the ratio of the extended semispan, $b_o/2$, to that of the actual semispan, $b/2$. With C defined as in equation (D28), for half plan forms with $0 < \lambda < 1$, all or a portion of the spanwise thickness distribution of the extended half plan form may be negative. This imposes no serious consequences since the distributions for $0 < \lambda < 1$ are obtained by subtracting the contributions for $\eta_t \leq \eta \leq 1$ from the distributions for $0 \leq \eta \leq 1$.

For extended half plan forms it is always possible to calculate the distribution at values of ξ for which the lower limit of integration corresponds to values of α_i for which the airfoil-section thickness is specified, and the upper limit of integration is always the leading or trailing edge. Hence, for extended half plan forms the first and last terms of equations (D22) and (D23) vanish. With this information plus conditions i to iv previously discussed in connection with the limits of integration, the approximate equations from which the distributions can be calculated for half plan forms with $0 \leq \lambda < 1$ are

$$\tilde{S}(\xi,K) \approx [\tau(\alpha)\psi(\alpha,\xi,K)-\tau'(\alpha)\Gamma(\alpha,\xi,K)]_{\alpha_\ell}^{\alpha_u} + \begin{cases} \sum_{i=i(\alpha_\ell)}^{2} \tau''(\alpha_{i-1}) \int_{\alpha_i}^{\alpha_{i-1}} \Gamma(\alpha,\xi,K)d\alpha & \text{for Case I} \\ \sum_{i=i(\alpha_\ell)+1}^{I-1} \tau''(\alpha_i) \int_{\alpha_i}^{\alpha_{i+1}} \Gamma(\alpha,\xi,K)d\alpha & \text{for Case II} \end{cases} \quad \text{(D29)}$$

$$\tilde{S}'(\xi,K) \approx [\tau'(\alpha)\Omega(\alpha,\xi,K)]_{\alpha_\ell}^{\alpha_u} - \begin{cases} \sum_{i=i(\alpha_\ell)}^{2} \tau''(\alpha_{i-1}) \int_{\alpha_i}^{\alpha_{i-1}} \Omega(\alpha,\xi,K)d\alpha & \text{for Case I} \\ \sum_{i=i(\alpha_\ell)+1}^{I-1} \tau''(\alpha_i) \int_{\alpha_i}^{\alpha_{i+1}} \Omega(\alpha,\xi,K)d\alpha & \text{for Case II} \end{cases} \quad \text{(D30)}$$

$$\tilde{S}''(\xi,K) \approx \begin{cases} \sum_{i=i(\alpha_\ell)}^{2} \tau''(\alpha_{i-1}) \int_{\alpha_i}^{\alpha_{i-1}} \Lambda(\alpha,\xi,K)d\alpha & \text{for Case I} \\ \sum_{i=i(\alpha_\ell)+1}^{I-1} \tau''(\alpha_i) \int_{\alpha_i}^{\alpha_{i+1}} \Lambda(\alpha,\xi,K)d\alpha & \text{for Case II} \end{cases} +$$

$$\left(2\frac{\partial\alpha_u}{\partial\xi} + \frac{\partial\alpha_u}{\partial\eta_u}\frac{d\eta_u}{d\xi}\right)\Phi(\eta_u)\tau'(\alpha_u)\frac{d\eta_u}{d\xi} -$$

$$\left(2\frac{\partial\alpha_\ell}{\partial\xi} + \frac{\partial\alpha_\ell}{\partial\eta_\ell}\frac{d\eta_\ell}{d\xi}\right)\Phi(\eta_\ell)\tau'(\alpha_\ell)\frac{d\eta_\ell}{d\xi} \quad \text{(D31)}$$

Sample calculation of $\tilde{S}(\xi,K)$.- For half plan forms with $0 < \lambda < 1$, first consider the extended half plan form and make a change of variable in equation (D27) by using equation (D26), hence

$$\Phi(\alpha,\xi,K) = (1-C)+C\frac{\xi-K}{\alpha-K} \quad \text{(D32)}$$

From a differentiation of equation (D26) with respect to α

$$\frac{d\eta}{d\alpha} = \frac{\xi-K}{(\alpha-K)^2} \tag{D33}$$

Substituting equations (D32) and (D33) in (D13) and performing the indicated integration

$$\psi(\alpha,\xi,K) = -(1-C)\left(\frac{\xi-K}{\alpha-K}\right) - \frac{C}{2}\left(\frac{\xi-K}{\alpha-K}\right)^2 \tag{D34}$$

Substituting equation (D34) in equation (D15) and performing the indicated integration

$$\Gamma(\alpha,\xi,K) = -(1-C)(\xi-K)\ln|\alpha-K| + \frac{C}{2}\frac{(\xi-K)^2}{\alpha-K} \tag{D35}$$

Substituting equation (D35) in the second term (for Case I) of equation (D29)

$$\sum_{i=i(\alpha_l)}^{2} \tau''(\alpha_{i-1}) \int_{\alpha_i}^{\alpha_{i-1}} \Gamma(\alpha,\xi,K)d\alpha$$

$$= -(1-C)(\xi-K) \sum_{i=i(\alpha_l)}^{2} \tau''(\alpha_{i-1})[(\alpha_{i-1}-K)(\ln|\alpha_{i-1}-K|-1)-$$

$$(\alpha_i-K)(\ln|\alpha_i-K|-1)] + \frac{C}{2}(\xi-K)^2 \sum_{i=i(\alpha_l)}^{2} \tau''(\alpha_i-1)(\ln|\alpha_{i-1}-K|-\ln|\alpha_i-K|)$$

for Case I (D36)

Each of the summations in equation (D36) is very large for α_l close to the value of K and infinite for $\alpha_l = K$. To avoid this singularity, it is therefore desirable to multiply and divide both terms of the right-hand side of equation (D36) by $\alpha_l - K$. Furthermore, since the uppermost limit of the stepwise integration (α_U) is -1 along the leading edge of the half plan form, equation (D36) can be written as a function of only the lower limit, α_l, and K. Thus

$$\sum_{i=i(\alpha_l)}^{2} \tau''(\alpha_{i-1}) \int_{\alpha_i}^{\alpha_{i-1}} \Gamma(\alpha,\xi,K)d\alpha = -(1-C)\left(\frac{\xi-K}{\alpha_l-K}\right) A_I(\alpha_l,K) +$$

$$\frac{C}{2}\left(\frac{\xi-K}{\alpha_l-K}\right)^2 B_I(\alpha_l,K) \quad \text{for Case I} \tag{D37}$$

where

$$A_I(\alpha_\ell,K) = (\alpha_\ell-K)\sum_{i=i(\alpha_\ell)}^{2}\tau''(\alpha_{i-1})[(\alpha_{i-1}-K)(\ell n|\alpha_{i-1}-K|-1) -$$

$$(\alpha_i-K)(\ell n|\alpha_i-K|-1)] \quad \text{for Case I} \tag{D38}$$

and

$$B_I(\alpha_\ell,K) = (\alpha_\ell-K)^2\sum_{i=i(\alpha_\ell)}^{2}\tau''(\alpha_{i-1})(\ell n|\alpha_{i-1}-K|-\ell n|\alpha_i-K|) \quad \text{for Case I} \tag{D39}$$

Similarly, since $\alpha_U = 1$ along the trailing edge,

$$\sum_{i=i(\alpha_\ell)+1}^{I-1}\tau''(\alpha_i)\int_{\alpha_i}^{\alpha_{i+1}}\Gamma(\alpha,\xi,K)d\alpha = -(1-C)\left(\frac{\xi-K}{\alpha_\ell-K}\right)A_{II}(\alpha_\ell,K) + \frac{C}{2}\left(\frac{\xi-K}{\alpha_\ell-K}\right)^2 B_{II}(\alpha_\ell,K) \quad \text{for Case II} \tag{D40}$$

where

$$A_{II}(\alpha_\ell,K) = (\alpha_\ell-K)\sum_{i=i(\alpha_\ell)+1}^{I-1}\tau''(\alpha_i)\,[(\alpha_{i+1}-K)(\ell n|\alpha_{i+1}-K|-1) -$$

$$(\alpha_i-K)(\ell n|\alpha_i-K|-1)] \quad \text{for Case II} \tag{D41}$$

and

$$B_{II}(\alpha_\ell,K) = (\alpha_\ell-K)^2\sum_{i=i(\alpha_\ell)+1}^{I-1}\tau''(\alpha_i)(\ell n|\alpha_{i+1}-K|-\ell n|\alpha_i-K|) \quad \text{for Case II} \tag{D42}$$

Substituting equations (D34), (D35), (D37), and (D40) in equation (D29) an expression for the area distribution of the extended half plan form is obtained as

$$\tilde{S}(\xi,K) \approx (1-C)\left(\frac{\xi-K}{\alpha_\ell-K}\right)[C(\alpha_\ell,K)-D(\alpha_\ell,K)] + \frac{C}{2}\left(\frac{\xi-K}{\alpha_\ell-K}\right)^2[E(\alpha_\ell,K)+F(\alpha_\ell,K)] \tag{D43}$$

where

$$C(\alpha_l,K) = \tau(\alpha_l) - \left(\frac{\alpha_l-K}{\alpha_u-K}\right)\tau(\alpha_u)-A(\alpha_l,K) \tag{D44}$$

$$D(\alpha_l,K) = (\alpha_l-K)[\tau'(\alpha_l)\ln|\alpha_l-K|-\tau'(\alpha_u)\ln|\alpha_u-K|] \tag{D45}$$

$$E(\alpha_l,K) = \tau(\alpha_l) - \left(\frac{\alpha_l-K}{\alpha_u-K}\right)^2\tau(\alpha_u)+B(\alpha_l,K) \tag{D46}$$

$$F(\alpha_l,K) = (\alpha_l-K)\left[\tau'(\alpha_l) - \left(\frac{\alpha_l-K}{\alpha_u-K}\right)\tau'(\alpha_u)\right] \tag{D47}$$

The left-hand side of equations (D44) to (D47) is correctly given as a function of only α_l and K even though α_u, $\tau(\alpha_u)$, and $\tau'(\alpha_u)$ appear in the right-hand side of the equations. For the extended half plan form it will be recalled that $\alpha_u = \alpha_U$ is always ∓ 1, $\tau(\alpha_u)$ (included for the general case) is zero along the leading edge but may not be zero along the trailing edge of the half plan form, and $\tau'(\alpha_u)$ is one constant value along the leading edge and another constant value along the trailing edge of the half plan form. For these sample calculations, it will be recalled that $\tau(\alpha_u)$ has been assumed zero along the trailing edge; consequently, the term containing $\tau(\alpha_u)$ in equations (D44) and (D46) vanishes. For Case I and Case II $A(\alpha_l,K)$ and $B(\alpha_l,K)$ are given by equations (D38) and (D39) and equations (D41) and (D42), respectively.

To evaluate equation (D43) it will be found convenient to calculate the values of $A(\alpha_l,K)$ through $F(\alpha_l,K)$ in tabular form for all values of K of interest and for all values of α_l corresponding to values of $-1 \le \alpha_i \le 1$ for which the basic airfoil-section thickness distribution is given. Then, depending upon the value of ξ, α_l is obtained from the table on page 53 and equation (D43) is evaluated with the aid of the tabulated values of $A(\alpha_l,K)$ through $F(\alpha_l,K)$.

Equation (D43) is also applicable to half plan forms with $\lambda = 0$, in which case the actual and extended half plan forms are identical.

Equation (D43) is applicable to all geometrically similar extended half plan forms. One such geometrically similar half plan form is the extended tip of the extended half plan form defined by $\eta_t \le \eta \le 1$. Hence, the area distribution of the extended tip can be easily found if, in equation (D43), α_l of the extended-tip half plan form is taken as α_t of the actual half plan form. Then $\tilde{S}(\xi,K)$ for the extended tip becomes

$$\tilde{S}(\xi,K) = \begin{cases} (1-C)\left(\frac{\xi-K}{\alpha_t-K}\right)[C(\alpha_t,K)-D(\alpha_t,K)] + \frac{C}{2}\left(\frac{\xi-K}{\alpha_t-K}\right)^2[E(\alpha_t,K)+F(\alpha_t,K)] \\ \qquad\qquad \text{for} \quad (K\eta_t-\lambda) \le \xi \le (K\eta_t+\lambda) \\ \text{Equation (D43)} \quad \text{for} \quad \xi \gtrless (K\eta_t \pm \lambda) \end{cases} \tag{D48}$$

If α_t happens to correspond to values of α_i for which the airfoil-section thickness is given, $C(\alpha_l,K)$ through $F(\alpha_l,K)$ have previously been calculated in finding $\tilde{S}(\xi,K)$ for the extended half plan form. Otherwise, these quantities can be obtained from individual or combined plots of the tabulated values of $C(\alpha_l,K)$ through $F(\alpha_l,K)$ versus their arguments; that is, the values of these quantities are read from the plots at values of α_l obtained by letting $\alpha_l = \alpha_t$. Hence, the area distribution of the half plan forms with $0 < \lambda < 1$ is given by the difference between equation (D43) for all values of ξ and equation (D48) for $(K\eta_t-\lambda) \le \xi \le (K\eta_t+\lambda)$.

Sample calculations of $\tilde{S}'(\xi,K)$.- Again the extended half plan forms will be considered first. All the terms of equation (D18) except $\partial\alpha/\partial\xi$ have been found in terms of α, ξ, and K in the sample calculation of $\tilde{S}(\xi,K)$. This term is evaluated from equations (D25) and (D26) as

$$\frac{\partial\alpha}{\partial\xi} = \frac{\alpha-K}{\xi-K} \tag{D49}$$

Substituting equations (D32), (D33), and (D49) in equation (D18) and performing the indicated integration yields

$$\Omega(\alpha,\xi,K) = (1-C)\ln|\alpha-K| - C\left(\frac{\xi-K}{\alpha-K}\right) \tag{D50}$$

From a comparison of equations (D35) and (D50) it can be easily determined from an inspection of equations (D36) to (D39) that by substituting equation (D50) in the second term, for Case I, of equation (D30) one can obtain

$$\sum_{i=i(\alpha_l)}^{2} \tau''(\alpha_{i-1}) \int_{\alpha_i}^{\alpha_{i-1}} \Omega(\alpha,\xi,K)d\alpha = (1-C)\frac{1}{\alpha_l-K}A_I(\alpha_l,K) - C\frac{\xi-K}{(\alpha_l-K)^2}B_I(\alpha_l,K)$$

for Case I (D51)

and similarly

$$\sum_{i=i(\alpha_l)+1}^{I-1} \tau''(\alpha_i) \int_{\alpha_i}^{\alpha_{i+1}} \Omega(\alpha,\xi,K)d\alpha = (1-C)\frac{1}{\alpha_l-K} A_{II}(\alpha_l,K) - C\frac{\xi-K}{(\alpha_l-K)^2} B_{II}(\alpha_l,K) \quad \text{for Case II}$$

(D52)

where $A(\alpha_l,K)$ and $B(\alpha_l,K)$ are given for Cases I and II by equations (D38) and (D39) and equations (D41) and (D42), respectively. Substituting equations (D50), (D51), and (D52) in equation (D30) an expression for the first derivative of the area distribution of the extended half plan form is obtained as

$$\tilde{S}'(\xi,K) \approx -(1-C)\frac{1}{\alpha_l-K}[A(\alpha_l,K)+D(\alpha_l,K)]+C\frac{\xi-K}{(\alpha_l-K)^2}[B(\alpha_l,K)+F(\alpha_l,K)] \tag{D53}$$

As in the case of the area distribution, $\tilde{S}'(\xi,K)$ for the extended half plan form (actual half plan form for $\lambda = 0$) is obtained from equation (D53) by using the proper value of α_l obtained from the table on page 53 for each value of ξ for which $\tilde{S}'(\xi,K)$ is calculated. Values of $A(\alpha_l,K)$, $B(\alpha_l,K)$, $D(\alpha_l,K)$, and $F(\alpha_l,K)$ are obtained from the previous calculations of $\tilde{S}(\xi,K)$. For the extended-tip half plan form $\tilde{S}'(\xi,K)$ is obtained by following the same procedure outlined in finding $\tilde{S}(\xi,K)$. That is, in the region for which $(K\eta_t-\lambda) \leq \xi \leq (K\eta_t+\lambda)$, α_l in equation (D53) is replaced by α_t, the values of $A(\alpha_l,K)$, $D(\alpha_l,K)$, and $F(\alpha_l,K)$ are obtained from the aforementioned tabulated values, or plots, by letting $\alpha_l = \alpha_t$, and the resulting values of $\tilde{S}'(\xi,K)$ are subtracted from those of the extended half plan form at the proper values of ξ. Obviously, for $\xi \gtrless (K\eta_t \pm \lambda)$, $\tilde{S}'(\xi,K)$ for the extended tip is given by equation (D53).

Sample calculation of $\tilde{S}''(\xi,K)$.- For the extended half plan forms, substituting equations (D32), (D33), and (D49) in equation (D20) yields the function

$$\Lambda(\alpha,\xi,K) = \frac{1-C}{\xi-K} + \frac{C}{\alpha-K} \tag{D54}$$

Using equation (D54), the first term of equation (D31) becomes

$$\frac{1-C}{\xi-K}[\tau'(\alpha_u)-\tau'(\alpha_l)] + \frac{C}{\alpha_l-K} B(\alpha_l,K) \tag{D55}$$

where $B(\alpha_l,K)$ for Cases I and II is given, respectively, by equations (D39) and (D42).

To evaluate the second and third terms of equation (D31) consider the equations of the leading and trailing edges of the extended half plan forms. In terms of both η and α variables

$$\eta = \frac{\xi \pm 1}{K \pm 1} \tag{D56}$$

and

$$\alpha = \mp 1 \tag{D57}$$

The upper and lower signs of the $\pm$ sign in equations (D56) and (D57) are used with the leading and trailing edges, respectively. First consider the evaluation of the second term of equation (D31) when the leading or trailing edge is the upper limit of integration. From equation (D49), evaluated at α_u, and equation (D57)

$$\frac{\partial \alpha_u}{\partial \xi} = \frac{K \pm 1}{K - \xi} \tag{D58}$$

Since $\partial\alpha_u/\partial\eta_u = d\alpha_u/d\eta_u = 1/(d\eta_u/d\alpha_u)$, from equation (D33), evaluated at α_u, and equation (D57)

$$\frac{\partial \alpha_u}{\partial \eta_u} = \frac{(K \pm 1)^2}{K - \xi} \tag{D59}$$

From a differentiation of equation (D56) with respect to ξ

$$\frac{d\eta_u}{d\xi} = \frac{1}{K \pm 1} \tag{D60}$$

From equation (D32), evaluated at α_u, and equation (D57)

$$\Phi(\eta_u) = (1-C) + C\,\frac{K - \xi}{K \pm 1} \tag{D61}$$

Using equations (D58) to (D61) one obtains for the second term (upper limit) of equation (D31)

$$\frac{3\tau'(\alpha_u)}{\xi - K}\left[\frac{(C\xi - K) \mp (1-C)}{K \pm 1}\right] \tag{D62}$$

A general expression identical to that of (D62) is similarly obtained for the last term (lower limit) of equation (D31).

For the extended half plan forms $\tilde{S}''(\xi,K)$ is found by properly combining expressions (D55) and (D62) (and its counterpart for the lower limit) for certain ranges of the value of ξ. Regardless of the value of K, for $-1 \le \xi \le 1$, the last term of equation (D31) vanishes, because $d\eta_l/d\xi = 0$ for these values of ξ. For $|K| > 1$, and for $|\xi| > 1$, when the leading edge of the extended half plan form is the lower limit, the trailing edge is the upper limit of integration and vice versa. Therefore, for the extended half plan form (actual half plan form $\lambda = 0$)

$$\tilde{S}''(\xi,K) = \begin{cases} \left[\frac{(K\mp 2)(1-C)+3(C\xi-K)}{(K\pm 1)(\xi-K)}\right]\tau'(\alpha_u) + \frac{C}{\alpha_l - K}B(\alpha_l,K) - \frac{1-C}{\xi-K}\tau'(\alpha_l) \\ \qquad\qquad\qquad\qquad\qquad\qquad\qquad\qquad \text{for } -1 \le \xi \le 1 \end{cases} \quad \text{(D63a)}$$

$$\begin{cases} \left[\frac{(K\mp 2)(1-C)+3(C\xi-K)}{(K\pm 1)(\xi-K)}\right]\tau'(\alpha_u) + \frac{C}{\alpha_l - K}B(\alpha_l,K) - \\ \left[\frac{(K\pm 2)(1-C)+3(C\xi-K)}{(K\mp 1)(\xi-K)}\right]\tau'(\alpha_l) \qquad\qquad \text{for } |\xi| > 1 \end{cases} \quad \text{(D63b)}$$

where the upper of the double signs is employed when the leading edge of the extended half plan form is the upper limit of integration and the lower sign is used when the trailing edge is the upper limit. It should be noted that equation (D63b) is constant for $C = 1$ (constant airfoil-section thickness ratio in the spanwise direction).

To calculate $\tilde{S}''(\xi,K)$ for the extended tip half plan form, the same procedure described in finding $\tilde{S}(\xi,K)$ and $\tilde{S}'(\xi,K)$ is employed. Again, α_l is replaced by α_t for the actual half plan form in equation (D63a) for values of $(K\eta_t-\lambda) \le \xi \le (K\eta_t+\lambda)$ and for $\xi \gtrless (K\eta_t \pm \lambda)$ equation (D63b) is used. The resulting $\tilde{S}''(\xi,K)$ is subtracted from that of the extended half plan form.

If the half plan forms considered previously have a more general airfoil section such that the airfoil-section thickness is not zero at the trailing edge, equations (D44) and (D46) are valid as shown, but for the values of ξ for which the trailing edge of the half plan forms is a limit of integration, the terms of equations (D17) and (D19) which were omitted in the above calculations must be evaluated.

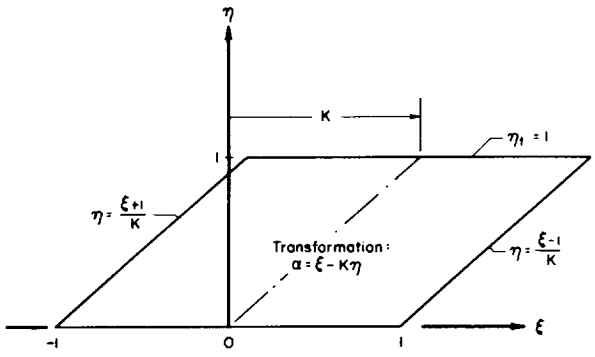

Sketch (f)

Complete Half Plan Forms, $\lambda = 1$

For the special case of half plan forms with $\lambda = 1$, the extended half plan form is semi-infinite and a different definition of K and different equations for the boundaries of the half plan form are needed. As noted in appendix A, the spanwise coordinate of half plan forms with $\lambda = 1$ is made dimensionless with respect to the actual semi-span, b/2. Hence the dimensionless half plan form for $\lambda = 1$ is defined as shown in sketch (f). With the half plan form so defined,

$$C = 1-\sigma \quad \text{for} \quad \lambda = 1$$

and the equations for the distributions derived above are, in general, applicable for $\lambda = 1$. However, for values of ξ in the region of the finite tip, $(K-1) \leq \xi \leq (K+1)$, the value of the upper limit defined by the α transformation noted in sketch (f) must be used in equations (D44) to (D47), that is,

$$\alpha_t = \xi - K\eta_t = \xi - K$$

Furthermore, unless the values of ξ in this region are so chosen that α_t corresponds to the values of α_i for which the airfoil-section thickness is given, the last term of equations (D22) and (D23) will not vanish and must be evaluated.

Exposed Half Plan Forms

In calculating the distributions of the exposed half plan forms of airplane-type configurations it is convenient to first calculate the distributions of the extended half plan forms. This provides an accurate determination of plots of $A(\alpha_l,K)$ through $F(\alpha_l,K)$. If $\eta_B = \eta_B(\xi)$ defines the body plan form, integrals of the type

$$\int_{\alpha_l=\alpha(\eta_B)}^{\alpha_u=\mp 1}$$

for the exposed portion of the extended half plan form can be evaluated in the manner described above for calculating the distributions of the half plan forms with $0 < \lambda < 1$. For values of ξ at which the distributions may be desired, it is unlikely that $\alpha(\eta_B)$ will correspond to values of α_i for which the airfoil-section thickness is given. Hence, values of $A(\alpha_l,K)$ through $F(\alpha_l,K)$ are obtained from plots of these quantities by letting $\alpha_l = \alpha(\eta_B)$. Furthermore, for values of ξ in the region of the juncture of the half plan form and body, the terms containing $d\eta_l/d\xi$ which were omitted above in finding $\tilde{S}'(\xi,K)$ and $\tilde{S}''(\xi,K)$ (see eqs. (D17) and (D19), respectively) must be evaluated since, generally, for practical configurations, $d\eta_B/d\xi \neq 0$. If the local values of $d\eta_B/d\xi$ are small enough to permit the approximation $d\eta_B/d\xi = 0$, it will be found convenient to treat the exposed extended half plan form as a complete extended half plan form and use equations (D29) to (D31). In so doing, however, care must be exercised in evaluating k_x, k_y, k_z, S_R, and C and in properly shifting the upper (positive η direction) and lower (negative η direction) sheared half plan forms when combining their distributions to calculate the zero-lift interference wave drag between the sheared half plan forms.

The approximate distribution equations in the sample calculations were derived by integrating the basic equations with respect to α in order to take advantage of the approximation made in appendix C for airfoil sections with nonanalytic thickness distributions. Although these approximate equations may be used for half plan forms for which the airfoil-section thickness distribution is given by a simple analytical expression, it is found more convenient, in such cases, to perform the integration of the basic distribution equations in terms of η as indicated by equations (D1) to (D3). For example, the thickness distribution of a parabolic-arc airfoil section, as shown in appendix C, is

$$\tau(\alpha) = 1-\alpha^2 \qquad \text{for} \quad -1 \leq \alpha \leq 1$$

From equation (C17)

$$\tau[\alpha(\xi,\eta,K)] = 1 - \left(\frac{\xi-K\eta}{\tilde{c}(\eta)}\right)^2$$

Therefore, from equation (D7)

$$\tau(\xi,\eta,K) = \Phi(\eta)\left[1 - \left(\frac{\xi-K\eta}{\tilde{c}(\eta)}\right)^2\right]$$

Hence, with the spanwise variation of the thickness, $\Phi(\eta)$, and the boundary of the half plan form specified (with the boundaries known, the spanwise variation of the half chord, $\tilde{c}(\eta)$, is automatically known) all the terms in equations (D1) to (D3) can be evaluated exactly. Furthermore, if $d\eta/d\xi$ for the boundary is continuous, as in the case of an elliptic plan-form wing, the calculation of the distributions is greatly simplified by virtue of the fact that a single equation specifies the limits of integration.

APPENDIX E

A PROCEDURE FOR CALCULATING LIFT DISTRIBUTIONS FOR SHEARED WINGS

The lifting-pressure distribution supported by a wing can be defined as the sum of several superposed distributions. These superposed lifting-pressure distributions can be written in coefficient form as

$$C_p(x,y) = \sum_{n=0}^{N} a_n x^n + \sum_{m=0}^{M} b_m y^m \tag{E1}$$

where x and y are the conventional rectangular coordinates. The constant coefficients a_n and b_m are determined by specified boundary conditions, such as lift, pitching moment, and desired properties of the lift distribution. In reference 9 a method was developed, independent of thickness, for warping delta and arrow plan-form wings with subsonic leading edges and supersonic trailing edges to support a desired lift distribution at 0° angle of attack. The method employed a particular form of equation (E1) which was considered adequate to determine the lifting-pressure distribution of this specialized group of wings with acceptable accuracy. In terms of the dimensionless coordinates defined in appendix A of this report, this particular form of equation (E1) can be written

$$\tilde{C}_p(\xi,\eta) = \tilde{a}_0 + \frac{\tilde{a}_1}{K_0+1}\xi + \tilde{b}_1|\eta| + \tilde{b}_2\eta^2 \tag{E2}$$

The longitudinal lift distribution is then easily obtained from

$$\tilde{L}(\xi) = \int_{\eta_l(\xi)}^{\eta_u(\xi)} \tilde{C}_p(\xi,\eta)\,d\eta \tag{E3}$$

where $\tilde{C}_p(\xi,\eta)$ is given by equation (E2), and $\eta_l(\xi)$ and $\eta_u(\xi)$ are boundaries of the dimensionless plan form.

Just as in the case of the area distribution, the lift distribution can be conveniently determined in terms of that for the sheared wings of each equivalent body of revolution. The local lifting pressure at any point in the plan form is independent of the shearing process. Therefore, with the aid of sketch (g) it is clear that the

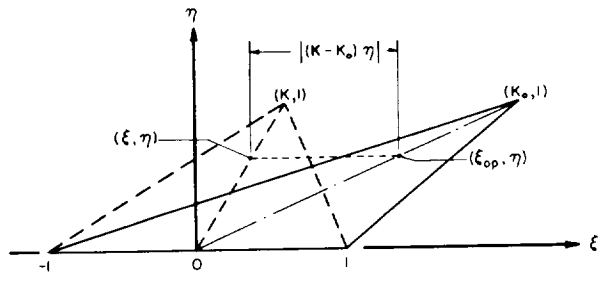

Sketch (g)

local pressure at any point in the sheared plan form, K, can be related to the same local pressure at the corresponding point in the original plan form, K_o, by the following transformation

$$\xi_{op} = \xi-(K-K_o)\eta \tag{E4}$$

where the subscript op denotes the original plan form. Using equation (E4) in equation (E2) the distribution of the lifting-pressure coefficient for sheared wings can be written

$$\tilde{C}_p(\xi,\eta,K) = \tilde{a}_o + \frac{\tilde{a}_1}{K_o+1}\xi + \left(\tilde{b}_1 - \frac{K-K_o}{K_o+1}\tilde{a}_1\right)|\eta| + \tilde{b}_2\eta^2 \tag{E5}$$

The integral of equation (E5) over the plan form in the η direction results in the frontal projection of the force distribution intercepted on the given wing by the parallel oblique planes. The direction of the frontal projection of the net force is perpendicular to the oblique planes (see sketch (a)). With the subscript p used to denote this fact, integration of equation (E5) yields

$$\tilde{L}_p(\xi,K) = \left[\left(\tilde{a}_o + \frac{\tilde{a}_1}{K_o+1}\xi\right)|\eta| + \frac{1}{2}\left(\tilde{b}_1 - \frac{K-K_o}{K_o+1}\tilde{a}_1\right)\eta^2 + \frac{1}{3}\tilde{b}_2|\eta|^3\right]_{\eta_l(\xi,K)}^{\eta_u(\xi,K)} \tag{E6}$$

The values of the limits of integration for the sheared wings are determined in the same manner described in appendix D for area distributions of sheared wings. However, in equation (E6) the limits are expressed in terms of the η integration rather than the α integration. Finally, it is the component of the force distribution in the ζ direction (i.e., the lift distribution) which is employed in equation (2) in this case. Hence, from sketch (a) it is clear that the lift in the ζ direction is

$$\tilde{L}(\xi,K) = \tilde{L}_p(\xi,K)\sin\theta \tag{E7}$$

and

$$\tilde{L}'(\xi,K) = \tilde{L}_p'(\xi,K)\sin\theta \tag{E8}$$

Upon substitution of equation (E8) in the dimensionless form of equation (2) of this report, it is clear that the total wave drag is most conveniently computed by separating the effects on the wave drag of thickness and lift, because only the lifting effect is affected by $\sin\theta$.

APPENDIX F

SPECIAL COMPUTING PROCEDURE FOR THE METHOD OF REFERENCE 3

If equation (3) of this report is integrated by parts, the zero-lift wave drag of any slender configuration can be expressed as a function of the first derivative of the area distribution of the configuration, $S'(x,\beta,\theta)$. From an expansion of $S'(x,\beta,\theta)$ in a Fourier sine series, the infinite series form of the supersonic area rule was developed in reference 2 for calculating zero-lift wave drag for slender-body thin-wing combinations; that is,

$$D(\beta) = \frac{q}{8}\int_0^{2\pi} \sum_{n=1}^{\infty} n[A_n(\beta,\theta)]^2 d\theta \tag{F1}$$

where

$$A_n(\beta,\theta) = \frac{2}{\pi}\int_{-\pi}^{0} \frac{\partial S(x,\beta,\theta)}{\partial x} \sin(n\varphi)d\varphi \tag{F2}$$

and

$$x = \frac{l_1(\beta,\theta)+l(\beta,\theta)}{2} \cos\varphi \tag{F3}$$

The zero-lift wave drag of the equivalent bodies of revolution is given, of course, by

$$D(\beta,\theta) = \frac{\pi}{4} q \sum_{n=1}^{\infty} n[A_n(\beta,\theta)]^2 \tag{F4}$$

The use of the Fourier series requires that application of the supersonic area rule be restricted to configurations for which each equivalent body of revolution satisfies the condition given by equation (4),

$$S'(-l_1,\beta,\theta) = S'(l,\beta,\theta) = 0$$

In reference 3 the Tchebichef form of harmonic analysis was employed to evaluate equation (F2). This permits zero-lift wave-drag calculations by the supersonic area rule from a knowledge of the area distribution of a configuration, $S(x,\beta,\theta)$.

The electronic-machine computing equipment at Ames is programed to evaluate the Fourier sine series coefficients and compute the total zero-lift wave drag of an equivalent body from the values of the area distribution determined by a telereader at 201 points equally spaced over the total length of an equivalent body. Equation (F4) requires an infinite number of terms of the series. However, the practical application of equation (F4) requires that the series be terminated at some value of n, say N, for which the series will converge. The existing machine-computing program is set up to provide zero-lift wave-drag solutions for N up to and including 49. In reference 3 it was demonstrated that for configurations with no discontinuities in the area distribution or the first derivative of the area distribution of a configuration $N = 25$ provides adequate convergence of the series, and the method yields accurate values of total zero-lift wave drag. This was found to be the case for pairs of bodies of revolution of this report which also had no singularities in the second derivative of the area distribution at the ends of the bodies. For pairs of bodies, at least one of which had singularities in the second derivative of the area distribution at the ends, all of the 49 terms available were required to obtain adequate convergence of the series.[4] For this reason 49 terms of the Fourier series for a 201-point analysis of the area distribution of a configuration were used in this report in order to consistently obtain the most accurate results by the method of reference 3.

In addition to the choice of N, there exists another factor which affects the convergence of a Fourier sine series. In reference 10 it is pointed out that in performing a Fourier series analysis of the derivative of the area distribution of a configuration the higher harmonics of the series will be suppressed if the smallest allowed value of the length of the configuration is used. Suppression of the higher harmonics results in a more rapid convergence and a more accurate result for a given N of the series. In the case of multiple-component configurations this is easily accomplished (as suggested in ref. 10) by analyzing the area distribution of each component over its individual length to obtain the zero-lift wave drag of each component alone and by analyzing the combined area distribution of any two components over their total combined length to obtain the zero-lift interference wave drag between components. The effectiveness of this type of individual-length analysis has been adequately demonstrated in the EVALUATION OF THE METHOD section of this report.

The machine-computing program for the method of reference 3 does not yield the zero-lift interference wave drag directly. However, in addition to the total zero-lift wave drag, the program output sheets list the

[4]For bodies 1x1 and 5x5 in the arrangement of figure 3(a), the series actually converges to the analytical value in the first two terms. However, to be consistent, data for these bodies computed by the method of reference 3 are presented for $N = 49$.

Fourier coefficients. The zero-lift interference wave drag can be obtained by proper application of these coefficients. For instance, the Fourier coefficients for a two-component configuration can be written

$$A_{T_n}(\beta,\theta) = A_{E_n}(\beta,\theta)+A_{H_n}(\beta,\theta) \tag{F5}$$

From substitution of equation (F5) in equation (F4) the zero-lift interference wave drag between components of an equivalent body of revolution is given by

$$D_{EH}(\beta,\theta) = \frac{\pi}{2} q \sum_{n=1}^{\infty} nA_{E_n}(\beta,\theta)A_{H_n}(\beta,\theta) \tag{F6}$$

Hence, by means of the Fourier coefficients of the program output sheet, the zero-lift interference wave drag can easily be calculated by manual computations in accordance with equation (F6).

The procedure described above was employed to calculate the dimensionless zero-lift interference wave drag at $M = 1$ for pairs of bodies of this report with $\tilde{\delta} = 0$ (figs. 3(a) and 3(c)). It was found convenient to compute these values according to the relation

$$\tilde{D}_{EH} = (\tilde{D}_{EH})_{n\ even}+(\tilde{D}_{EH})_{n\ odd} \tag{F7}$$

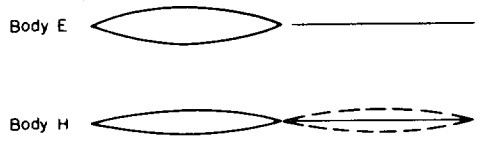

The separate terms of equation (F7) were also used to compute the interference at $M = 1$ for the pairs of bodies of this report with $\tilde{\delta} = 2$ (fig. 3(b)) from the relation

$$\tilde{D}_{EH} = (\tilde{D}_{EH})_{n\ even}-(\tilde{D}_{EH})_{n\ odd} \tag{F8}$$

The derivation of equation (F8) can best be understood by considering the two bodies shown by the solid lines in the upper part of sketch (h). If the area distributions of bodies E and H are analyzed in a Fourier series over the length $-1 \le \xi \le 1$, the contributions to the total area distribution of the even and odd parts of the Fourier series, $\tilde{S}_e(\xi)$ and $\tilde{S}_o(\xi)$, respectively, can be constructed for each body as shown in the sketch.

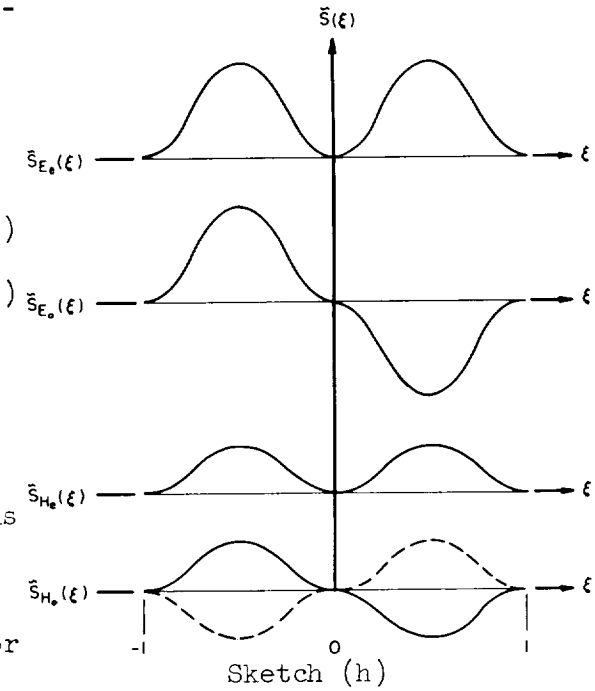

Sketch (h)

The zero-lift interference wave drag between bodies E and H consists of the sum of the zero-lift interference wave-drag contributions of the even parts of the area distribution and that between the odd parts of the area distribution (see eq. (F7)). The zero-lift interference wave drag between the even and odd parts of the area distribution is identically zero (see, e.g., bodies 1×5 of table II). If body H were positioned as shown by the dashed lines ($\tilde{\delta} = 2$), the contribution to the total area distribution of body H of the even part of its area distribution would be the same as before, but the contribution of the odd part of its area distribution would be given by the dashed curve. This dashed curve is exactly the negative of $\tilde{S}_{H_O}(\xi)$ for the original position of body H. Consequently, the zero-lift interference wave drag at M = 1 for the configurations with $\tilde{\delta} = 2$ was calculated by using equation (F8) and the data previously obtained from equation (F7) for the configurations with $\tilde{\delta} = 0$ but analyzed over a length equal to the total combined length of the bodies with $\tilde{\delta} = 2$. Although this procedure has been employed herein to obtain M = 1 interference drag for only $\tilde{\delta} = 2$, it should be noted that the general procedure is applicable for all $\tilde{\delta} > 0$.

REFERENCES

1. Lomax, Harvard: The Wave Drag of Arbitrary Configurations in Linearized Flow as Determined by Areas and Forces in Oblique Planes. NACA RM A55A18, 1955.

2. Jones, Robert T.: Theory of Wing-Body Drag at Supersonic Speeds. NACA Rep. 1284, 1956.

3. Holdaway, George H., and Mersman, William A.: Application of Tchebichef Form of Harmonic Analysis to the Calculation of Zero-Lift Wave Drag of Wing-Body-Tail Combinations. NACA RM A55J28, 1956.

4. Nelson, Robert L., and Welsh, Clement J.: Some Examples of the Applications of the Transonic and Supersonic Area Rules to the Prediction of Wave Drag. NACA RM L56D11, 1957.

5. Sears, W. R.: General Theory of High Speed Aerodynamics. Princeton Series, vol. VI of High Speed Aerodynamics and Jet Propulsion, Princeton Univ. Press, 1954, pp. 235-249.

6. Cahn, Maurice S., and Olstad, Walter B.: A Numerical Method for Evaluating Wave Drag. NACA TN 4258, 1958.

7. Jarmalow, K., and Vandrey, F.: An Exact Method for the Rapid Calculation of the Area Distributions of Wings of Trapezoidal Geometry Based on a New Interpretation of the Area Rule. Eng. Rep. No. 7689, Glenn L. Martin Co., Aug. 24, 1955.

8. Holdaway, George H., and Hatfield, Elaine W.: Investigation of Symmetrical Body Indentations Designed to Reduce the Transonic Zero-Lift Wave Drag of a 45° Swept Wing With an NACA 64A006 Section and With a Thickened Leading-Edge Section. NACA RM A56K26, 1957.

9. Tucker, Warren A.: A Method for the Design of Sweptback Wings Warped to Produce Specified Flight Characteristics at Supersonic Speeds. NACA Rep. 1226, 1955. (Supersedes NACA RM L51F08)

10. Baldwin, Barrett S., and Dickey, Robert R.: Application of Wing-Body Theory to Drag Reduction at Low Supersonic Speeds. NACA RM A54J19, 1955.

TABLE I.- ZERO-LIFT WAVE-DRAG EQUATIONS FOR SEVERAL CONFIGURATIONS

Configuration	Component	Zero-lift wave drag for equivalent-body component			
		Component alone		Interference between components	
		Equation	Averaging process*	Equation	Averaging process*
E **	E	(24)	None required	---	---
E or	E	(28)	None required	---	---
E H	E	(28)	None required	(42)	Analytical (Inherent in equation (42))
	H				
*** P_1 W_1 B W_2 P_2	W_1	(28)	Graphical	(34) or (42) for $\beta d = 0$	Graphical
	W_2				
	W_1	(28)	Graphical	--do--	Graphical
	B		None required		
	W_1	(28)	Graphical	--do--	Graphical
	P_1		None required		
	W_1	(28)	Graphical	--do--	Graphical
	P_2		None required		
	P_1	(28)	None required	(42)	Analytical (Inherent in equation (42))
	P_2				
	P_1	(28)	None required	(42)	Analytical (Inherent in equation (42))
	B				

* $\frac{1}{2\pi}\int_0^{2\pi} D(\beta,\theta)d\theta$

**For this configuration only, $S'(l) \neq 0$.

***W_2B, W_2P_1, W_2P_2, and P_2B are treated in the same manner as W_1B, W_1P_2, W_1P_1, and P_1B, respectively, because of the symmetry of the sheared configurations for $0 \leq \theta \leq \pi$ and $\pi \leq \theta \leq 2\pi$.

TABLE II.- DIMENSIONLESS ZERO-LIFT INTERFERENCE WAVE DRAG AT MACH NUMBER 1 FOR CONFIGURATIONS OF FIGURE 3

1	2	3	4	5	6	7	8	9
Bodies	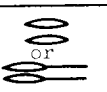	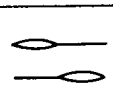		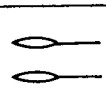	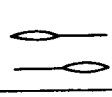		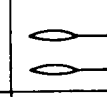	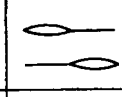
	$\tilde{\delta} = 0$	$\tilde{\delta} = 2$	$\tilde{\delta} = 0$	$\tilde{\delta} = 0$	$\tilde{\delta} = 2$	$\tilde{\delta} = 0$	$\tilde{\delta} = 0$	$\tilde{\delta} = 2$
	Analytical		Method of reference 3			Present method		
1*x1*	7.064	1.068	7.065	6.909	1.053	7.1	7.1	0.98
1*x2	5.892			5.885	.538	5.9	5.9	.51
1*x3	5.152			5.153	.359	5.2	5.2	.35
1*x4	4.636			4.636	.280	4.6	4.6	.28
1*x5*	0			-.208	.650			.59
1*x6	0			0	.245			.22
1*x7	0			.004	.120			.12
1*x8	0			0	.074			.074
2x2	7.368	.316	7.368	7.367	.318	7.367	7.358	.316
2x3	7.733			7.728	.234	7.730	7.728	.234
2x4	7.744			7.742	.191	7.741	7.736	.191
2x5*	0			.007	.286			.26
2x6	0			.004	.119			.119
2x7	0			0	.068			.069
2x8	0			0	.045			.045
3x3	9.014	.178	9.014	9.015	.178	9.012	9.003	.178
3x4	9.658			9.658	.148	9.650	9.650	.148
3x5*	0			.001	.166			.16
3x6	0			0	.081			.081
3x7	0			0	.049			.048
3x8	0			0	.033			.033
4x4	10.86	.123	10.86	10.85	.124	10.85	10.84	.124
4x5*	0			0	.123			.12
4x6	0			0	.062			.062
4x7	0			0	.038			.038
4x8	0			0	.026			.026
5*x5*	4.710	-.487	4.733	4.549	-.452	4.7	4.7	-.42
5*x6	2.946			2.942	-.158	2.9	2.9	-.14
5*x7	2.061			2.063	-.070	2.1	2.0	-.067
5*x8	1.545			1.546	-.039	1.5	1.5	-.041
6x6	2.947	-.055	2.947	2.945	-.056	2.946	2.941	-.055
6x7	2.578			2.578	-.029	2.578	2.573	-.030
6x8	2.213			2.213	-.018	2.212	2.209	-.018
7x7	2.576	-.017	2.576	2.576	-.017	2.575	2.570	-.017
7x8	2.414			2.414	-.011	2.414	2.411	-.011
8x8	2.413	-.007	2.413	2.412	-.007	2.412	2.406	-.007

*Denotes body with singularities in $\tilde{S}''(\xi)$ at the ends.

TABLE III.- DIMENSIONLESS TOTAL ZERO-LIFT WAVE DRAG AT MACH NUMBER 1 FOR SEVERAL CONFIGURATIONS OF FIGURE 3

1	2	3	4	5	6	7	8	9
Bodies							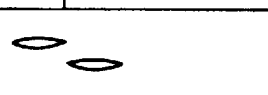	
	Total or individual length		Total or individual length		Total length		Individual length	
	Analytical		Method of reference 3	Present method	Method of reference 3	Present method	Method of reference 3	Present method
1*x1*	14.128	8.132	14.170	14.2	7.962 (-2.09)	8.08 (-0.64)	8.138 (0.07)	8.08 (-0.64)
2x2	14.736	7.684	14.736	14.734	7.685 (0.01)	7.674 (-0.13)	7.686 (0.03)	7.683 (-0.01)
3x3	18.028	9.192	18.028	18.024	9.193 (0.01)	9.181 (-0.12)	9.192 (0.00)	9.190 (-0.02)
4x4	21.72	10.983	21.72	21.70	10.974 (-0.08)	10.964 (-0.17)	10.984 (0.01)	10.974 (-0.08)
5*x5*	9.420	4.223	9.466	9.4	4.097 (-2.98)	4.28 (1.35)	4.281 (1.37)	4.28 (1.35)
6x6	5.894	2.892	5.894	5.892	2.889 (-0.10)	2.886 (-0.21)	2.891 (-0.03)	2.891 (-0.03)
7x7	5.152	2.559	5.152	5.150	2.559 (0.00)	2.553 (-0.23)	2.559 (0.00)	2.558 (-0.04)
8x8	4.826	2.406	4.826	4.824	2.405 (-0.04)	2.399 (-0.29)	2.406 (0.00)	2.405 (-0.04)

*Body with singularities in $\tilde{S}''(\xi)$ at the ends.

TABLE IV.- VALUES OF THE DIMENSIONLESS ZERO-LIFT INTERFERENCE WAVE-DRAG INTEGRAL FUNCTION, $\tilde{I}(\tilde{a}_{ij}, \tilde{B})$

	$\tilde{I}(\tilde{a}_{ij}, \tilde{B})$*															
$\tilde{a}_{ij}$ \ $\tilde{B}$	0	0.2	0.4	0.6	0.8	1.0	1.2	1.4	1.6	1.8	2.0	2.2	2.4	2.6	2.8	3.0
0	0	0	0	0	0	0	0	0	0	0	0	0	0	0	0	0
.01	-.000461															
.02	-.001565															
.03	-.003156															
.04	-.005150															
.05	-.007489															
.06	-.010128															
.07	-.013030															
.08	-.016165															
.09	-.019504															
.10	-.023026															
.11	-.026708															
.12	-.030532															
.13	-.034480															
.14	-.038536															
.15	-.042685															
.16	-.046914															
.17	-.051210															
.18	-.055559															
.19	-.059952															
.20	-.064378															
.21	-.068825	.000017														
.22	-.073284	.000095														
.23	-.077746	.000262														
.24	-.082202	.000536														
.25	-.086643	.000935														
.26	-.091062	.001472														
.27	-.095450	.002160														
.28	-.099801	.003011														
.29	-.104105	.004036														
.30	-.108358	.005243														
.31	-.112551	.006644														
.32	-.116678	.008245														
.33	-.120733	.010056														
.34	-.124710	.012083														
.35	-.128603	.014336														
.36	-.132406	.016820														
.37	-.136113	.019542														
.38	-.139719	.022510														
.39	-.143219	.025730														
.40	-.146607	.029206														
.41	-.149878	.032946	.000012													
.42	-.153027	.036955	.000067													
.43	-.156050	.041240	.000185													
.44	-.158942	.045803	.000380													
.45	-.161698	.050651	.000664													

* $\tilde{I}(\tilde{a}_{ij}, \tilde{B}) = \frac{1}{\pi}\int_0^{\pi} (\tilde{a}_{ij} - B\cos\theta)^2 \ln\left|\tilde{a}_{ij} - \tilde{B}\cos\theta\right| d\theta$; equation (B2)

$\tilde{a}_{ij} = \xi_{E_i} - (\xi_{H_j} + \bar{\delta})$; equation (B3)

$\tilde{B} = \frac{\beta d}{l}$; equation (B4)

TABLE IV.- VALUES OF THE DIMENSIONLESS ZERO-LIFT INTERFERENCE WAVE-DRAG INTEGRAL FUNCTION, $\tilde{I}(\tilde{a}_{ij}, \tilde{B})$ - Continued

$\tilde{I}(\tilde{a}_{ij}, \tilde{B})$																
$\tilde{a}_{ij}$ \ $\tilde{B}$	0	0.2	0.4	0.6	0.8	1.0	1.2	1.4	1.6	1.8	2.0	2.2	2.4	2.6	2.8	3.0
.46	-.164313	.055790	.001046	0	0	0	0	0	0	0	0	0	0	0	0	0
.47	-.166784	.061225	.001537													
.48	-.169106	.066958	.002144													
.49	-.171275	.072996	.002876													
.50	-.173287	.079343	.003739													
.51	-.175137	.086003	.004741													
.52	-.176822	.092981	.005887													
.53	-.178337	.100281	.007186													
.54	-.179680	.107907	.008641													
.55	-.180846	.115862	.010259													
.56	-.181831	.124152	.012046													
.57	-.182632	.132780	.014005													
.58	-.183246	.141749	.016144													
.59	-.183669	.151063	.018465													
.60	-.183897	.160727	.020974													
.61	-.183928	.170743	.023676	.000010												
.62	-.183757	.181115	.026574	.000055												
.63	-.183382	.191847	.029674	.000152												
.64	-.182799	.202942	.032980	.000311												
.65	-.182006	.214402	.036494	.000543												
.66	-.180999	.226233	.040223	.000856												
.67	-.179774	.238435	.044167	.001257												
.68	-.178330	.251014	.048333	.001755												
.69	-.176663	.263971	.052724	.002354												
.70	-.174771	.277311	.057343	.003061												
.71	-.172649	.291035	.062194	.003883												
.72	-.170297	.305147	.067278	.004824												
.73	-.167709	.319651	.072604	.005889												
.74	-.164885	.334547	.078171	.007084												
.75	-.161821	.349841	.083982	.008412												
.76	-.158515	.365534	.090041	.009879												
.77	-.154963	.381629	.096353	.011490												
.78	-.151164	.398087	.102919	.013247												
.79	-.147114	.415036	.109741	.015155												
.80	-.142812	.432352	.116826	.017220												
.81	-.138254	.450083	.124172	.019443	.000009											
.82	-.133438	.468227	.131786	.021828	.000048											
.83	-.128362	.486791	.139669	.024381	.000131											
.84	-.123024	.505773	.147823	.027103	.000270											
.85	-.117420	.525179	.156252	.029998	.000471											
.86	-.111549	.545010	.164957	.033071	.000743											
.87	-.105407	.565269	.173943	.036323	.001090											
.88	-.098994	.585957	.183211	.039759	.001522											
.89	-.092306	.607079	.192766	.043381	.002041											
.90	-.085342	.628635	.202607	.047193	.002654											
.91	-.078099	.650627	.212738	.051196	.003369											
.92	-.070574	.673058	.223161	.055396	.004185											
.93	-.062766	.695932	.233881	.059793	.005111											
.94	-.054673	.719249	.244899	.064392	.006147											
.95	-.046292	.743011	.256214	.069195	.007301											
.96	-.037622	.767221	.267831	.074204	.008576											
.97	-.028659	.791881	.279755	.079424	.009974											
.98	-.019403	.816995	.291983	.084854	.011501											
.99	-.009850	.842562	.304521	.090501	.013161											

TABLE IV.- VALUES OF THE DIMENSIONLESS ZERO-LIFT INTERFERENCE WAVE-DRAG INTEGRAL FUNCTION, $\tilde{I}(\tilde{a}_{1j}, \tilde{B})$ - Continued

$\tilde{I}(\tilde{a}_{1j}, \tilde{B})$																
$\tilde{a}_{1j}$ \ $\tilde{B}$	0	0.2	0.4	0.6	0.8	1.0	1.2	1.4	1.6	1.8	2.0	2.2	2.4	2.6	2.8	3.0
1.00	0	.868587	.317372	.096363	.014955	0	0	0	0	0	0	0	0	0	0	0
1.01	.010150	.895069	.330482	.102446	.016887	.000001										
1.02	.020603	.922012	.344012	.108750	.018962	.000042										
1.03	.031359	.949417	.357808	.115279	.021182	.000118										
1.04	.042421	.977287	.371923	.122036	.023550	.000241										
1.05	.053791	1.005623	.386361	.129023	.026069	.000422										
1.06	.065471	1.034428	.401123	.136240	.028743	.000663										
1.07	.077462	1.063704	.416210	.143691	.031573	.000975										
1.08	.089767	1.093450	.431626	.151379	.034566	.001362										
1.09	.102388	1.123672	.447371	.159305	.037719	.001827										
1.10	.115325	1.154370	.463450	.167473	.041039	.002376										
1.11	.128582	1.185545	.479861	.175884	.044525	.003014										
1.12	.142160	1.217201	.496608	.184539	.048182	.003747										
1.13	.156060	1.249338	.513693	.193442	.052014	.004575										
1.14	.170284	1.281957	.531120	.202593	.056023	.005505										
1.15	.184835	1.315063	.548886	.211996	.060207	.006539										
1.16	.199714	1.348654	.566995	.221654	.064574	.007679										
1.17	.214922	1.382736	.585452	.231567	.069125	.008934										
1.18	.230462	1.417308	.604253	.241737	.073861	.010303										
1.19	.246335	1.452371	.623406	.252162	.078785	.011790										
1.20	.262543	1.487929	.642909	.262858	.083897	.013397										
1.21	.279087	1.523981	.662763	.273812	.089204	.015130	.000007									
1.22	.295970	1.560533	.682971	.285031	.094705	.016991	.000038									
1.23	.313192	1.597581	.703539	.296519	.100403	.018982	.000106									
1.24	.330755	1.635132	.724462	.308274	.106299	.021107	.000218									
1.25	.348662	1.673183	.745745	.320300	.112398	.023366	.000384									
1.26	.366913	1.711738	.767388	.332602	.118699	.025766	.000605									
1.27	.385510	1.750802	.789395	.345175	.125206	.028304	.000889									
1.28	.404456	1.790370	.811767	.358025	.131920	.030989	.001242									
1.29	.423750	1.830447	.834503	.371156	.138844	.033818	.001667									
1.30	.443396	1.871034	.857610	.384563	.145978	.036797	.002171									
1.31	.463394	1.912133	.881083	.398253	.153326	.039927	.002754									
1.32	.483746	1.953747	.904930	.412227	.160890	.043212	.003422									
1.33	.504453	1.995873	.929148	.426487	.168671	.046651	.004178									
1.34	.525518	2.038517	.953739	.441031	.176669	.050248	.005027									
1.35	.546941	2.081678	.978709	.455865	.184890	.054006	.005974									
1.36	.568724	2.125359	1.004055	.470989	.193333	.057928	.007016									
1.37	.590868	2.169561	1.029781	.486405	.202002	.062014	.008164									
1.38	.613376	2.214287	1.055886	.502114	.210897	.066269	.009414									
1.39	.636248	2.259534	1.082372	.518119	.220018	.070691	.010775									
1.40	.659486	2.305308	1.109244	.534420	.229372	.075283	.012245									
1.41	.683091	2.351608	1.136497	.551019	.238957	.080052	.013828	.000006								
1.42	.707065	2.398475	1.164141	.567917	.248775	.084993	.015531	.000035								
1.43	.731408	2.445795	1.192171	.585117	.258828	.090117	.017349	.000100								
1.44	.756124	2.493683	1.220590	.602622	.269119	.095416	.019292	.000206								
1.45	.781212	2.542106	1.249402	.620428	.279648	.100897	.021359	.000358								
1.46	.806675	2.591062	1.278603	.638540	.290417	.106562	.023552	.000561								
1.47	.832514	2.640555	1.308200	.656962	.301427	.112410	.025876	.000825								
1.48	.858729	2.690581	1.338191	.675692	.312682	.118446	.028332	.001151								
1.49	.885323	2.741147	1.368579	.694730	.324180	.124673	.030920	.001546								
1.50	.912296	2.792252	1.399363	.714085	.335928	.131090	.033647	.002012								
1.51	.939651	2.843899	1.430550	.733750	.347921	.137698	.036510	.002551								
1.52	.967388	2.896085	1.462135	.753730	.360165	.144498	.039515	.003172								
1.53	.995509	2.948817	1.494124	.774028	.372663	.151499	.042662	.003872								

TABLE IV.- VALUES OF THE DIMENSIONLESS ZERO-LIFT INTERFERENCE WAVE-DRAG INTEGRAL FUNCTION, $\tilde{I}(\tilde{a}_{ij}, \tilde{B})$ - Continued

$\tilde{a}_{ij}$ \ $\tilde{B}$	0	0.2	0.4	0.6	0.8	1.0	1.2	1.4	1.6	1.8	2.0	2.2	2.4	2.6	2.8	3.0
	$\tilde{I}(\tilde{a}_{ij}, \tilde{B})$															
1.54	1.024015	3.002092	1.526515	.794641	.385411	.158696	.045959	.004660	0	0	0	0	0	0	0	0
1.55	1.052907	3.055914	1.559311	.815574	.398415	.166091	.049394	.005535	↓	↓	↓	↓	↓	↓	↓	↓
1.56	1.082187	3.110224	1.592515	.836827	.411673	.173690	.052984	.006503								
1.57	1.111856	3.165202	1.626123	.858405	.425191	.181488	.056724	.007567								
1.58	1.141915	3.220668	1.660140	.880303	.438968	.189494	.060621	.008724								
1.59	1.172366	3.276686	1.694569	.902528	.453002	.197705	.064672	.009983								
1.60	1.203209	3.333260	1.729410	.925075	.467304	.206122	.068875	.011347								
1.61	1.234447	3.390386	1.764664	.947955	.481863	.214750	.073241	.012814	.000004							
1.62	1.266079	3.448065	1.800329	.971157	.496691	.223588	.077767	.014394	.000030							
1.63	1.298108	3.506303	1.836412	.994694	.511783	.232641	.082456	.016082	.000090							
1.64	1.330535	3.565094	1.872911	1.018561	.527144	.241910	.087310	.017880	.000188							
1.65	1.363361	3.624448	1.909823	1.042758	.542775	.251391	.092332	.019799	.000331							
1.66	1.396587	3.684360	1.947160	1.067344	.558675	.261087	.097521	.021830	.000522							
1.67	1.430214	3.744834	1.984917	1.092165	.574844	.271002	.102878	.023984	.000768							
1.68	1.464244	3.805869	2.023096	1.117368	.591289	.281142	.108408	.026262	.001074							
1.69	1.498677	3.867470	2.061693	1.142913	.608012	.291499	.114111	.028662	.001443							
1.70	1.533516	3.929634	2.100718	1.168795	.625007	.302082	.119992	.031191	.001880							
1.71	1.568760	3.992364	2.140166	1.195068	.642278	.312889	.126046	.033850	.002384							
1.72	1.604412	4.055663	2.180042	1.221585	.659830	.323925	.132279	.036634	.002965							
1.73	1.640473	4.119524	2.220344	1.248489	.677661	.335182	.138695	.039554	.003619							
1.74	1.676943	4.183961	2.261078	1.275740	.695777	.346671	.145288	.042608	.004358							
1.75	1.713823	4.248969	2.302239	1.303338	.714168	.358394	.152065	.045797	.005179							
1.76	1.751116	4.314544	2.343830	1.331281	.732848	.370345	.159035	.049130	.006084							
1.77	1.788822	4.380696	2.385855	1.359572	.751814	.382530	.166183	.052599	.007076							
1.78	1.826942	4.447421	2.428316	1.388213	.771061	.394948	.173522	.056210	.008161							
1.79	1.865477	4.514720	2.471207	1.417201	.790598	.407603	.181048	.059967	.009342							
1.80	1.904430	4.582598	2.514537	1.446544	.810427	.420497	.188764	.063870	.010620	↓	↓	↓	↓	↓	↓	↓
1.81	1.943798	4.651050	2.558301	1.476240	.830544	.433629	.196677	.067923	.011994	.000003						
1.82	1.983586	4.720084	2.602492	1.506284	.850954	.446995	.204782	.072122	.013470	.000031						
1.83	2.023794	4.789696	2.647151	1.536690	.871653	.460610	.213081	.076474	.015051	.000085						
1.84	2.064424	4.859884	2.692233	1.567448	.892648	.474466	.221579	.080978	.016737	.000179						
1.85	2.105473	4.930662	2.737760	1.598565	.913937	.488563	.230276	.085637	.018528	.000314						
1.86	2.146946	5.002017	2.783728	1.630040	.935524	.502909	.239172	.090452	.020437	.000490						
1.87	2.188844	5.073962	2.830138	1.661872	.957406	.517498	.248264	.095426	.022452	.000724						
1.88	2.231167	5.146486	2.876996	1.694069	.979588	.532335	.257564	.100556	.024584	.001012						
1.89	2.273916	5.219599	2.924295	1.726623	1.002070	.547420	.267067	.105852	.026830	.001360						
1.90	2.317093	5.293300	2.972044	1.759544	1.024852	.562761	.276777	.111309	.029199	.001769						
1.91	2.360697	5.367588	3.020240	1.792824	1.047938	.578347	.286692	.116932	.031687	.002253						
1.92	2.404732	5.442464	3.068885	1.826474	1.071323	.594191	.296816	.122723	.034297	.002794						
1.93	2.449196	5.517933	3.117982	1.860488	1.095019	.610284	.307145	.128674	.037032	.003413						
1.94	2.494092	5.593993	3.167532	1.894869	1.119016	.626631	.317690	.134798	.039894	.004113						
1.95	2.539421	5.670647	3.217530	1.929618	1.143318	.643240	.328445	.141091	.042886	.004884						
1.96	2.585183	5.747892	3.267982	1.964740	1.167934	.660100	.339416	.147556	.046000	.005734						
1.97	2.631380	5.825735	3.318888	2.000234	1.192858	.677230	.350598	.154203	.049254	.006674						
1.98	2.678013	5.904167	3.370255	2.036094	1.218086	.694608	.361996	.161013	.052639	.007698						
1.99	2.725082	5.983202	3.422067	2.072328	1.243630	.712252	.373613	.168002	.056160	.008809						
2.00	2.772589	6.062831	3.474347	2.108934	1.269486	.730158	.385449	.175175	.059816	.010015	↓	↓	↓	↓	↓	↓
2.01	2.820534	6.143059	3.527082	2.145918	1.295652	.748327	.397498	.182523	.063610	.011310	.000009					
2.02	2.868919	6.223888	3.580275	2.183275	1.322132	.766762	.409775	.190049	.067549	.012708	.000031					
2.03	2.917745	6.305320	3.633931	2.221013	1.348930	.785461	.422277	.197759	.071622	.014196	.000087					
2.04	2.967012	6.387350	3.688049	2.259124	1.376046	.804426	.434995	.205652	.075847	.015786	.000170					
2.05	3.016722	6.469985	3.742626	2.297614	1.403481	.823661	.447945	.213727	.080211	.017480	.000301					
2.06	3.066875	6.553219	3.797668	2.336489	1.431234	.843163	.461116	.221995	.084723	.019276	.000470					

TABLE IV.- VALUES OF THE DIMENSIONLESS ZERO-LIFT INTERFERENCE WAVE-DRAG INTEGRAL FUNCTION, $\tilde{I}(\tilde{a}_{ij}, \tilde{B})$ - Continued

	$\tilde{I}(\tilde{a}_{ij}, \tilde{B})$															
$\tilde{a}_{ij}$ \ $\tilde{B}$	0	0.2	0.4	0.6	0.8	1.0	1.2	1.4	1.6	1.8	2.0	2.2	2.4	2.6	2.8	3.0
2.07	3.117473	6.637061	3.853175	2.375741	1.459306	.862938	.474511	.230446	.089389	.021183	.000695	0	0	0	0	0
2.08	3.168516	6.721511	3.909146	2.415380	1.487693	.882982	.488141	.239082	.094193	.023196	.000963					
2.09	3.220006	6.806561	3.965590	2.455397	1.516407	.903300	.501998	.247912	.099155	.025314	.001294					
2.10	3.271944	6.892224	4.022496	2.495800	1.545445	.923888	.516083	.256934	.104274	.027552	.001680					
2.11	3.324329	6.978491	4.079870	2.536586	1.574807	.944755	.530402	.266150	.109545	.029897	.002136					
2.12	3.377164	7.065373	4.137713	2.577757	1.604488	.965899	.544954	.275558	.114971	.032359	.002660					
2.13	3.430450	7.152860	4.196030	2.619316	1.634502	.987313	.559739	.285157	.120547	.034945	.003240					
2.14	3.484186	7.240960	4.254815	2.661269	1.664841	1.009008	.574759	.294957	.126293	.037639	.003902					
2.15	3.538375	7.329725	4.314071	2.703606	1.695512	1.030982	.590020	.304951	.132188	.040460	.004636					
2.16	3.593017	7.419000	4.373800	2.746330	1.726504	1.053238	.605509	.315145	.138255	.043413	.005445					
2.17	3.648113	7.508941	4.434006	2.789448	1.757828	1.075772	.621247	.325537	.144484	.046478	.006333					
2.18	3.703664	7.599497	4.494688	2.832955	1.789488	1.098591	.637216	.336134	.150869	.049674	.007309					
2.19	3.759670	7.690666	4.555846	2.876858	1.821473	1.121690	.653433	.346934	.157425	.052995	.008366					
2.20	3.816134	7.782457	4.617481	2.921153	1.853800	1.145073	.669889	.357940	.164145	.056448	.009512					
2.21	3.873055	7.874861	4.679591	2.965843	1.886453	1.168746	.686588	.369145	.171035	.060029	.010740	.000004				
2.22	3.930434	7.967888	4.742178	3.010932	1.919446	1.192698	.703524	.380550	.178090	.063747	.012061	.000030				
2.23	3.988274	8.061530	4.805251	3.056411	1.952769	1.216940	.720717	.392172	.185324	.067594	.013478	.000082				
2.24	4.046573	8.155797	4.868804	3.102292	1.986436	1.241470	.738155	.404003	.192726	.071585	.014987	.000165				
2.25	4.105334	8.250684	4.932836	3.148571	2.020450	1.266289	.755831	.416040	.200307	.075705	.016595	.000292				
2.26	4.164557	8.346189	4.997352	3.195252	2.054772	1.291401	.773763	.428285	.208050	.079970	.018302	.000446				
2.27	4.224243	8.442325	5.062351	3.242304	2.089457	1.316801	.791937	.440743	.215980	.084370	.020111	.000662				
2.28	4.284394	8.539076	5.127829	3.289808	2.124475	1.342496	.810369	.453420	.224087	.088915	.022011	.000925				
2.29	4.345009	8.636460	5.193801	3.337685	2.159836	1.368483	.829052	.466299	.232369	.093596	.024011	.001236				
2.30	4.406089	8.734462	5.260256	3.385969	2.195542	1.394760	.847985	.479407	.240824	.098426	.026157	.001609				
2.31	4.467637	8.833095	5.327196	3.434661	2.231583	1.421337	.867171	.492723	.249467	.103407	.028385	.002046				
2.32	4.529651	8.932359	5.394625	3.483756	2.267983	1.448205	.886615	.506259	.258290	.108519	.030727	.002532				
2.33	4.592134	9.032248	5.462543	3.533254	2.304720	1.475377	.906309	.520005	.267297	.113796	.033177	.003092				
2.34	4.655086	9.132775	5.530941	3.583158	2.341808	1.502842	.926261	.533982	.276488	.119222	.035739	.003724				
2.35	4.718509	9.233917	5.599842	3.633467	2.379237	1.530608	.946473	.548174	.285874	.124793	.038421	.004428				
2.36	4.782402	9.335694	5.669235	3.684188	2.417019	1.558672	.966942	.562590	.295430	.130521	.041213	.005190				
2.37	4.846767	9.438108	5.739110	3.735322	2.455144	1.587031	.987671	.577219	.305192	.136395	.044126	.006050				
2.38	4.911604	9.541152	5.809486	3.786859	2.493626	1.615704	1.008659	.592081	.315128	.142431	.047159	.006966				
2.39	4.976915	9.644835	5.880355	3.838813	2.532457	1.644670	1.029906	.607166	.325262	.148628	.050311	.007983				
2.40	5.042700	9.749142	5.951717	3.891178	2.571637	1.673943	1.051422	.622482	.335584	.154970	.053589	.009073				
2.41	5.108960	9.854086	6.023571	3.943953	2.611169	1.703519	1.073199	.638016	.346101	.161475	.056980	.010246	.000002			
2.42	5.175696	9.959671	6.095933	3.997140	2.651054	1.733402	1.095244	.653801	.356811	.168150	.060529	.011497	.000030			
2.43	5.242909	10.065900	6.168778	4.050743	2.691300	1.763593	1.117553	.669779	.367716	.174981	.064185	.012855	.000080			
2.44	5.310600	10.172750	6.242131	4.104766	2.731894	1.794090	1.140122	.686000	.378815	.181973	.067962	.014296	.000151			
2.45	5.378768	10.280251	6.315976	4.159199	2.772841	1.824892	1.162958	.702447	.390111	.189127	.071889	.015832	.000277			
2.46	5.447416	10.388389	6.390326	4.214049	2.814157	1.856006	1.186064	.719137	.401605	.196455	.075944	.017461	.000424			
2.47	5.516545	10.497161	6.465174	4.269324	2.855819	1.887432	1.209446	.736055	.413297	.203947	.080113	.019181	.000626			
2.48	5.586153	10.606584	6.540530	4.325004	2.897848	1.919159	1.233094	.753208	.425193	.211597	.084428	.021005	.000880			
2.49	5.656244	10.716641	6.616381	4.381112	2.940232	1.951204	1.257011	.770593	.437283	.219421	.088873	.022924	.001177			
2.50	5.726817	10.827344	6.692736	4.437640	2.982979	1.983563	1.281204	.788219	.449587	.227416	.093463	.024952	.001537			
2.51	5.797873	10.938691	6.769596	4.494590	3.026084	2.016233	1.305662	.806078	.462084	.235592	.098190	.027078	.001956			
2.52	5.869414	11.050682	6.846961	4.551967	3.069553	2.049211	1.330402	.824175	.474792	.243924	.103058	.029304	.002426			
2.53	5.941439	11.163313	6.924830	4.609759	3.113388	2.082523	1.355409	.842512	.487701	.252434	.108063	.031650	.002958			
2.54	6.013950	11.276597	7.003207	4.667973	3.157580	2.116134	1.380702	.861085	.500817	.261118	.113213	.034096	.003562			
2.55	6.086947	11.390525	7.082085	4.726614	3.202139	2.150074	1.406258	.879902	.514136	.269980	.118510	.036651	.004231			
2.56	6.160432	11.505096	7.161476	4.785687	3.247073	2.184323	1.432096	.898951	.527676	.279018	.123952	.039322	.004969			
2.57	6.234404	11.620317	7.241376	4.845178	3.292362	2.218888	1.458211	.918261	.541415	.288234	.129543	.042104	.005786			
2.58	6.308865	11.736192	7.321790	4.905095	3.338014	2.253781	1.484615	.937802	.555363	.297628	.135269	.044995	.006678			
2.59	6.383816	11.852717	7.402704	4.965441	3.384040	2.288991	1.511288	.957589	.569527	.307204	.141155	.048007	.007633			

TABLE IV.- VALUES OF THE DIMENSIONLESS ZERO-LIFT INTERFERENCE WAVE-DRAG INTEGRAL FUNCTION, $\tilde{I}(a_{ij}, \tilde{B})$ - Concluded

	$\tilde{I}(\tilde{a}_{ij}, \tilde{B})$															
$\tilde{a}_{ij}$ \ $\tilde{B}$	0	0.2	0.4	0.6	0.8	1.0	1.2	1.4	1.6	1.8	2.0	2.2	2.4	2.6	2.8	3.0
2.60	6.459257	11.969889	7.484133	5.026219	3.430436	2.324520	1.538249	.977618	.583904	.316965	.147186	.051132	.008683	0	0	0
2.61	6.535190	12.087710	7.566076	5.087427	3.477202	2.360369	1.565491	.997895	.598497	.326899	.153368	.054384	.009808	.000009		
2.62	6.611614	12.206185	7.648527	5.149059	3.524337	2.396541	1.593013	1.018422	.613294	.337022	.159706	.057750	.011015	.000022		
2.63	6.688531	12.325317	7.731505	5.211127	3.571846	2.433043	1.620814	1.039190	.628318	.347333	.166192	.061237	.012304	.000081		
2.64	6.765941	12.445098	7.814984	5.273627	3.619721	2.469868	1.648899	1.060214	.643549	.357828	.172843	.064852	.013688	.000155		
2.65	6.843845	12.565537	7.898978	5.336556	3.667976	2.507016	1.677279	1.081486	.659003	.368498	.179641	.068583	.015155	.000268		
2.66	6.922244	12.686629	7.983488	5.399917	3.716594	2.544490	1.705934	1.103010	.674675	.379364	.186599	.072455	.016721	.000417		
2.67	7.001139	12.808375	8.068524	5.463710	3.765591	2.582287	1.734884	1.124785	.690561	.390417	.193719	.076447	.018363	.000605		
2.68	7.080531	12.930781	8.154063	5.527943	3.814965	2.620421	1.764120	1.146808	.706665	.401661	.200993	.080559	.020108	.000849		
2.69	7.160419	13.053836	8.240131	5.592607	3.864720	2.658870	1.793643	1.169090	.722999	.413101	.208433	.084809	.021955	.001143		
2.70	7.240805	13.177567	8.326771	5.657710	3.914840	2.697664	1.823456	1.191619	.739559	.424722	.216024	.089193	.023894	.001480		
2.71	7.321690	13.301944	8.413816	5.723253	3.965340	2.736772	1.853559	1.214411	.756331	.436542	.223789	.093697	.025931	.001883		
2.72	7.403075	13.426982	8.501441	5.789228	4.016221	2.776221	1.883952	1.237453	.773333	.448553	.231714	.098348	.028064	.002339		
2.73	7.484959	13.552679	8.589583	5.855641	4.067481	2.816000	1.914630	1.260750	.790551	.460753	.239810	.103127	.030307	.002848		
2.74	7.567345	13.679034	8.678246	5.922498	4.119122	2.856108	1.945619	1.284309	.807998	.473160	.248060	.108040	.032646	.003432		
2.75	7.650232	13.806057	8.767438	5.989794	4.171142	2.896553	1.976885	1.308122	.825670	.485757	.256480	.113100	.035095	.004068		
2.76	7.733621	13.933748	8.857144	6.057529	4.223547	2.937327	2.008456	1.332201	.843574	.498556	.265080	.118291	.037657	.004784		
2.77	7.817514	14.062096	8.947379	6.125707	4.276327	2.978446	2.040313	1.356538	.861711	.511545	.273834	.123616	.040319	.005568		
2.78	7.901910	14.191100	9.038139	6.194324	4.329492	3.019894	2.072466	1.381128	.880063	.524740	.282769	.129096	.043095	.006424		
2.79	7.986810	14.320784	9.129424	6.263380	4.383044	3.061679	2.104917	1.405989	.898666	.538137	.291863	.134711	.045980	.007343		
2.80	8.072216	14.451125	9.221235	6.332890	4.436975	3.103796	2.137673	1.431111	.917482	.551731	.301141	.140462	.048977	.008352		
2.81	8.158128	14.582129	9.313570	6.402836	4.491299	3.146254	2.170718	1.456495	.936531	.565523	.310584	.146371	.052084	.009434	.000014	
2.82	8.244546	14.713803	9.406438	6.473240	4.545994	3.189062	2.204068	1.482144	.955820	.579520	.320213	.152425	.055312	.010588	.000040	
2.83	8.331472	14.846148	9.499847	6.544080	4.601084	3.232197	2.237719	1.508063	.975346	.593724	.330010	.158616	.058661	.011834	.000077	
2.84	8.418906	14.979158	9.593745	6.615366	4.656566	3.275677	2.271666	1.534238	.995090	.608134	.339982	.164960	.062125	.013159	.000152	
2.85	8.506849	15.112840	9.688204	6.687102	4.712432	3.319485	2.305919	1.560678	1.015082	.622749	.350145	.171460	.065695	.014578	.000251	
2.86	8.595301	15.247186	9.783180	6.759286	4.768690	3.363647	2.340459	1.587388	1.035302	.637566	.360463	.178097	.069398	.016074	.000400	
2.87	8.684263	15.382217	9.878693	6.831912	4.825326	3.408153	2.375317	1.614377	1.055767	.652598	.370971	.184893	.073228	.017661	.000589	
2.88	8.773736	15.517899	9.974744	6.904997	4.882363	3.452999	2.410476	1.641625	1.076472	.667840	.381668	.191838	.077168	.019340	.000825	
2.89	8.863720	15.654262	10.071315	6.978525	4.939791	3.498185	2.445944	1.669152	1.097407	.683283	.392531	.198948	.081238	.021106	.001092	
2.90	8.954217	15.791302	10.168436	7.052507	4.997606	3.543721	2.481712	1.696938	1.118587	.698935	.403589	.206193	.085436	.022974	.001424	
2.91	9.045227	15.929005	10.266077	7.126936	5.055817	3.589601	2.517780	1.725003	1.140001	.714804	.414833	.213611	.089761	.024923	.001813	
2.92	9.136751	16.067390	10.364251	7.201829	5.114416	3.635820	2.554156	1.753336	1.161656	.730881	.426248	.221177	.094210	.026986	.002251	
2.93	9.228788	16.206450	10.462971	7.277173	5.173414	3.682402	2.590842	1.781948	1.183560	.747179	.437848	.228905	.098793	.029128	.002756	
2.94	9.321341	16.346179	10.562219	7.352963	5.232804	3.729315	2.627837	1.810832	1.205703	.763681	.449642	.236783	.103513	.031396	.003305	
2.95	9.414409	16.486589	10.662001	7.429212	5.292586	3.776581	2.665136	1.839985	1.228080	.780409	.461619	.244830	.108355	.033747	.003921	
2.96	9.507994	16.627675	10.762324	7.505917	5.352763	3.824204	2.702757	1.869416	1.250721	.797346	.473798	.253034	.113323	.036202	.004616	
2.97	9.602096	16.769443	10.863185	7.583072	5.413344	3.872177	2.740692	1.899124	1.273597	.814503	.486136	.261403	.118438	.038757	.005364	
2.98	9.696716	16.911882	10.964587	7.660682	5.474317	3.920493	2.778922	1.929105	1.296716	.831864	.498691	.269925	.123683	.041431	.006183	
2.99	9.791854	17.055003	11.066531	7.738733	5.535690	3.969157	2.817474	1.959374	1.320083	.849459	.511429	.278612	.129063	.044207	.007084	
3.00	9.887511	17.198791	11.169043	7.817280	5.597463	4.018185	2.856334	1.989905	1.343700	.867259	.524358	.287482	.134586	.047090	.008042	
3.01	9.983687	17.343278	11.272030	7.896268	5.659627	4.067550	2.895507	2.020728	1.367564	.885289	.537484	.296503	.140243	.050064	.009091	.000004
3.02	10.080385	17.488437	11.375590	7.975710	5.722196	4.117274	2.934993	2.051838	1.391683	.903529	.550791	.305684	.146046	.053181	.010219	.000038
3.03	10.177603	17.634277	11.479696	8.055622	5.785170	4.167360	2.974793	2.083205	1.416045	.921997	.564296	.315047	.151983	.056385	.011409	.000073
3.04	10.275342	17.780798	11.584344	8.135984	5.848548	4.217784	3.014920	2.114870	1.440655	.940696	.578004	.324575	.158066	.059723	.012686	.000148
3.05	10.373605	17.928000	11.689534	8.216815	5.912312	4.268576	3.055350	2.146812	1.465523	.959615	.591900	.334270	.164290	.063169	.014051	.000249
3.06	10.472390	18.075888	11.795260	8.298109	5.976505	4.319730	3.096097	2.179040	1.490645	.978736	.606004	.344127	.170654	.066727	.015500	.000379
3.07	10.571699	18.224461	11.901552	8.379863	6.041078	4.371227	3.137167	2.211545	1.516015	.998099	.620294	.354167	.177170	.070397	.017023	.000564
3.08	10.671532	18.373720	12.008376	8.462081	6.106061	4.423087	3.178554	2.244343	1.541639	1.017686	.634783	.364382	.183830	.074194	.018644	.000787
3.09	10.771890	18.523660	12.115737	8.544754	6.171449	4.475304	3.220254	2.277427	1.567515	1.037508	.649471	.374766	.190625	.078116	.020338	.001060
3.10	10.872774	18.674290	12.223663	8.627895	6.237246	4.527888	3.262291	2.310797	1.593651	1.057550	.664363	.385245	.197577	.082150	.022145	.001389

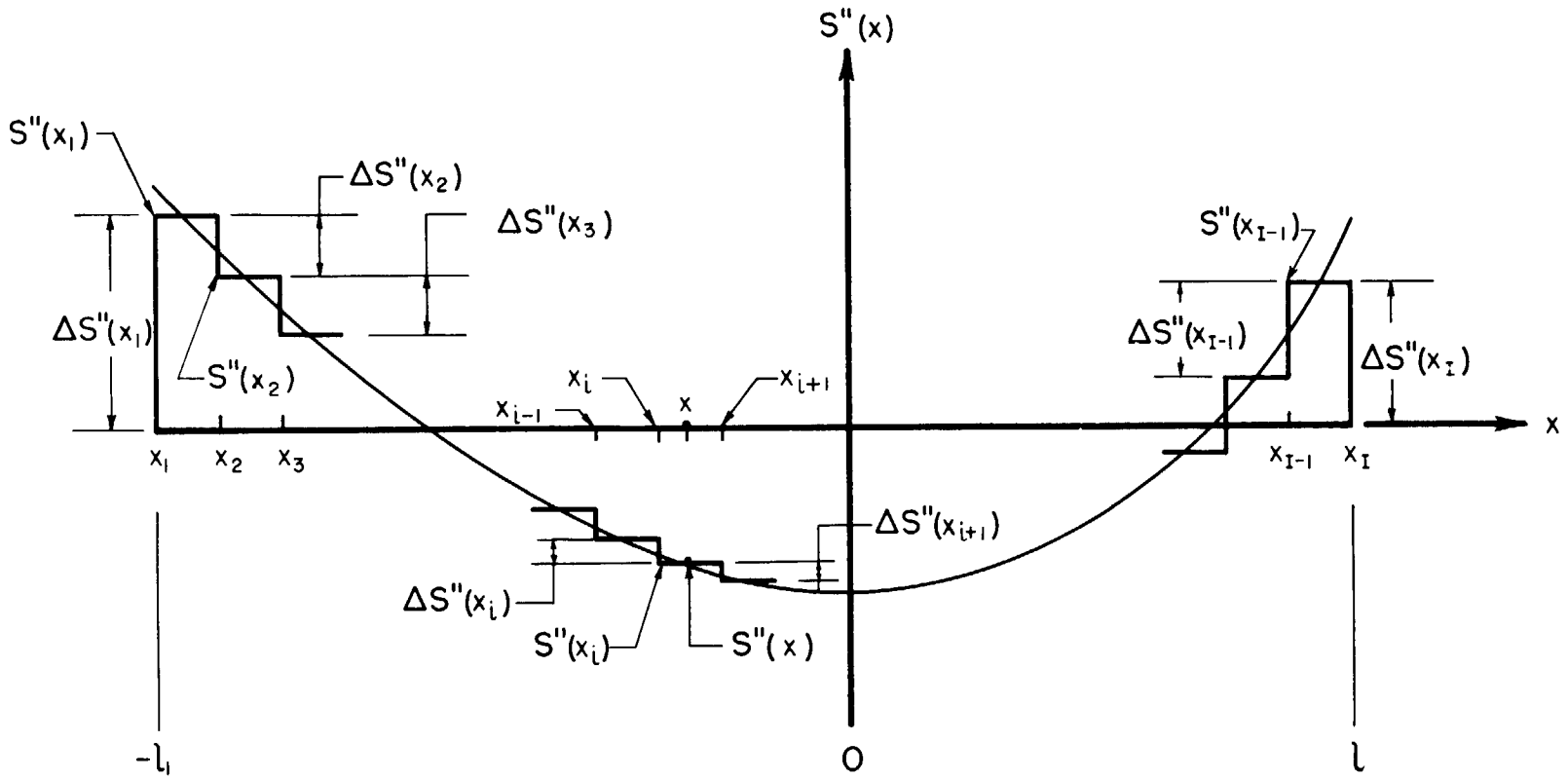

Figure 1.- Sketch showing the equal-interval approximation of the second derivative of the area distribution of an equivalent body of revolution.

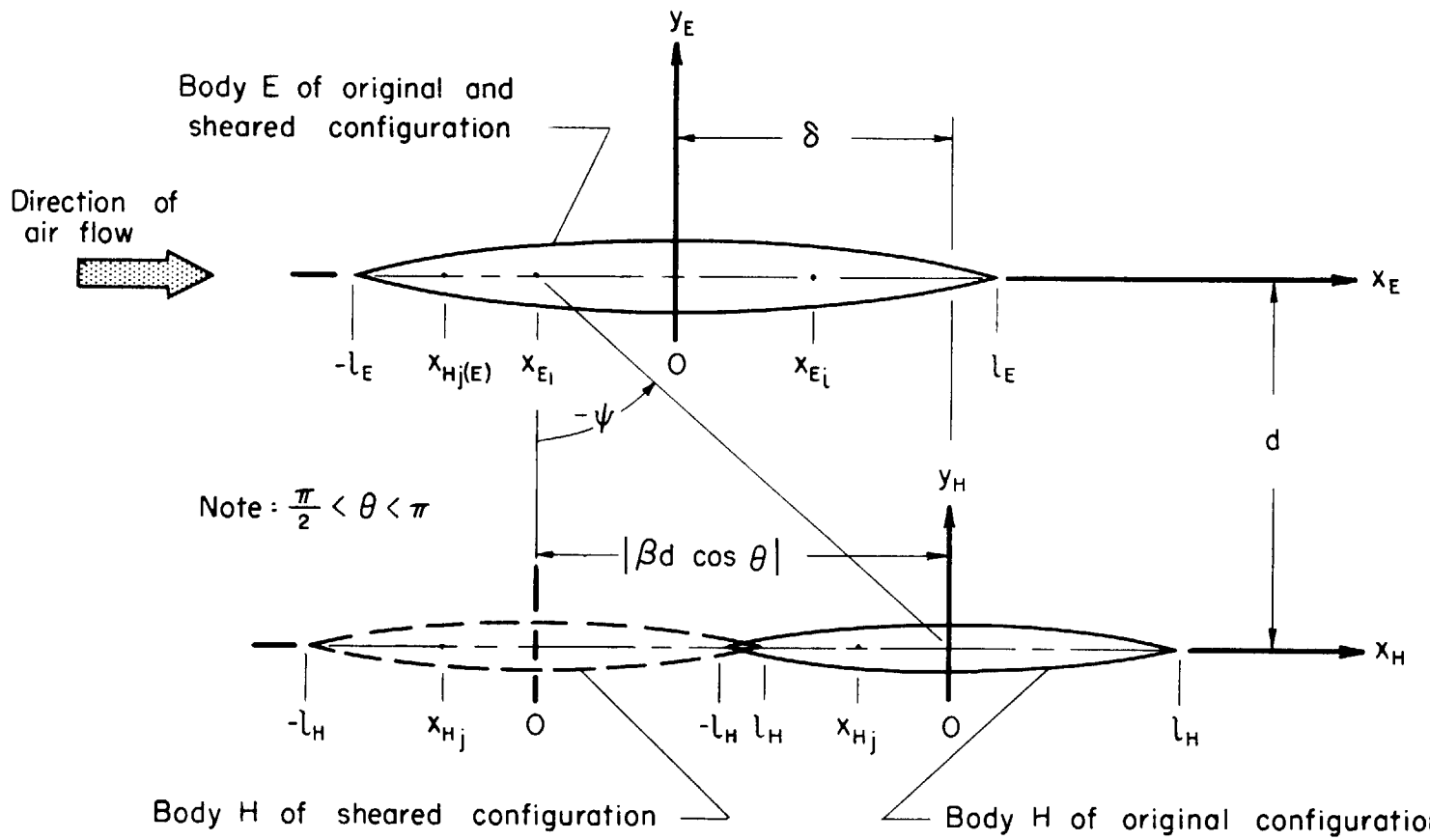

Figure 2.- Sketch showing a pair of bodies of revolution and a typical sheared configuration.

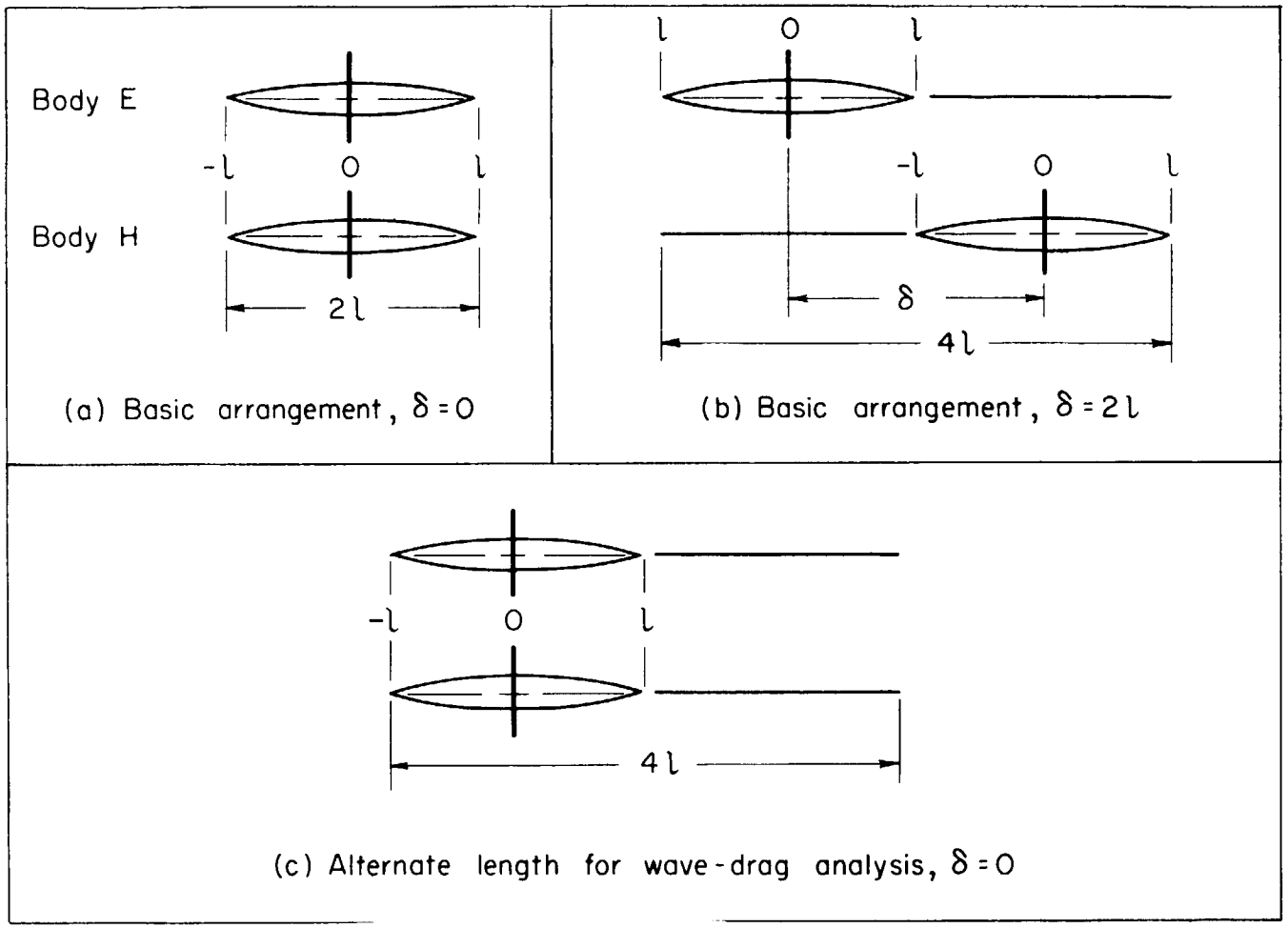

Figure 3.- Sketch showing the two basic arrangements of the pairs of bodies of revolution and the lengths over which the wave-drag analysis is performed.

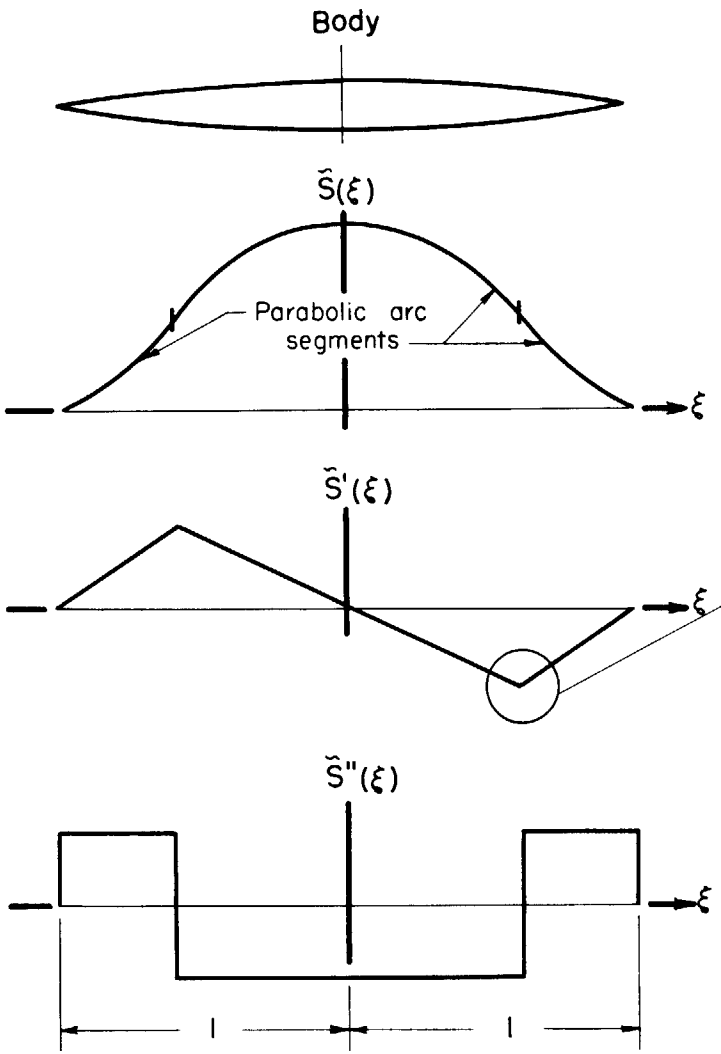

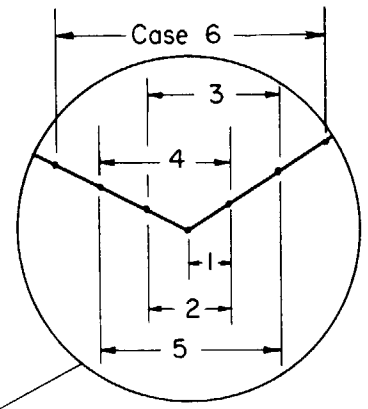

Location of equal-interval points for cases of the drag analyses listed below.

Case no.	No. of points	$\frac{2}{\pi S_o^2}\tilde{D}_{\tilde{S}''_m(\xi)}$	Percent error
1	200	3.140	0
2	100	3.132	.25
3	67	3.125	.48
4	67	3.125	.48
5	50	3.113	.86
6	25	3.085	1.75
$\frac{2}{\pi S_o^2}\tilde{D}_{Analytical} = 3.140$			

Figure 4.- Effect of the choice of the number and location of the equally spaced points used in the wave-drag analysis.

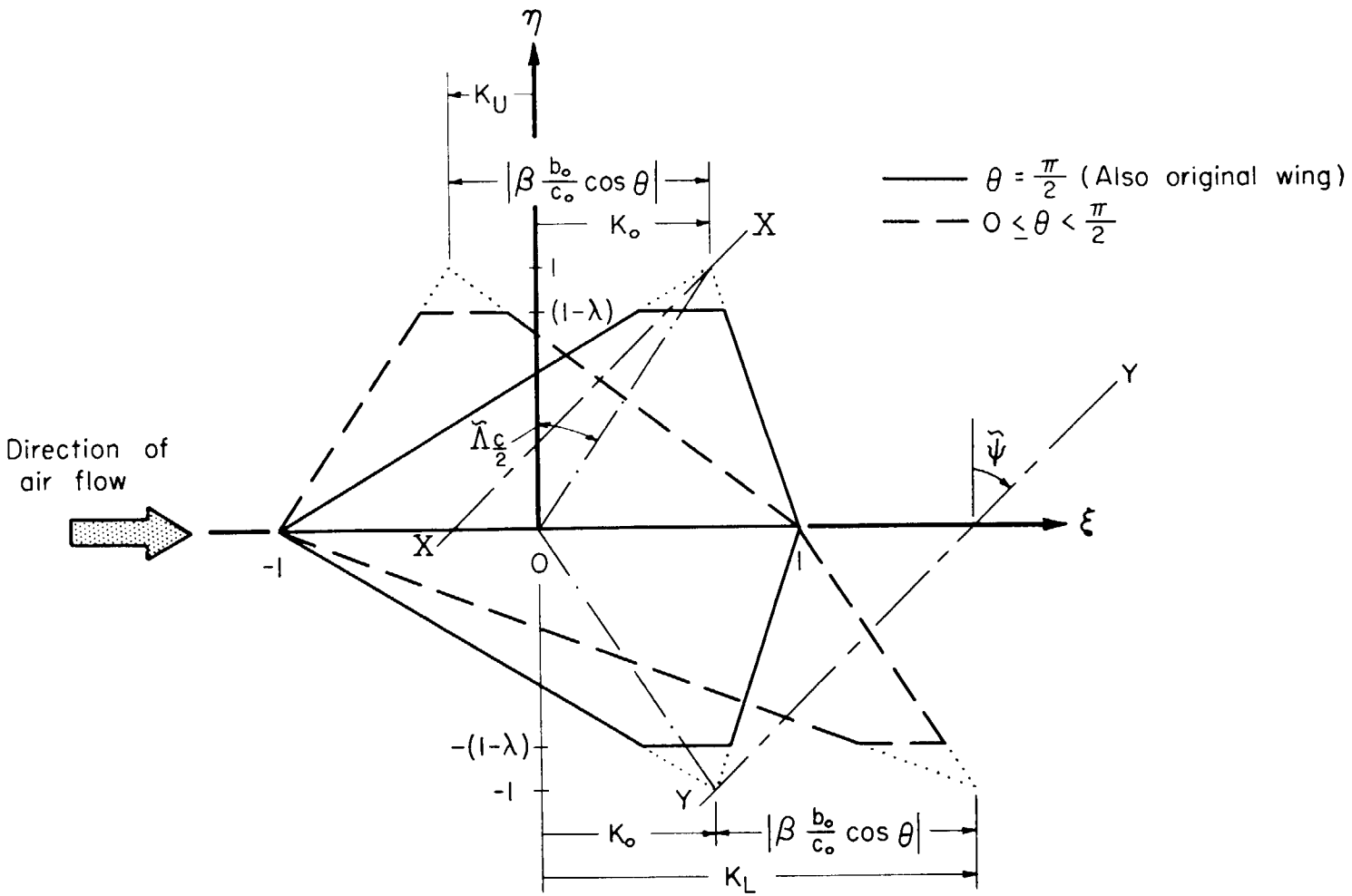

Figure 5.- Sketch, in dimensionless coordinates, showing the relationship of sheared wings to β and θ.

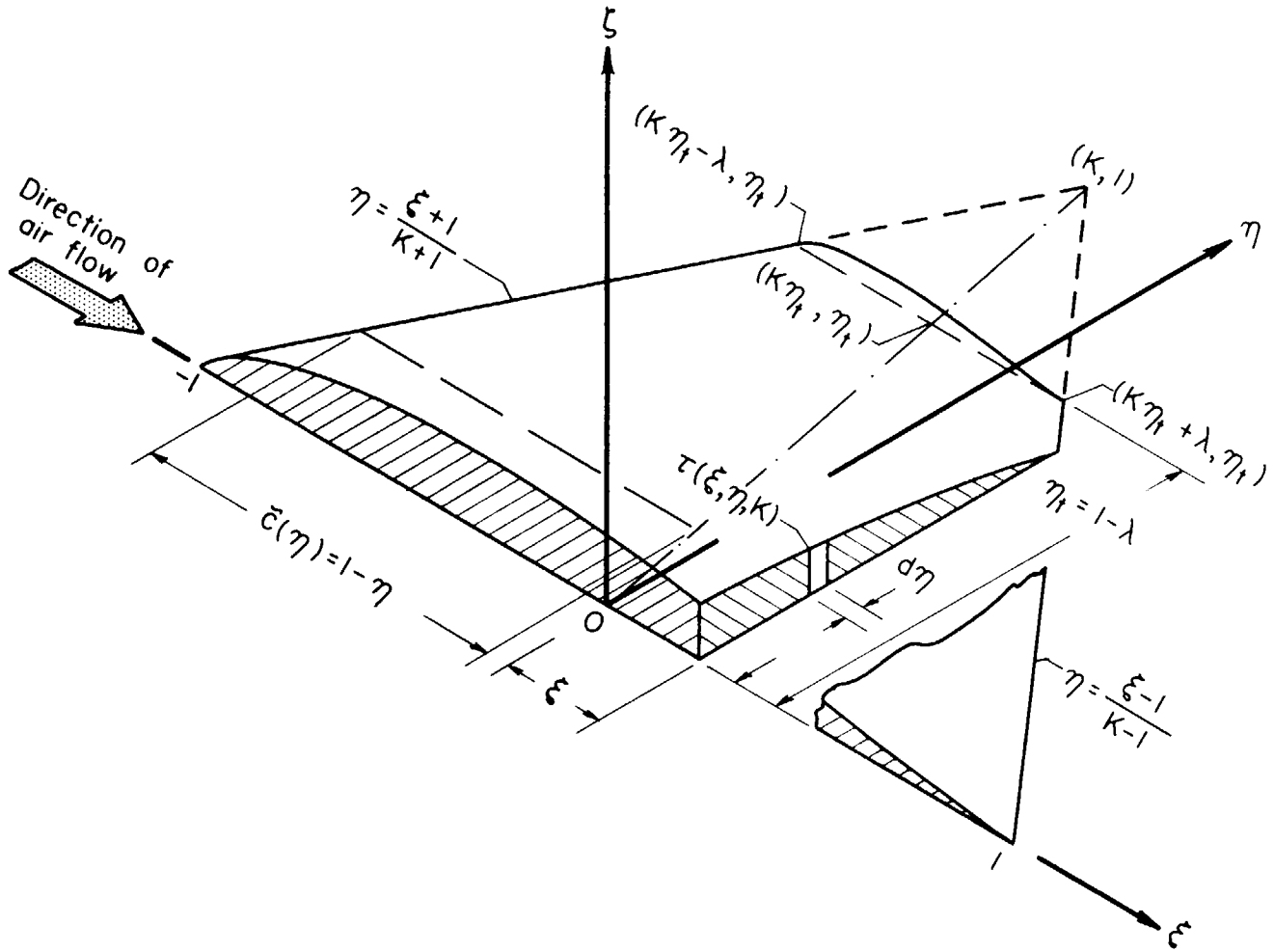

Figure 6.- Typical half plan form, in dimensionless coordinates, for wings and tail surfaces.

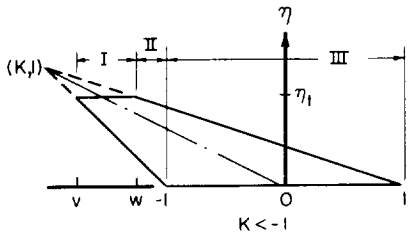

K < -1

Case II

Region I, $v \le \xi \le w$, $\int_{\alpha_l}^{\alpha_u} = \int_{-1}^{1} - \int_{\alpha_t}^{1}$

Region II, $w < \xi < -1$, $\int_{\alpha_l}^{\alpha_u} = \int_{-1}^{1}$

Region III, $-1 \le \xi \le 1$, $\int_{\alpha_l}^{\alpha_u} = \int_{\xi}^{1}$

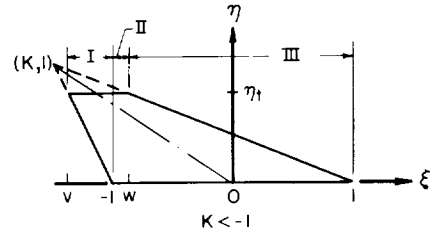

K < -1

Region I, $v \le \xi < -1$, $\int_{\alpha_l}^{\alpha_u} = \int_{-1}^{1} - \int_{\alpha_t}^{1}$

Region II, $-1 \le \xi \le w$, $\int_{\alpha_l}^{\alpha_u} = \int_{\xi}^{1} - \int_{\alpha_t}^{1}$

Region III, $w < \xi \le 1$, $\int_{\alpha_l}^{\alpha_u} = \int_{\xi}^{1}$

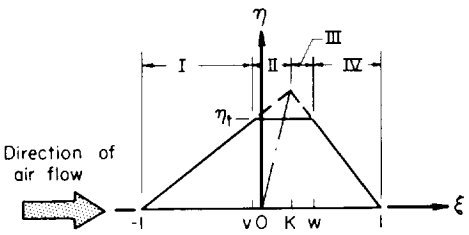

Region I, $-1 \le \xi < v$, $\int_{\alpha_l}^{\alpha_u} = \int_{\xi}^{-1}$

Region II, $v \le \xi \le K$, $\int_{\alpha_l}^{\alpha_u} = \int_{\xi}^{-1} - \int_{\alpha_t}^{-1}$

} Case I, $\xi \le K$, $\alpha_u < \alpha_l$

Region III, $K < \xi \le w$, $\int_{\alpha_l}^{\alpha_u} = \int_{\xi}^{1} - \int_{\alpha_t}^{1}$

Region IV, $w < \xi \le 1$, $\int_{\alpha_l}^{\alpha_u} = \int_{\xi}^{1}$

} Case II, $\xi > K$, $\alpha_u > \alpha_l$

$-1 \le K \le 1$

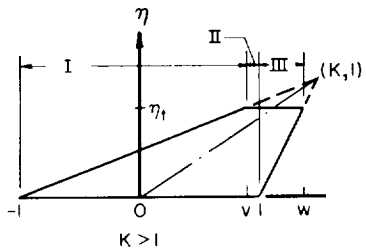

K > 1

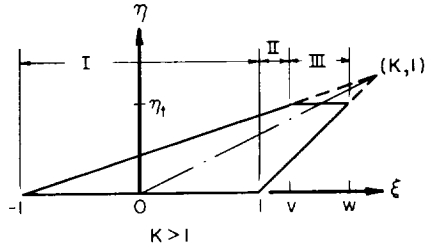

K > 1

Case I

Region I, $-1 \le \xi < v$, $\int_{\alpha_l}^{\alpha_u} = \int_{\xi}^{-1}$

Region II, $v \le \xi \le 1$, $\int_{\alpha_l}^{\alpha_u} = \int_{\xi}^{-1} - \int_{\alpha_t}^{-1}$

Region III, $1 < \xi \le w$, $\int_{\alpha_l}^{\alpha_u} = \int_{1}^{-1} - \int_{\alpha_t}^{-1}$

Region I, $-1 \le \xi \le 1$, $\int_{\alpha_l}^{\alpha_u} = \int_{\xi}^{-1}$

Region II, $1 < \xi < v$, $\int_{\alpha_l}^{\alpha_u} = \int_{1}^{-1}$

Region III, $v \le \xi \le w$, $\int_{\alpha_l}^{\alpha_u} = \int_{-1}^{-1} - \int_{\alpha_t}^{-1}$

Note: $v = K\eta_t - \lambda$; $w = K\eta_t + \lambda$

(a) Half plan forms for $0 < \lambda < 1$

Figure 7.- Regions and limits of α integration for dimensionless half plan forms.

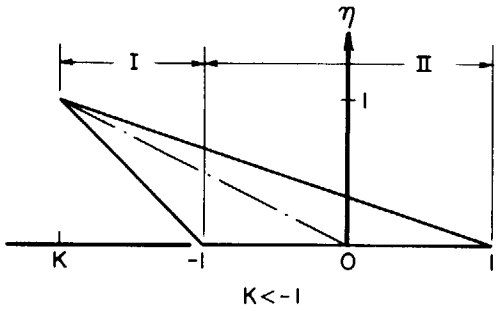

$K < -1$

Case II

Region I, $K \le \xi < -1$, $\int_{\alpha_l}^{\alpha_u} = \int_{-1}^{1}$

Region II, $-1 \le \xi \le 1$, $\int_{\alpha_l}^{\alpha_u} = \int_{\xi}^{1}$

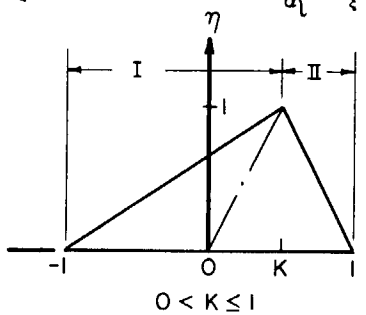

$0 < K \le 1$

Case I, Region I, $1 \le \xi \le K$, $\int_{\alpha_l}^{\alpha_u} = \int_{\xi}^{-1}$

Case II, Region II, $K < \xi \le 1$, $\int_{\alpha_l}^{\alpha_u} = \int_{\xi}^{1}$

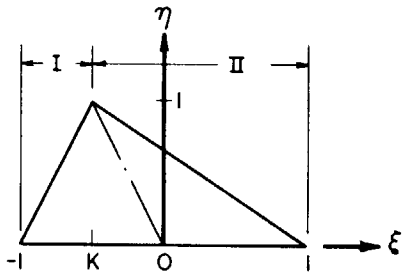

$-1 \le K \le 0$

Case I, Region I, $-1 \le \xi \le K$, $\int_{\alpha_l}^{\alpha_u} = \int_{\xi}^{-1}$

Case II, Region II, $K < \xi \le 1$, $\int_{\alpha_l}^{\alpha_u} = \int_{\xi}^{1}$

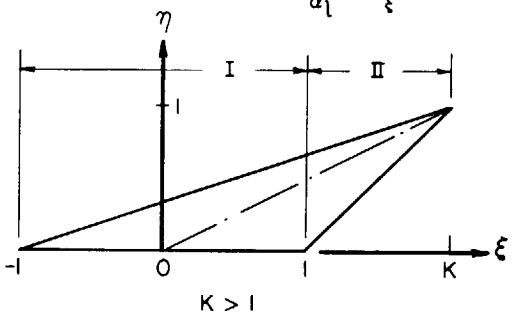

$K > 1$

Case I

Region I, $-1 \le \xi \le 1$, $\int_{\alpha_l}^{\alpha_u} = \int_{\xi}^{-1}$

Region II, $1 < \xi \le K$, $\int_{\alpha_l}^{\alpha_u} = \int_{1}^{-1}$

(b) Half plan forms for $\lambda = 0$.

Figure 7.- Concluded.

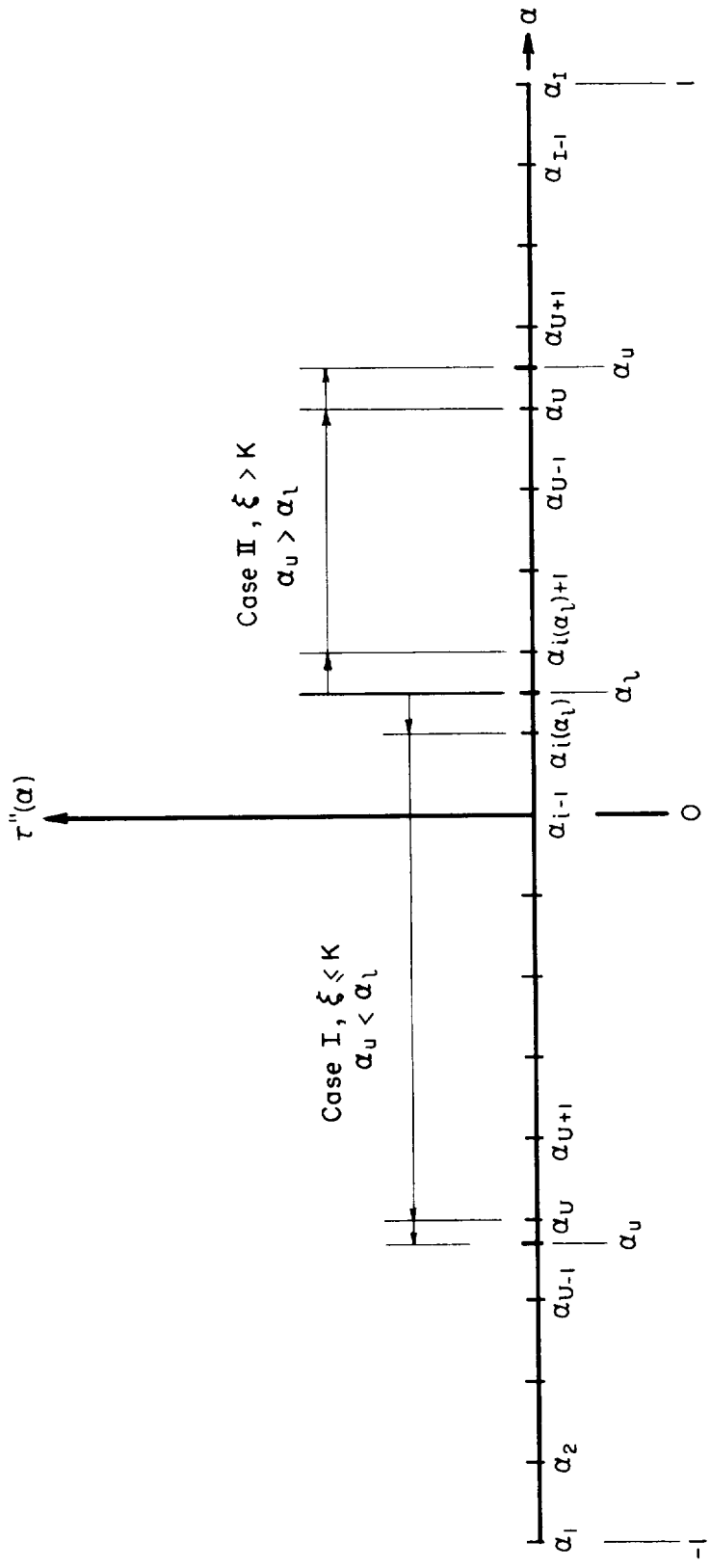

Figure 8.- Stepwise limits and direction of α integration.

NASA MEMO 1-16-59A
National Aeronautics and Space Administration.
A NUMERICAL METHOD FOR CALCULATING THE WAVE DRAG OF A CONFIGURATION FROM THE SECOND DERIVATIVE OF THE AREA DISTRIBUTION OF A SERIES OF EQUIVALENT BODIES OF REVOLUTION. Lionel L. Levy, Jr., and Kenneth K. Yoshikawa. April 1959. 91p. diagrs., tabs. (NASA MEMORANDUM 1-16-59A)

By a simple approximation of the second derivative of the area distribution, the wave drag of a configuration is expressed in a finite series which can be evaluated numerically. Results calculated by the present method for specific configurations have been found to agree well with analytical and other numerical results. The finite series form of the present method is particularly attractive in its application to the calculation of zero-lift interference wave drag between any pair of components of a configuration.

Copies obtainable from NASA, Washington

1. Bodies - Shape Variables (1.3.2)
2. Airplanes - Components in Combination (1.7.1.1)
3. Missiles - Components in Combination (1.7.2.1)

I. Levy, Lionel L., Jr.
II. Yoshikawa, Kenneth K.
III. NASA MEMO 1-16-59A

NASA

NASA MEMO 1-16-59A
National Aeronautics and Space Administration.
A NUMERICAL METHOD FOR CALCULATING THE WAVE DRAG OF A CONFIGURATION FROM THE SECOND DERIVATIVE OF THE AREA DISTRIBUTION OF A SERIES OF EQUIVALENT BODIES OF REVOLUTION. Lionel L. Levy, Jr., and Kenneth K. Yoshikawa. April 1959. 91p. diagrs., tabs. (NASA MEMORANDUM 1-16-59A)

By a simple approximation of the second derivative of the area distribution, the wave drag of a configuration is expressed in a finite series which can be evaluated numerically. Results calculated by the present method for specific configurations have been found to agree well with analytical and other numerical results. The finite series form of the present method is particularly attractive in its application to the calculation of zero-lift interference wave drag between any pair of components of a configuration.

Copies obtainable from NASA, Washington

1. Bodies - Shape Variables (1.3.2)
2. Airplanes - Components in Combination (1.7.1.1)
3. Missiles - Components in Combination (1.7.2.1)

I. Levy, Lionel L., Jr.
II. Yoshikawa, Kenneth K.
III. NASA MEMO 1-16-59A

NASA

NASA MEMO 1-16-59A
National Aeronautics and Space Administration.
A NUMERICAL METHOD FOR CALCULATING THE WAVE DRAG OF A CONFIGURATION FROM THE SECOND DERIVATIVE OF THE AREA DISTRIBUTION OF A SERIES OF EQUIVALENT BODIES OF REVOLUTION. Lionel L. Levy, Jr., and Kenneth K. Yoshikawa. April 1959. 91p. diagrs., tabs. (NASA MEMORANDUM 1-16-59A)

By a simple approximation of the second derivative of the area distribution, the wave drag of a configuration is expressed in a finite series which can be evaluated numerically. Results calculated by the present method for specific configurations have been found to agree well with analytical and other numerical results. The finite series form of the present method is particularly attractive in its application to the calculation of zero-lift interference wave drag between any pair of components of a configuration.

Copies obtainable from NASA, Washington

1. Bodies - Shape Variables (1.3.2)
2. Airplanes - Components in Combination (1.7.1.1)
3. Missiles - Components in Combination (1.7.2.1)

I. Levy, Lionel L., Jr.
II. Yoshikawa, Kenneth K.
III. NASA MEMO 1-16-59A

NASA

NASA MEMO 1-16-59A
National Aeronautics and Space Administration.
A NUMERICAL METHOD FOR CALCULATING THE WAVE DRAG OF A CONFIGURATION FROM THE SECOND DERIVATIVE OF THE AREA DISTRIBUTION OF A SERIES OF EQUIVALENT BODIES OF REVOLUTION. Lionel L. Levy, Jr., and Kenneth K. Yoshikawa. April 1959. 91p. diagrs., tabs. (NASA MEMORANDUM 1-16-59A)

By a simple approximation of the second derivative of the area distribution, the wave drag of a configuration is expressed in a finite series which can be evaluated numerically. Results calculated by the present method for specific configurations have been found to agree well with analytical and other numerical results. The finite series form of the present method is particularly attractive in its application to the calculation of zero-lift interference wave drag between any pair of components of a configuration.

Copies obtainable from NASA, Washington

1. Bodies - Shape Variables (1.3.2)
2. Airplanes - Components in Combination (1.7.1.1)
3. Missiles - Components in Combination (1.7.2.1)

I. Levy, Lionel L., Jr.
II. Yoshikawa, Kenneth K.
III. NASA MEMO 1-16-59A

NASA